Title

Towards more biologically plausible computational models of the cerebellum with emphasis on the molecular layer interneurons

Permalink

https://escholarship.org/uc/item/9n45f5rz

Author

Lennon, William Charles

Publication Date

2015

Peer reviewed|Thesis/dissertation

UNIVERSITY OF CALIFORNIA, SAN DIEGO

Towards more biologically plausible computational models of the cerebellum
with emphasis on the molecular layer interneurons

A dissertation submitted in partial satisfaction of the requirements for the
degree of Doctor of Philosophy

in

Electrical Engineering (Intelligent Systems, Robotics and Control)

by

William Charles Lennon, Jr.

Committee in charge:

    Professor Robert Hecht-Nielsen, Chair
    Professor Clark Guest, Co-Chair
    Professor Jeffrey Elman
    Professor Lawrence Larson
    Professor Laurence Milstein
    Professor Douglas Nitz

2015

The Dissertation of William Charles Lennon, Jr. is approved, and it is acceptable in quality and form for publication on microfilm and electronically:

_____

_____

_____

_____

_____

Co-Chair

_____

Chair

University of California, San Diego

2015

DEDICATION

To my loving wife, Katie, and my parents, Bill and Cyndy, for shaping me.

EPIGRAPH

"The eye sees only what the mind is prepared to comprehend"

-- Robertson Davies

TABLE OF CONTENTS

LIST OF FIGURES

LIST OF TABLES

ACKNOWLEDGEMENTS

After five years of graduate work, so many acknowledgements and thanks are due to the amazing people in my life. First, to my long-time mentor, Robert Hecht-Nielsen. You inspired me and encouraged me to achieve far more than I ever thought I was capable of. I am infinitely grateful for the decade of mentorship you have given me, from my high school senior project to doctoral dissertation.

I am also deeply indebted to and thankful for my committee co-chair, Clark Guest, for helping me navigate through the turbulence of graduate school and for your steady, sound advice. I am grateful to the rest of the committee, Professors Jeff Elman, Larry Larson, Larry Milstein and Doug Nitz, for their support and guidance over the years. I would also like to thank Harvey Karten for serving on my committee before his retirement and for the valuable conversations on cerebellar and brainstem anatomy we shared.

I am thankful for the opportunity that the National Science Foundation provided for me to spend the summer of 2013 working in Japan. My gracious host, Tadashi Yamazaki, has become a wonderful scientific mentor, collaborator and friend. The work in this dissertation would not have happened without him.

While in graduate school, I had the privilege of working with a cast of brilliant and entertaining characters. Rupert Minnett, Andrew Smith, Mehrdad Yazdani, Geoffrey Gamble and Gavin Henderson, I enjoyed all of our time together and will miss our conversations. I am also grateful for the friends I made in graduate school, Kiran Sikka, Justin Grevich, all of the neuroscience graduate students, and many more. I am also grateful for all of the friends I

made outside of school, Haw-minn Lu, Misha Erekhinsky, Julia and Rich Stoner, Syrus Nemat-Nasser, Bilal Shaw, Steve Anton and many more.

I am grateful for Shu Chien, Lori Guardiano-Durkin and Ken Tomory at the Institute of Engineering in Medicine for providing a wonderful work opportunity. I learned a tremendous amount from you all.

To all of my friends and family, I am fortunate to have such wonderful people in my life. Your support over the past five years has been indispensible for completing this work. I thank Andrew Bates for showing me what hard work really is. I would also like to thank Kaitlin Wood for the fun, albeit very slow, games of Dominion. Thanks to Bryan and Cat, Matt and Mindi, Jeff and Mariah, Jens and Drew, Kelsey, and Travis and Kaitlin for sharing many experiences of acute ethanol-induced cerebellar disruption with me.

I am especially thankful for my parents, for making me, and for loving and nurturing me. I could not have done it without you.

Most importantly, I thank my wife and best friend, Katie. Your love and support has permeated every aspect of my life since we met.

Chapter 3, in full, is a reprint with minor revisions of the material as it appears in *Frontiers in Computational Neuroscience*. William Lennon, Robert Hecht-Nielsen, Tadashi Yamazaki. "A spiking network model of the cerebellar Purkinje cells and molecular layer interneurons exhibiting irregular firing". Vol. 8, pp. 1-10, 2014. The dissertation author is the primary investigator and author of this material.

Chapter 4, in part, has been submitted for publication of the material. William Lennon, Tadashi Yamazaki, Robert Hecht-Nielsen. The dissertation author is the primary investigator and author of this material.

Chapter 5, in part, is currently being prepared for submission for publication of the material. William Lennon, Tadashi Yamazaki, Robert Hecht-Nielsen. The dissertation author is the primary investigator and author of this material.

VITA

2009	Bachelor of Arts, Mathematics Bachelor of Science, Business Administration University of California, Berkeley
2011	Master of Science, Electrical Engineering (Intelligent Systems, Robotics and Control) University of California, San Diego
2014	Candidate of Philosophy, Electrical Engineering (Intelligent Systems, Robotics and Control) University of California, San Diego
2010-2015	Graduate Student Researcher University of California, San Diego
2015	Doctor of Philosophy, Electrical Engineering (Intelligent Systems, Robotics and Control) University of California, San Diego

PUBLICATIONS

William Lennon, Tadashi Yamazaki and Robert Hecht-Nielsen. Temporal difference learning at parallel fiber - molecular layer interneuron synapses. In preparation.

William Lennon, Tadashi Yamazaki and Robert Hecht-Nielsen. A model of learning at the parallel fiber - molecular layer interneuron synapses. *Submitted.*

Tadashi Yamazaki, Soichi Nagao, **William Lennon**, and Shigeru Tanaka (2015). Modeling memory consolidation during post-training periods in cerebellovestibular learning. *Proceedings of the National Academy of Sciences of the United States of America*, in press.

William Lennon, Robert Hecht-Nielsen, Tadashi Yamazaki (2014). A spiking network model of cerebellar Purkinje cells and molecular layer interneurons exhibiting irregular firing. *Frontiers in Computational Neuroscience*, 8(157), 1-10.

William Lennon, Robert Hecht-Nielsen, Tadashi Yamazaki. A simulation of cerebellar function with learning at parallel fiber – molecular layer interneurons. Program No. 341.09. 2014 Neuroscience Meeting Planner. Washington DC: Society for Neuroscience, 2014. Online. 44th Annual Meeting of Society for Neuroscience, Nov 15-19, Washington DC, USA.

William Lennon, Tadashi Yamazaki, Robert Hecht-Nielsen. A computational model of the cerebellum with learning at the parallel fiber - basket cell synapses. 21st Joint Symposium on Neural Computation, May 17, 2014, CalIT2 Auditorium, University of California at Irvine.

William Lennon, Tadashi Yamazaki, Robert Hecht-Nielsen. A computational model of the cerebellum with learning at the parallel fiber - basket cell synapses. Program No. 469.18. 2013 Neuroscience Meeting Planner. San Diego, CA: Society for Neuroscience, 2013. Online. 43rd Annual Meeting of Society for Neuroscience, Nov 9-13, San Diego, California, USA.

William Lennon, Tadashi Yamazaki, Robert Hecht-Nielsen. A Computational Investigation into the Role of Molecular Layer Interneurons in the Cerebellar Cortex. JSPS Summer Program Orientation.   SOKENDAI Graduate University for Advanced Studies, Hayama, Tokyo, Japan. June 2013.

Rupert Minnett, Andrew Smith, **William Lennon**, Robert Hecht-Nielsen (2011). Neural network tomography: Network replication from output surface geometry. *Neural Networks*, 24(5), 484-492.

William Lennon, Rupert Minnett, Andrew Smith, Robert Hecht-Nielsen. Direct positioning of a neural network's hidden units. Program No. 209.5. 2010 Neuroscience Meeting Planner. San Diego, CA: Society for Neuroscience, 2010.

ABSTRACT OF THE DISSERTATION

Towards more biologically plausible computational models of the cerebellum
with emphasis on the molecular layer interneurons

by

William Charles Lennon, Jr.

Doctor of Philosophy in Electrical Engineering (Intelligent Systems, Robotics
and Control)

University of California, San Diego, 2015

Professor Robert Hecht-Nielsen, Chair
Professor Clark Guest, Co-Chair

We join the efforts of over a century of modern scientific inquiry to
understand *what* the cerebellum does and *how* the cerebellum implements its
function. A myriad of anatomical and physiological facts about the cerebellum
exist and have been woven into theories of cerebellar computation, but most of

these theories ignore the role of a certain neuron type in the cerebellar cortex - - the molecular layer interneurons (MLIs). In this body of work, we propose mathematical models for the anatomy, physiology and synaptic plasticity of these neurons in order to characterize their role in cerebellar function.

First, we introduce a simple model of the physiology of the MLI which exhibits spontaneous firing as observed *in vivo*. Further, we model the synaptic connectivity of MLIs with other MLIs and with Purkinje cells (PKJs). We validate the model by simulating the network of MLIs and PKJs and show that it reproduces the irregular firing activity of MLIs and PKJs as observed *in vitro*.

Second, we introduce a phenomenological model of plasticity at parallel fiber (PF) - MLI synapses. We show via computer simulation that this model reproduces the changes in synaptic efficacy observed *in vitro* under a number of experimental protocols. Further, we hypothesize what biological mechanisms govern plasticity at this synapse and give rise to the model we introduce.

Finally, we show analytically that the model of plasticity at PF-MLI synapses can implement temporal difference learning at these synapses under certain assumptions about the function of cerebellar cortical circuitry. This result supports the idea that reinforcement learning is the method of learning used by the cerebellum.

Chapter 1   Introduction

1.1   Why study the cerebellum?

The cerebellum is a mysterious brain structure. Despite being the target of intense scientific inquiry for over a century (Glickstein et al., 2009), we still cannot answer the basic question, "What does the cerebellum do?". In contrast, brain structures like the motor cortex seem to have clearer answers to this question: to voluntarily control movement (Kandel, 2013). To illustrate this, consider the difference in the effects of an acute lesion (e.g. by stroke) to the motor cortex versus the cerebellar cortex (let's assume we lesion the respective sub-regions in both structures involved in arm movements). When the motor cortex is damaged, the individual experiences flaccid paralysis, in addition to other symptoms (Fulton, 1935). In contrast, a lesion to the cerebellum leaves the individual with the ability to move, but the movements are imprecise, uncoordinated, and require tremendous mental effort to achieve (Kandel, 2013). So then, what is the cerebellum doing to make these movements smooth, precise and effortless? Even stranger, there are rare cases of individuals who are born without a cerebellum and lead relatively normal lives (Romaniello and Borgatti, 2013).

All of this is not to say that the cerebellum is exclusively involved in motor function. Over the last two decades, many lines of evidence have led to the consensus that the cerebellum is also involved in cognitive function (Koziol et al., 2014). Lesions to the regions of the cerebellum involved in cognitive function in humans lead to seemingly analogous deficits in cognition as in

motor function, termed *dysmetria of thought* (Schmahmann, 2004). The fact that the circuitry is stereotyped throughout the entire cerebellar cortex implies that whatever the cerebellum is doing for movement, it is doing the same for cognition.

Despite not having a unified understanding of cerebellar function, our knowledge of the anatomy and physiology of this structure is rich. In addition, new subtleties are being learned as a result of experimental techniques such as optogenetics. Such detailed knowledge of the cerebellar circuitry lends itself well to theoretical and computational investigation of cerebellar function. Not surprisingly, shortly after the first blueprint-like diagrams of cerebellar circuits were published (Eccles et al., 1967) the first theoretical and mathematical models of cerebellar computation emerged (Grossberg, 1969;Marr, 1969;Albus, 1971).

1.2 Two fundamental questions

We have already explicitly stated one important question, "What does the cerebellum do?". The other, which we have stated implicitly is, "How does the cerebellum do this?". Or, more formally, "What function does the cerebellum compute and how does it implement this computation in neuronal circuitry?". The former is a top-down inquiry from the level of behavior while the latter is bottom-up from the level of neurons and synapses. Our understanding of the cerebellum must also come from understanding the context in which it operates. That is, by understanding what the role of the cerebellum is in the system which it co-exists -- the set of brain structures which it co-evolved to support and be supported by -- in order to achieve

behavioral success for the organism. Fully understanding how the cerebellum works will likely require all of these approaches. The approach taken for the research presented in this dissertation is motivated by *in vitro, in vivo,* and behavioral results but constructs a bottom-up model to explain cerebellar function.

1.3 The role of the molecular layer interneurons

The molecular layer interneurons (MLIs) are a type of *inhibitory interneuron* found in the cerebellar cortex that historically have been overlooked by theorists and experimentalists in models of cerebellar function. The MLIs provide feedforward inhibition onto the historically recognized "principal" neuron of the cerebellar cortex -- the Purkinje cell (PKJ) -- which provides the sole output of the cerebellar cortex. Because the PKJs have such a remarkable morphology, an immense number of synaptic inputs from parallel fibers (PFs), and form the sole output of the cerebellar cortex, they have been the focus of experimental and theoretical cerebellar neuroscience for the last century. The MLIs were relegated to the role of providing "sculpting" and "global" inhibition to prevent runaway PKJ excitation, a decidedly second-class role in neural systems.

Recent evidence (reviewed in Chapter 2) suggests a more significant role for these neurons in cerebellar function. A number of clues led to the idea that these neurons have a more sophisticated role in cerebellar function. First, PKJs fire spontaneously in absence of all synaptic input (Hausser and Clark, 1997), so observed decreases in PKJ firing require inhibition provided by MLIs (Miyashita and Nagao, 1984;Jirenhed et al., 2007). Second, plasticity exists at synapses formed by and onto MLIs, so feedforward inhibition can be learned

(Gao et al., 2012). Finally, genetically modified mice lacking MLI-PKJ feedforward inhibition exhibit significant motor learning deficits (Wulff et al., 2009). The accumulation of this evidence and the holes in previous theories of cerebellar function are what motivated the research in this dissertation. Namely, that by understanding the role of MLIs and including them in mechanistic explanations of how the cerebellum learns and operates, we would be able to explain more experimental and behavioral data.

1.4 The role of theoretical and computational neuroscience

The role of *theoretical neuroscience* is to distil experimental results into theoretical models of a neural system which correctly predicts new, unknown experimental results. The goal of *computational neuroscience* is to describe the function of neural systems mathematically and carry out computer simulations of these models which reproduce existing experimental results and predict new, untested experimental results. A computational model is "good" when it is as simple as possible, accounts for all of the extant experimental results, and consistently predicts new results. Essentially, the role of these disciplines is to compress the volume of neuroscience facts into the most minimal form and provide experimentalists with avenues for research with a high probability of yielding new insight.

1.5 Summary and Contributions

Chapter 2 introduces background material about cerebellar anatomy, physiology and functional circuitry of the cerebellum which emphasizes the role of the MLIs.

Chapter 3 presents a computational model of the MLI and the network formed by spontaneously active MLIs and Purkinje cells connected according to known anatomy that exhibits activity similar to that observed *in vitro.*

Chapter 4 presents a theory of learning at parallel fiber - MLI synapses and carries out a number of computer simulations which show this model reproduces experimental evidence of plasticity observed *in vitro.*

Chapter 5 extends the work of Chapter 4 and shows that this model of plasticity at parallel fiber - MLI synapses implements a form of learning known as temporal difference learning.

Chapter 6 concludes the dissertation and presents promising opportunities for future research on the molecular layer interneurons.

Chapter 2   Background and Motivation: Anatomy and Physiology of the Cerebellum

This chapter introduces the essential anatomy and physiology of the cerebellum to provide context to our study of the molecular layer interneurons (MLIs). Additionally, this chapter describes the "trail of breadcrumbs" which led to the fundamental research question proposed in this dissertation, "What is the role of the molecular layer interneurons?". While this chapter will briefly review the gross anatomy, microscopic anatomy and physiology, it is no substitute for an excellent introductory textbook chapter on the cerebellum (e.g. Principles of Neural Science, 5th edition).

In the most basic sense, a *neural system* is composed of individual processing units (neurons, glia, etc.) which are connected in some way to influence each other (synapses, gap junctions, etc.) whose state dynamically changes in response to input stimuli. The state of all or some subset of the processing units can then be used as output. E.g. a generic neural system takes sensory information as input and generates motor control signals as output. *Neuroanatomy* is the "blue-print" or "wiring diagram" describing the structure and connectivity of neural systems, and *neurophysiology* is the set of "rules" which govern the state dynamics of the constituents of the neural system (neurons, synapses, etc). Neural systems change their response to the same input stimuli via *learning*, typically by *synaptic plasticity* -- changes in the

efficacy of synapses. The cerebellum is ideal for studying neural systems because its anatomy is relatively simple and well-known (but not exhaustively known), stereotyped throughout the entire cerebellum (Llinas et al., 2004) and conserved across vertebrates (Butler and Hodos, 2005). Further, we know a tremendous amount about cerebellar neurophysiology and are constantly learning more about the synaptic plasticity.
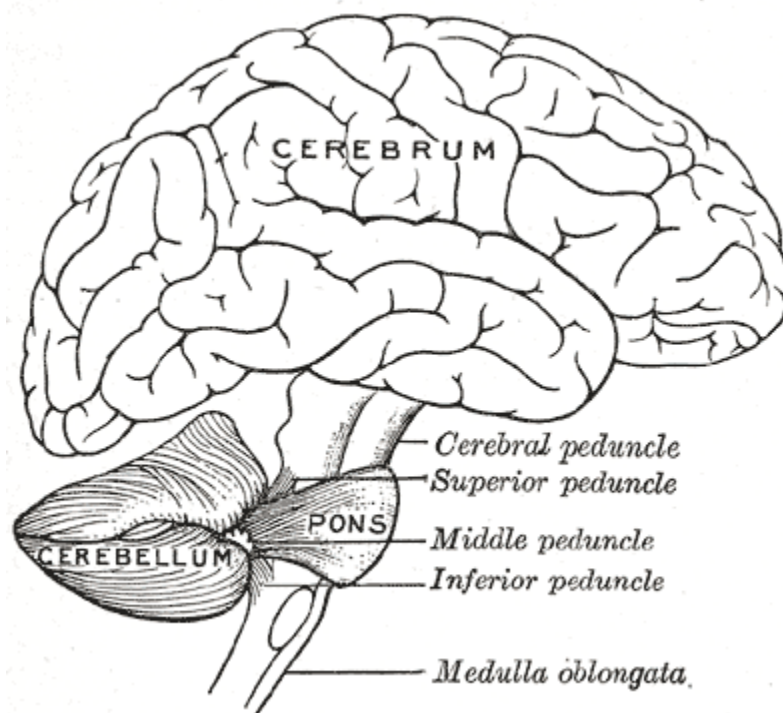
Figure 2.1 The gross anatomy of the human brain with the cerebellum depicted as a foliated structure situated caudal to the cerebrum and posterior to the brain stem. Also denoted are the three fiber pathways to/from the cerebellum -- the superior, middle and inferior peduncles. "Gray677" from Gray's Anatomy. Licensed under Public Domain via Wikimedia Commons.

2.1 Gross Anatomy

The cerebellar cortex is a grossly visible foliated structure composed of two hemispheres (Figure 2.1), while other parts of the cerebellum (discussed below) are embedded in the interior of the cerebellum or reside within the brainstem and require dissection of the neural tissue to observe (Figure 2.2).

One remarkable property about the cerebellum is that the neuronal circuitry is stereotyped throughout the entire cerebellar cortex; that is, the same pattern of connections among neuron types is observed in any part of the cerebellar cortex (described in the next section). Despite this, regions of the cerebellar cortex (and corresponding components in the brain stem) are functionally specialized (Kandel, 2013). E.g. the medial portion, referred to as the spinocerebellum, is involved in body and limb movement, while the lateral portions of the hemispheres known as the cerebrocerebellum appear to be involved in cognitive functions and motor planning. Table 2.1 shows the gross anatomical regions and their connections. There are several other regions which won't be mentioned. Since the anatomy is uniform across regions, the input and output connections determine their function. For the remainder of the dissertation, unless otherwise mentioned, we will consider only the generalized circuitry of the cerebellum to investigate its function. We refer to this a *stereotypical microcircuit.*

Nucleus dentatus   *Superior peduncle*
Corpora quadrigemina

Pons

Inferior olivary nucleus
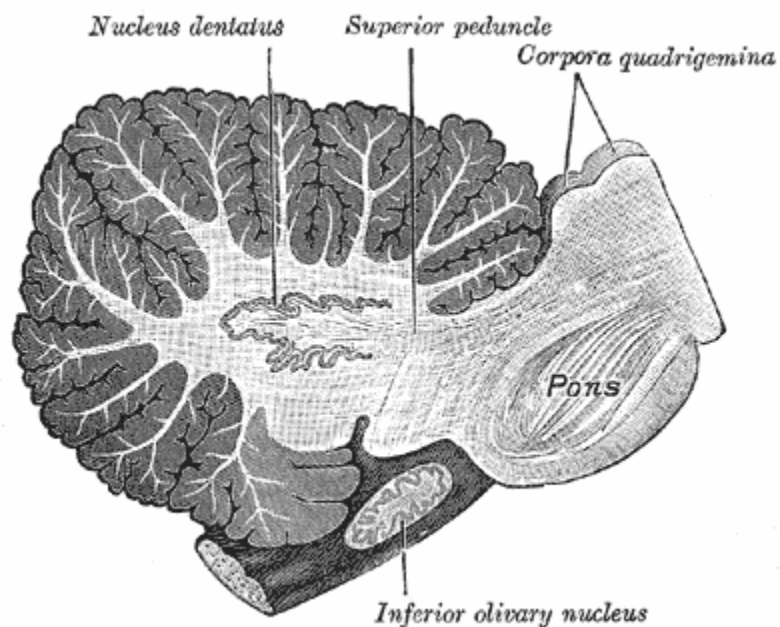
Figure 2.2 A midsagittal section of the cerebellum depicting the components that are not grossly visible including the dentate nucleus and inferior olive. "Gray707". Licensed under Public Domain via Wikimedia Commons.

Table 2.1 Major inputs and outputs to the cerebellum

Functional Subdivision	Inputs	Outputs
Vestibulocerebellum	Semicircular canals, vestibular nuclei, superior colliculus, visual cortex (via pontine nuclei)	vestibular nuclei
Spinocerebellum	spinocerebellar tract,	cerebral cortex, brain stem
Cerebrocerebellum	Cerebral cortex, especially parietal lobe (via pontine nuclei)	primary motor cortex and premotor cortex via ventrolateral thalamus, red nucleus

The cerebellum is composed of three main components: the cerebellar cortex (CC), deep cerebellar nuclei/vestibular nuclei (DCN/VN) and inferior olive (IO) (Figures 2.2 & 2.3). The cortex is the largest structure, being grossly visible without dissection into the neural tissue, situated caudal to the occipital lobe and posterior to the brain stem. The DCN and IO are embedded within the brainstem and only visible upon dissection. Together, these structures form the basic circuit of the cerebellum. Input information (e.g. sensory, cognitive state, etc.) to the cerebellum is distributed to both the CC and DCN/VN via the mossy fibers (MFs). In most cases, this information arrives via the pontine nuclei (PN) located in the pons. In some cases, e.g. vestibular, it arrives directly from the sensory organ (Itō, 1984). Information then flows from CC to DCN/VN via a purely inhibitory projection made up from the axons of a single neuron type -- the Purkinje cell (PKJ). From the DCN/VN information flows to nuclei outside the cerebellum to affect behavior (e.g. motor nuclei controlling eye movements, via thalamus to cerebral cortex, etc.). Information arriving to the IO is relayed to the cerebellar cortex. This information can come directly from sensory systems (e.g. skin receptors, retina, etc.) via the spinal cord and brain stem nuclei (Itō, 1984) or from the cerebral cortex via the red nucleus (Burman et al., 2000). There is also an inhibitory feedback pathway from DCN/VN to IO (Itō, 2012).

Figure 2.3 The circuitry formed by the gross anatomical constituents of the cerebellum. Excitatory connections are depicted with a solid filled circle, inhibitory with an open fill, and mixed with an error.

2.2 Microscopic Anatomy

By some estimates, over half of the neurons in the mammalian brain are found in the cerebellum, largely comprised of neurons with tiny cell bodies called granule cells (GRs) (Williams and Herrup, 1988). GRs will be the starting point for our description of the cerebellar cortex as they are the input stage for information flow into the cerebellar cortex. Mossy fibers (MF) emanating from the pontine nuclei (PN) form intricate synapses onto granule cells in a special arrangement called a *rosette*. MFs and GRs are both excitatory and release glutamate as their neurotransmitter (Itō, 2012).

The cerebellar cortex is a laminar structure composed of three layers: the granule layer (innermost), the Purkinje layer and the molecular layer (outermost). Each layer is named for the principal cell bodies they house but the axons and dendrites of these cells may extend into other layers. Unsurprisingly, the granule layer contains the cell bodies of GRs, in addition to a number of other cell types: Golgi cells (GO), Lugaro cells (LC), and unipolar brush cells (UBC) (Table 2.2). In addition to receiving MF input, GOs also receive significant input from GRs, and in turn provide inhibitory

inputs to GRs. The functional significance of this GR-GO circuit is discussed in a later section.

Table 2.2 Summary of neuronal constituents of the cerebellar cortex and their connections.

Neuron type	Synapse polarity	Cell Body Location	Main Inputs	Main targets
Granule cell (GR)	Excitatory	Granular Layer	MF	GO, MLI, PKJ
Golgi cell (GO)	Inhibitory	Granular Layer	GR, MF	GR
Unipolar Brush Cell (UBC)	Excitatory	Granular Layer	MF	GR, UBC
Lugaro cell	Inhibitory	Granular Layer	PKJ	MLI, GO
Molecular Layer Interneuron (MLI)	Inhibitory	Molecular Layer	PF	MLI, PKJ
Purkinje cell (PKJ)	Inhibitory	Purkinje Layer	PF, MLI	MLI, DCN

The Purkinje layer exclusively houses the cell bodies of Purkinje cells (PKJs) while the PKJ dendrites extend into the molecular layer and form a remarkable and extensive two-dimensional planar dendritic arborization (Figure 2.4). The GRs give rise to axons that extend upwards toward the molecular layer, forming synapses onto the PKJs along the way, and then branch in two directions forming a "T" passing through the 2D PKJ dendrites in an orthogonal orientation forming *en passant* synapses (Figure 2.5). These branched axons are known as parallel fibers (PFs). While individual PFs make only a few synapses onto a single PKJ, because the GRs are so numerous, PKJs receive may receive up to 200,000 PF-PKJ synapses in human (Llinas et al., 2004). However, only a fraction (~15%) of these synapses are electrically

active resulting in an effective number of synapses on the order tens of thousands (Isope and Barbour, 2002).
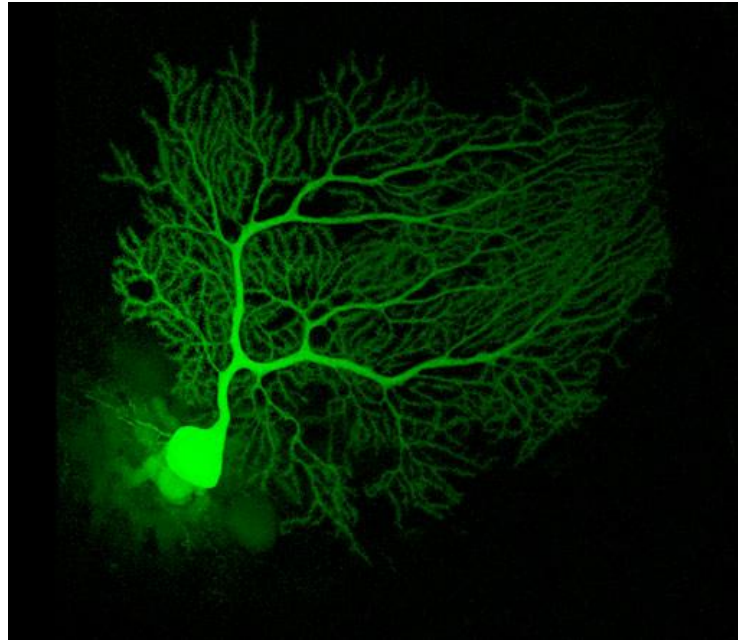
Figure 2.4 A Purkinje cell injected with a fluorescent dye. The exquisite dendritic arborization extends into a nearly two dimensional plane. "3 recon 512x512" by Project leader: Maryann Martone. Experimenters: Andrea Thor & Diana Price - Cell Centered Database, National Center for Microscopy and Imaging Research, University of California. Microscopy product ID: 3Image basename: e1cb4a5. Licensed under CC BY 3.0 via Wikimedia Commons.

The molecular layer is home to the cell bodies of basket cells (BC) and stellate cells (SC). Historically, these neurons have been classified as two distinct neuron types but more recent anatomical and physiological evidence suggests they are a single neuron type with morphological variation along a spectrum (Sultan and Bower, 1998;Ruigrok et al., 2011;Chu et al., 2012). Collectively they are referred to as the molecular layer interneurons (MLIs). BCs were named so because they were found in the lower molecular layer and their axons form dense basket-like structures around the PKJ cell bodies

forming many synapses (Palay and Chan-Palay, 1974). Like basket-type cells, stellate-type cells' dendrites span the molecular layer and receive input from PFs and other MLIs, however they're typically found in the outer ⅔ of the molecular layer and their prototypical axonal input to PKJs are onto the PKJ dendrites. It's now known that stellate-type MLIs can also from basket-type synapses onto PKJs (Jorntell and Ekerot, 2003). MLIs are inhibitory neurons and form a vast network through inhibitory synapses with other MLIs and PKJs (Rieubland et al., 2014). In addition, MLIs are connected via gap junctions, a type of electrical synapse. While PKJ axons are the sole output of the cerebellar cortex, targeting the DCN/VN, they also provide recurrent collaterals to MLIs in the lower molecular layer (typically basket-type MLIs) (Chan-Palay, 1971). PKJs also provide inhibitory recurrent inputs to other PKJs during development, but apparently not in adult animals (Watt et al., 2009), suggesting there is some developmental process which utilizes these connections.

The second and last source of input to the cerebellar cortex (the other being mossy fibers) is the CF -- the axon originating from cell bodies located in the IO. The climbing fiber wraps itself around PKJs like a vine and forms numerous synapses onto the PKJ having a powerful excitatory effect on the PKJ when active (Itō, 2012). Each PKJ receives only one CF but each neuron in the IO can form up to 10 CFs, i.e. 10:1 divergence (Llinas et al., 2004). The CF also has an excitatory effect onto MLIs but through a different means of transmission. CFs do not make direct synapses onto MLIs but instead excite them through *spillover transmission*, i.e. neurotransmitter released from CFs spills over from the release site to places where AMPA and NMDA receptors

are located (Szapiro and Barbour, 2007). As a result, CF-MLI excitation has a volume effect and is less specific than CF-PKJ input. In contrast to PKJs, MLIs can be excited by multiple CFs. The termination zone of CF inputs into the cerebellar cortex is perpendicular to the span of parallel fibers (Llinas et al., 2004).

Figure 2.5 A depiction of cerebellar circuitry composed of the major neuronal constituents. Here, mf (MF), cf (CF), GrC (GR), Goc (GO), pf (PF), , PC (PKJ), DCN-C (DCN/VN), IO-C (IO). Reproduced under the Creative Commons License from (D'Angelo and Casali, 2012).

2.3 Specific Physiology

There are an immense number of physiological details known about the cerebellum, of which entire textbooks are devoted. Only the most pertinent

facts to understanding the functional perspective and results presented in Chapters 3-5 will be presented here.

Beginning with the input layer of the cerebellar cortex, GRs are only sparsely active, firing spontaneously at ˜1 Hz, but fire high frequency bursts of up to several hundred hertz when active (Chadderton et al., 2004;van Beugen et al., 2013). This low level of GR activity is mediated by a blanket of GO inhibition. Thus, converging MF input to GRs must be sufficiently strong and synchronized to surpass a threshold and then GRs are highly excited. This results in a spatiotemporally sparse coding of the sensory input among GRs.

PKJs fire spontaneously at rates of about 50 Hz while an animal is at rest (Armstrong and Edgley, 1984). Surprisingly, this spontaneously firing is not due to the immense number of PF inputs, but is an intrinsic mechanism to the PKJ (Hausser and Clark, 1997;Raman and Bean, 1999); that is, when all excitatory and inhibitory inputs to PKJs are removed, PKJs continue to fire spontaneously. MLIs also fire spontaneously at rates of about 15-30 Hz (Hausser and Clark, 1997). The activity of both MLIs and PKJs is increased by excitatory inputs from PFs and CFs. Likewise, MLI and PKJ activity is decreased by MLI inhibitory inputs (Park et al., 2012). Finally, climbing fibers fire at a low irregular rate ˜1 Hz (Itō, 2012).

2.4 Synaptic plasticity

Synaptic plasticity refers to learning-related changes in the efficacy of synapses. Effectively, this translates to the ability of a pre-synaptic neuron to influence the membrane potential or action potential firing probability of a post-synaptic neuron. Synaptic plasticity in the cerebellar cortex takes place both pre-synaptically and post-synaptically through a variety of mechanisms

and at both excitatory and inhibitory synapse types (Gao et al., 2012). In particular, PF-MLI, PF-PKJ and MLI-PKJ synapses have been shown to undergo plasticity, in addition to others.

The most studied locus of learning and memory in the cerebellar cortex is the PF-PKJ synapse. Plasticity at this synapse was hypothesized in purely theoretical models of cerebellar function by David Marr and James Albus and later confirmed experimentally by Masao Ito (Itō, 2012). The basic "learning rule" is that long-term potentiation (LTP) at this synapse occurs when PFs fire alone while long-term depression (LTD) occurs when PFs fire at nearly the same time as CFs impinging onto the same PKJ. The latter is termed "conjunctive LTD". Thus, CFs act as a "teaching" signal which reduce the efficacy of PF-PKJ synapses presenting a stimulus pattern at the time of CF activation. This led to the idea that PKJs can reduce their activity in response to a learned stimulus in order to disinhibit the DCN/VN to elicit movement. Most models used this as the primary mechanism for learning and memory. However, PKJs have been shown to fire spontaneously in absence of all synaptic inputs (Hausser and Clark, 1997), so simply decreasing the efficacy of PF-PKJ synapses does not account for the pauses of PKJ activity seen in learned behaviors (Jirenhed et al., 2007).

Feedforward inhibition from MLIs is one mechanism for reducing PKJ activity, and this feedforward inhibition can be learned by synaptic plasticity at PF-MLI and MLI-PKJ synapses (Gao et al., 2012). *In vivo* experiments showing PF-MLI receptive field changes with CF stimulation suggest a complementary and synergist learning rule to conjunctive LTD at PF-PKJ synapses (Jorntell and Ekerot, 2002;2003;2011). Namely, conjunctive PF and CF activation results in PF-MLI LTP while PF activation alone leads to LTD.

However, this learning rule does not account for PF-MLI LTP in absence of CF input observed *in vitro* (Rancillac and Crepel, 2004;Smith and Otis, 2005). A theoretical model of learning at PF-MLI synapses is proposed in Chapter 4 and the experimental results are reviewed and discussed extensively.

2.5 Functional Circuitry

Here, a mental model of the functional components of the cerebellum is presented by abstracting away from individual neurons to form *functional circuits* composed of one or more neuron types. In reality, this is only a cartoon of the functional elements of the cerebellum that does not account for some neuron types and the three-dimensional geometry of actual cerebellar neuroanatomy. Nonetheless, it is useful as a model for thinking about cerebellar computation.

The cerebellar cortex can be roughly divided into two functional circuits: the GR-GO loop (blue circuit in Figure 2.6) and PKJ-MLI network (red circuit). The sole output of the cerebellar cortex -- the PKJ axons -- targets the DCN/VN (purple circuit). Two inputs to the cerebellum are present and target the cortex and DCN/VN: the MFs (black), largely from the pontine nuclei, and CFs (green) arising from the inferior olive The MFs carry the organism's state information (i.e. sensory information, motor control signals, cognitive processes, etc.) to the cerebellum and the CFs carry motor and cognitive control "error" information. This error signal induces synaptic plasticity at synapses in the red circuit to modify the MLI-PKJ response to the state information towards a response that results in no error.
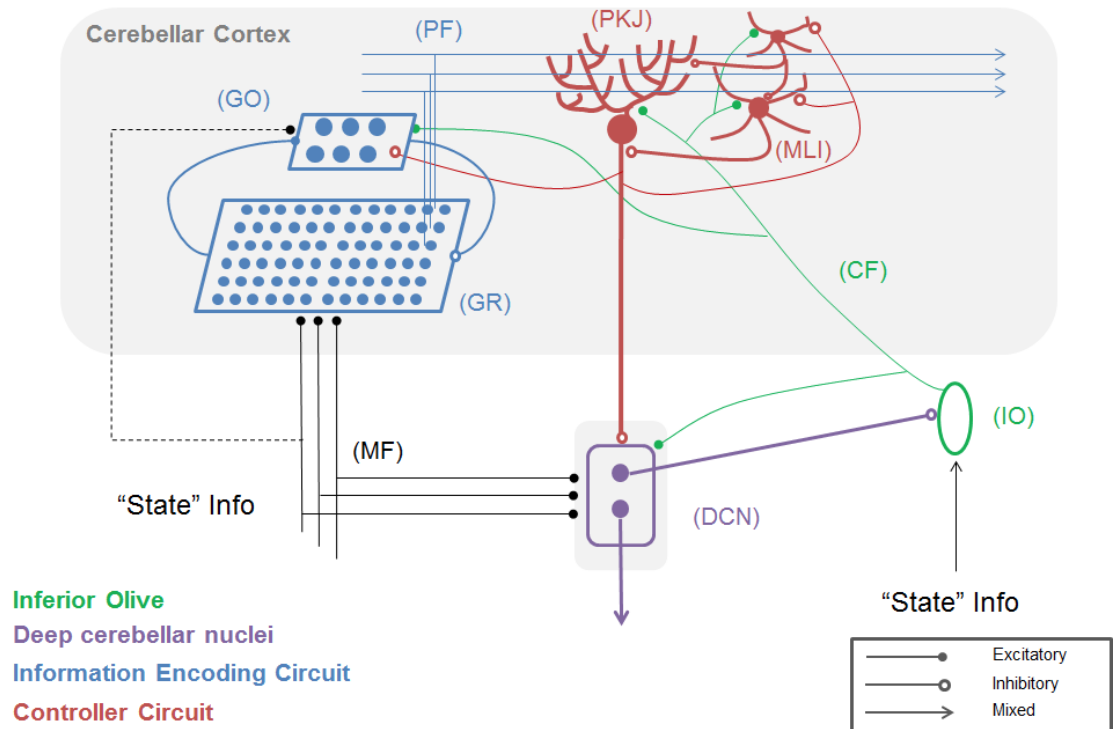
Figure 2.6 Functional circuitry of the cerebellum. Several circuit components are depicted: GR-GO circuit (blue), MLI-PKJ circuit (red), DCN (purple), IO (green), MF (black).

Several groups have proposed that the GR-GO loop (blue circuit) is involved in encoding state information conveyed by the MFs in a usable form by the downstream circuit, by forming sparse, distributed, and temporally evolving representations of state information (Marr, 1969;Buonomano and Mauk, 1994;Yamazaki and Tanaka, 2005). The representation formed by a set of GRs switching their activity on and off asynchronously over some period of time in response to an input stimulus can be thought of as forming a reproducible *temporal barcode* of that stimulus. Yamazaki and Nagao (2012) propose a computational model of this circuit that can encode spatiotemporal information for both gain and timing control. Thus the blue circuit can be considered as a spatiotemporal feature encoding component of the cerebellum,

providing the red circuit with state information encoded in a suitable form. Although not depicted, unipolar brush cells also likely participate in this circuit to achieve this function.

The function of the red circuit is to use the encoded state information provided by the PFs to modulate the activity of the DCN -- the final output nuclei of the cerebellum -- to achieve the accurate, coordinated and well-timed orchestration of movement and thought (e.g. to achieve a calibrated vestibulo-ocular reflex while wearing corrective lenses, etc.). Since PKJs are the sole output of the cerebellar cortex, the success of the behavior hinges on the appropriate spatiotemporal pattern of PKJ activity to contribute to the appropriate DCN response, which in turn affects the response of the target of the DCN. In effect, this amounts to learning the appropriate *gain* (spatio-) and *timing* (temporal) of PKJ inhibition onto the neurons of the DCN. Since PKJs are spontaneously active at about 50 Hz their activity can either increase or decrease the amount of inhibition onto the DCN. A decrease in inhibition is also referred to as *disinhibition*. The simplest way of increasing PKJ inhibition onto DCN targets is for PF inputs to excite the PKJ, and the clearest way of disinhibition PKJ targets is by MLIs inhibiting PKJs.

A popular theory is that CFs provide a supervised error learning signal to the cerebellar cortex that acts to selectively modify synaptic strengths to change the input-output response that does not generate error signals (Doya, 1999). More generally, the CFs can be considered to encode an error signal in the context of the organism's world (sensory or cognitive environment) in response to the presence or absence of a behavior, as in the case of a reinforcement learning signal (Swain et al., 2011). This synaptic modification guides the stimulus-response pattern of the PKJ-MLI circuit towards a

reduction in the error signal and thus a successful behavior. In some cases, these error signals appear to be hard-wired as in the retinal slip signal of the VOR (Itō, 1984). In other cases, these signals may be more dynamic, such as the signals conveyed to the IO from the cerebral cortex (Habas et al., 2010). For completeness, an alternative theory views CFs as conveying timing signals for the execution of behaviors (Llinas, 2011).

Learning also occurs at synapses in the DCN (Zheng and Raman, 2010) and theoretical models support the idea that motor learning memories are consolidated here (Yamazaki et al., 2015).

The focus of the work presented in Chapters 3-5 is how the MLI-PKJ (red) circuit learns to operate on the state information to effectively modulate the activity of the DCN for the adaptive control of movement in the presence of feedback error signals from the CFs.

2.6 Functional Role of MLIs

The hypothesis that motivated the work presented in this dissertation is that the functional role of MLIs is the precise control of PKJ disinhibition of the deep cerebellar nuclei (DCN) and that PF-MLI, MLI-MLI, and MLI-PKJ synapses are important locations of learning and memory for adaptive control. This is supported by recent optogenetic experiments allowing precise control of MLI firing *in vivo* that shows MLI activity can directly control movement kinematics (Heiney et al., 2014).

The role of MLI feedforward inhibition can most clearly be seen in the conditioned eyeblink response in animals, a type of Pavlovian response where the animal learns to blink its eye in response to a conditioned stimulus (CS) to avoid an aversive unconditioned stimulus (CS). In the naive animal, recordings

from PKJs in the part of the cerebellum responsible for generating eyeblink control signals fire spontaneously at about 50 Hz throughout the presentation of the CS (Jirenhed et al., 2007). After training and the acquisition of an appropriately timed eyeblink, the PKJs exhibit a strong pause in the firing activity. Since the PKJ spontaneous firing is intrinsic to the PKJ and not due to the total PF synaptic input, this pause is likely due to MLI feedforward inhibition.

The role of MLI inhibition can also be seen in the vestibulo-ocular reflex (VOR) of animals by local application of chemical blockers of GABA (Miyashita and Nagao, 1984). During application, the amplitude of PKJ firing during VOR is increased and the phase is shifted by 180 degrees due to block of feedforward inhibition.

Following the detailed investigation of the anatomy and physiology of the cerebellum (Eccles et al., 1967), the first theories of cerebellar learning emerged (Grossberg, 1969;Marr, 1969;Albus, 1971). Albus hypothesized that long-term depression (LTD) at the PF-PKJ synapses would be sufficient to modify cerebellar output in response to some stimulus pattern and error signal. Following experimental verification of LTD at these synapses (Ito, 1982), PF-PKJ LTD became the dominant mechanism of learning in cerebellar learning theory. This theory, that LTD (i.e. a weakening of synaptic efficacy) at the PF-PKJ synapses driven by concomitant activation of CFs and PFs is the principal form of learning in the cerebellar cortex has dominated for the last 30 years. Recent evidence suggests that targeted blocking of LTD at these synapses does not yield remarkable motor deficits in animal models (Schonewille et al., 2011). Moreover, blocking long-term potentiation (LTP) (i.e. a strengthening of synaptic efficacy) at PF-PKJ synapses or removing

plasticity at molecular layer interneurons (MLIs) (PF-MLI and MLI-PKJ together) results in profound motor deficits in animal models (Gao et al., 2012). Either LTD at PF-PKJ synapses is not the principal form of learning in the cerebellar cortex, or its loss is compensated for by other mechanisms of plasticity (e.g. plasticity at MLIs), or it is some combination of the two.

Chapter 3   A spiking network model of cerebellar Purkinje cells and molecular layer interneurons exhibiting irregular firing

While the anatomy of the cerebellar microcircuit is well studied, how it implements cerebellar function is not understood. A number of models have been proposed to describe this mechanism but few emphasize the role of the vast network Purkinje cells (PKJs) form with the molecular layer interneurons (MLIs) − the stellate and basket cells. We propose a model of the MLI-PKJ network composed of simple spiking neurons incorporating the major anatomical and physiological features. In computer simulations, the model reproduces the irregular firing patterns observed in PKJs and MLIs *in vitro* and a shift toward faster, more regular firing patterns when inhibitory synaptic currents are blocked. In the model, the time between PKJ spikes is shown to be proportional to the amount of feedforward inhibition from an MLI on average. The two key elements of the model are: (1) spontaneously active PKJs and MLIs due to an endogenous depolarizing current, and (2) adherence to known anatomical connectivity along a parasagittal strip of cerebellar cortex. We propose this model to extend previous spiking network models of the cerebellum and for further computational investigation into the role of irregular firing and MLIs in cerebellar learning and function.

3.1 Introduction

The cerebellum is thought to be involved in producing smooth and coordinated movements which are both spatially and temporally precise. How the cerebellum achieves this is not understood. One approach to elucidate this mechanism is to construct a model from known anatomy and physiology to explain how the constituent neurons compute the function implemented by the cerebellum. Numerous theoretical and computational models have been proposed (Grossberg, 1969;Marr, 1969;Albus, 1971;Fujita, 1982;Medina et al., 2000;Dean et al., 2010;Yamazaki and Nagao, 2012), however few of these models emphasize the functional role of the molecular layer interneurons (MLIs). Typically, these inhibitory interneurons are described as providing "global inhibition" or "sculpting" the overall response of the Purkinje cells (PKJs); however, recent experimental evidence questions this hypothesis (Bower, 2010;Jorntell et al., 2010). We seek to understand the role of the MLIs in concert with the PKJs which they form a vast network with by means of computational modeling.

A key feature of the network of MLIs and PKJs is that these neurons fire spontaneously in absence of excitatory synaptic input (Hausser and Clark, 1997;Raman and Bean, 1997). When inhibitory synaptic currents are blocked *in vitro*, MLIs and PKJs fire regularly (Hausser and Clark, 1997). In the presence of inhibitory synaptic currents, they exhibit relatively irregular firing. Understanding how PKJ spontaneous activity is modified to control their targets in the deep cerebellar nuclei and vestibular nuclei (DCN/VN) is central to understanding the operation of the cerebellar cortex. In conditioned eye blink response (CER) learning, PKJs learn to make an appropriately timed

pause in firing in response to a conditioned stimulus, which in turn disinhibits their DCN targets and elicits an eye blink (Jirenhed et al., 2007). Since PKJs are spontaneously active and blocking excitatory synaptic inputs to PKJs only modestly decreases the spontaneous PKJ activity *in vivo* (Cerminara and Rawson, 2004) and *in vitro* (Hausser and Clark, 1997), a decrease in efficacy at parallel fiber (PF) to PKJ synapses is insufficient to explain the learned pause in PKJ activity. Feedforward inhibition provided by MLIs may be one mechanism to produce this pause. Furthermore, using an optogenetic technique to increase the firing rates of a target population of MLIs in awake mice, movements can be elicited and kinematics controlled by varying the photostimulation parameters (Heiney et al., 2014). Finally, in mutant mice lacking PKJ gamma-aminobutyric acid A ($GABA_A$) receptors, effectively removing MLI feedforward inhibition, motor learning deficits are observed (Wulff et al., 2009). The accumulating evidence points to a greater functional role for MLIs than previous theories suggest.

In this study we construct a spiking network model of spontaneously active MLIs and PKJs composed of leaky integrate-and-fire neuron models connected according to known anatomy. We show that despite using simple neuron models, this network reproduces the irregular ISIs observed in PKJs and MLIs *in vitro*. We further show that the relative contribution of MLI-MLI feedback inhibition to produce irregular firing in MLIs is greater than the PKJ-MLI feedback inhibition contribution. Finally, this model provides a substrate for additional experiments investigating the functional role of irregular firing patterns and MLIs in cerebellar learning and function.

3.2 Materials and methods

3.2.1 Network Model

The network is composed of PKJs and MLIs and is modeled after a 1 mm x 32 μm microzone of the cerebellar cortex with the long axis extending parasagittally. In cats, 330 PKJs are contained within a 1 mm^2 sheet of cerebellar cortex arranged in a grid-like arrangement (Palkovits et al., 1971). We therefore modeled 16 PKJs along a one dimensional grid with an even 64 μm spacing between cell body centers and assume PKJ cell bodies are 32 μm in diameter. The network includes 160 MLIs in accordance with the anatomical data of a 10:1 ratio of MLIs to PKJs (Korbo et al., 1993). Thus, each PKJ has 10 nearest MLIs; three are designated as lower molecular layer interneurons and are eligible to receive PKJ recurrent collaterals (described below). Figure 3.1 illustrates the network and basic connectivity. Synapse formation in the network is probabilistic subject to the anatomical constraints described next.
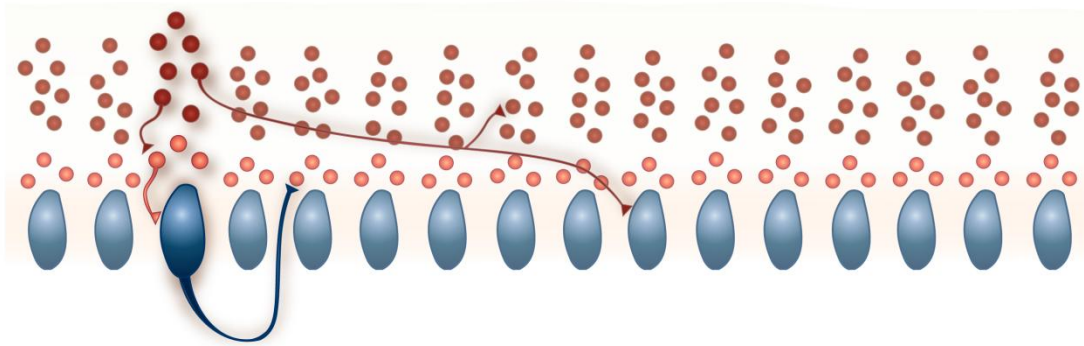
Figure 3.1 A schematic of the model network. 160 MLIs (red) and 16 PKJs (blue) were simulated. Each PKJ has 10 corresponding MLIs that are closest to it along the long axis. Of the 10 closest, three are eligible to receive PKJ recurrent collaterals (shown in a lighter shade of red) and seven are ineligible to receive PKJ recurrent collaterals (shown in a darker shade of red). Examples of allowed connections are shown. All synapses are inhibitory. Further details on the network connectivity are described in the Methods section.

In vivo, PKJ recurrent collaterals extend parasagittally and can span more than 200 μm, appearing to contact both PKJs and MLIs in the lower molecular layer (Chan-Palay, 1971;Hawkes and Leclerc, 1989;O'Donoghue et al., 1989;Apps and Hawkes, 2009). (Watt et al., 2009) showed PKJ recurrent collaterals extend asymmetrically and predominantly terminate within 100 μm of the parent cell soma but do not make functional synapses onto PKJs after post-natal day 21. To model this, PKJs in our network model extend their recurrent collaterals asymmetrically in the vicinity of the two nearest PKJs and can form synapses onto MLIs in the lower molecular layer, i.e. the first three of ten MLIs corresponding to a particular PKJ. We chose a probability of forming a PKJ-MLI synapse such that, on average, each eligible MLI receives one PKJ input and each PKJ forms synapses onto three MLIs. Table 3.1 summarizes these convergence and divergence values. We assume the model network belongs to an adult animal and do not allow PKJ to PKJ connections.

In vivo, MLI axons extend parasagittally and terminate up to 500 μm away from the parent soma, contacting both PKJs and other MLIs (Itō, 1984). In the model, we assume MLI axons extend asymmetrically and span a distance of eight PKJs. Each MLI axon branches in one direction or the other determined randomly with equal probability; i.e. an MLI can form synapses with MLIs and PKJs either to its left or to its right, but not both directions. We chose a probability of forming MLI-PKJ synapses such that, on average, 20 MLIs formed synapses onto one PKJ, consistent with the anatomical data (Eccles et al., 1967;Palay and Chan-Palay, 1974). Synapse formation is determined by iterating through the list of candidate target neurons for a

source neuron and randomly drawing a value from *Unif(0,1)* ; if the drawn value is less than some chosen probability, then a synapse is formed. Thus, all target neurons within the axon span had an equal probability of forming a synapse whereas those neurons outside this distance had zero probability of forming synapses. We also chose a probability of forming MLI-MLI synapses such that, on average, each MLI received inputs from four other MLIs, consistent with physiological data (Hausser and Clark, 1997;Kondo and Marty, 1998). While gap junctions between MLIs are known to exist (Mann-Metzer and Yarom, 1999), we chose to model only chemical synapses as a first approximation to this network.

Peak inhibitory post synaptic conductances (IPSCs) for each neuron type are summarized in Table 3.1. These peak IPSCs are multiplied by synaptic weights, specific to each synapse (Eq. 2). Synaptic weights are drawn from a random distribution to simulate the diversity of synaptic conductances up to the peak conductance as observed *in vitro,* e.g. (Kondo and Marty, 1998). MLI-MLI synapse weights are drawn from a uniform distribution between 0 and 1, i.e. $w_{MLI \to MLI}$ ~ *Unif(0,1)* ; also, $w_{MLI \to PKJ}$ ~ *Unif(0,1.2 5)* and $w_{PKJ \to MLI}$ ~ *Unif(0,1)* .

3.2.2 Neuron Model

Neurons are modeled as conductance-based leaky integrate-and-fire units (Gerstner and Kistler, 2002). The membrane potential, $V(t)$, is governed by Eq.(1), where C is the membrane capacitance, g_{leak} is a constant leak conductance, $g_{ahp}(t)$ is an after-hyperpolarization (AHP) conductance

(described by Eq.(4)), $g_{GABA}(t)$ is the inhibitory GABA conductance and $I_{spont}(t)$ is a spontaneous depolarizing current (described below). E_{leak}, E_{ahp}, E_{GABA} are the respective reversal potentials. Table 3.1 summarizes the physiological values used in the neuron models derived from the literature. The model did not include any excitatory synaptic conductances.

$$C\frac{dV}{dt} = -g_{leak}(V(t) - E_{leak}) - g_{ahp}(t)(V(t) - E_{ahp}) - g_{GABA}(t)(V(t) - E_{GABA}) + I_{spont}(t) \qquad (3.1)$$

The total synaptic conductance is described by Eq.(2), where $\bar{g}_{GABA}$ is the maximum synaptic conductance, w_i is the weight of the ith synapse, $\alpha(t)$ is the conductance kinetics function described by Eq.(3), and $\delta_i(t)$ is a Dirac delta function for the ith synapse onto a target neuron, indicating whether the presynaptic neuron has spiked at time t. τ_{GABA} is the inhibitory conductance time constant.

$$g_{GABA}(t) = \bar{g}_{GABA}\sum_i w_i \int_{-\infty}^{t} \alpha(t-s)\delta_i(s)ds \qquad (3.2)$$

$$\alpha(t) = \exp(-t/\tau_{GABA}) \qquad (3.3)$$

When the membrane potential for the neuron model surpasses $V_{threshold}$, the neuron emits a spike and an AHP conductance is triggered. The AHP is described by Eq.(4), where t_{spiked} is the time the neuron last spiked and τ_{ahp} is a time constant.

$$g_{ahp}(t - t_{spiked}) = \exp(\frac{-(t - t_{spiked})}{\tau_{ahp}}) \qquad (3.4)$$

The spontaneous firing activity of MLIs and PKJs has been shown to be an intrinsic neuron property and not driven by the background activity of parallel fibers (Hausser and Clark, 1997). In PKJs, the spontaneous firing is primarily mediated by tetrodotoxin (TTX) sensitive sodium channels which produce a sub-threshold depolarizing current (Raman and Bean, 1999). While the mechanism for this endogenous current in MLIs is not well studied, MLIs presumably share a similar mechanism to PKJs since blocking TTX-sensitive sodium channels abolishes this sub-threshold depolarizing response in MLIs (Midtgaard, 1992). To model this spontaneous activity of MLIs and PKJs, we inject a random depolarizing current drawn from a gamma distribution, $I_{spont}(t) \sim \Gamma(\kappa, \beta)$ (in units of nA), every time step of the simulation. A gamma distribution was chosen since its support is strictly non-negative and has flexible shape and scale (controlled by κ and β, respectively). We performed a grid search over κ and β for MLIs and PKJs separately to find the parameters which resulted in the neuron model reproducing the mean firing rate and inter-spike interval coefficient of variation (CV) that was close to the example data reported in (Hausser and Clark, 1997) in the presence of GABA blockers. Table 3.1 summarizes gamma distribution parameters for each neuron type. Figures 3.2&3.3 A-C show the resulting neuron model activity when neurons are isolated, i.e. no synaptic inputs are present.

Table 3.1 A summary of the neuron model and network parameters. PKJ, Purkinje cell (De Schutter and Bower, 1994a;Puia et al., 1994); MLI, molecular layer interneuron (Midtgaard, 1992;Hausser and Clark, 1997;Kondo and Marty, 1998;Lachamp et al., 2009). −, nonexistent. Convergence and divergence values are averages since the network is constructed randomly subject to anatomical constraints. *, Convergence was calculated on average for the entire population of MLIs, despite PKJ-MLI synapses only being made on the lower molecular layer interneurons.

	Neuron Type	
Cell parameters	PKJ	MLI
$V_{threshold}$ (mV)	-55.0	-53.0
C (pF)	107.0	14.6
$\bar{g}_{leak}$ (nS)	2.32	1.6
E_{leak} (mV)	-68.0	-68.0
$\bar{g}_{GABA}$ (nS)	1.0	4.0
E_{GABA} (mV)	-75.0	-82.0
τ_{GABA} (msec)	10.0	4.6
$\bar{g}_{AHP}$ (nS)	100.0	50.0
E_{AHP} (mV)	-70.0	-82.0
τ_{AHP} (msec)	2.5	2.5
κ	0.430303	3.966333
β	0.195962	0.006653
MLI convergence	20	4
PKJ convergence	--	.3*
MLI divergence	2	4
PKJ divergence	--	3

We used the PKJ model parameters from (Yamazaki and Nagao, 2012) but replaced the constant spontaneous current with one drawn from a gamma distribution. A single neuron model for basket and stellate cells was derived from physiological data reported in the literature (Table 3.1). Anatomical and physiological evidence suggests that basket and stellate cells belong to one homogenous group of interneurons whose properties vary smoothly by depth of the soma in the molecular layer (Sultan and Bower, 1998;Ruigrok et al., 2011;Chu et al., 2012) and which share common receptive field properties (Jorntell and Ekerot, 2003). Since PKJs and MLIs are modeled as single

compartment neuron models, we combine the effects of stellate-type synapses onto the PKJ dendrites with basket-type synapses onto the PKJ somas (Eccles et al., 1967;Palay and Chan-Palay, 1974) by modeling a single idealized MLI that makes synapses of one type onto the model PKJ.

3.2.3 Software & Data Analysis

Simulations were performed using BRIAN Simulator, a Python library for spiking neural network simulations (Goodman and Brette, 2009). Simulations were carried out using Euler's method for temporal integration with a time step of 0.25 ms for numerical stability. Data analysis and plotting were performed using BRIAN Simulator, SciPy, Matplotlib, Plotly and custom software written in Python. The source code for these experiments will be made freely available online.

Artificial action potential (AP) waveforms were drawn for Figures 3.2A,D; 3.3A,D; 3.5A,B. For Figures 3.2 and 3.3, a value of 0 mV was inserted when the spike occurred. For Figure 5, these waveforms were a hand-crafted series of six values at 0.25 ms intervals for a total AP waveform length of 1.5 ms. Exact values can be found in the published code. Mean, variances and coefficient of variations were computed assuming a normal distribution in all cases to make the values comparable to (Hausser and Clark, 1997).

3.3 Results

3.3.1 Model PKJs and MLIs in isolation exhibit regular firing

First, we examined the spike patterns of isolated MLI and PKJ neuron models (no synaptic currents) with spontaneous depolarizing currents. The

top rows of Figures 3.2 and 3.3 show the response of a model MLI and PKJ, respectively, under these conditions. The random current was sufficient to drive the neuron past threshold potential to fire spontaneously (Figures 3.2, 3.3A). A histogram of the inter-spike intervals (ISIs) reveals the degree of regularity of firing by the average baseline firing rate of the neuron and variability in timing between spike pairs (Figures 3.2, 3.3B). These results are consistent with MLIs and PKJs recorded *in vitro* when GABAergic transmission has been blocked chemically (Hausser and Clark, 1997). The model PKJ produced a mean firing rate of 38.9 Hz and an ISI coefficient of variation (CV) of 0.17 compared to 40 Hz and 0.18, respectively, for an exemplar neuron *in vitro* (Hausser and Clark, 1997). The model MLI produced a mean firing rate of 29.1 Hz and an ISI CV of 0.14 compared to 30 Hz and 0.14, respectively, for an exemplar neuron *in vitro* (Hausser and Clark, 1997). The model MLI appeared slightly more skewed towards longer ISIs compared to the *in vitro* data, possibly due to longer recording times of 300 seconds in our experiments. While the model PKJ ISI histogram appeared symmetric, it failed a test of normality (Shapiro-Wilk test, $p<10^{-12}$) as did the MLI ISI histogram (Shapiro-Wilk test, $p<10^{-38}$). Tests of normality were not reported by (Hausser and Clark, 1997), though the authors noted Gaussian-shaped ISI histograms. A spike autocorrelogram revealed regularity in trains of successive spikes with several peaks at integer multiples of the baseline frequency (Figures 3.2, 3.3C). These results suggest that a simple neuron model with a spontaneous random current is capable of reproducing similar spike timing phenomena as observed *in vitro* under conditions of GABAergic transmission block.
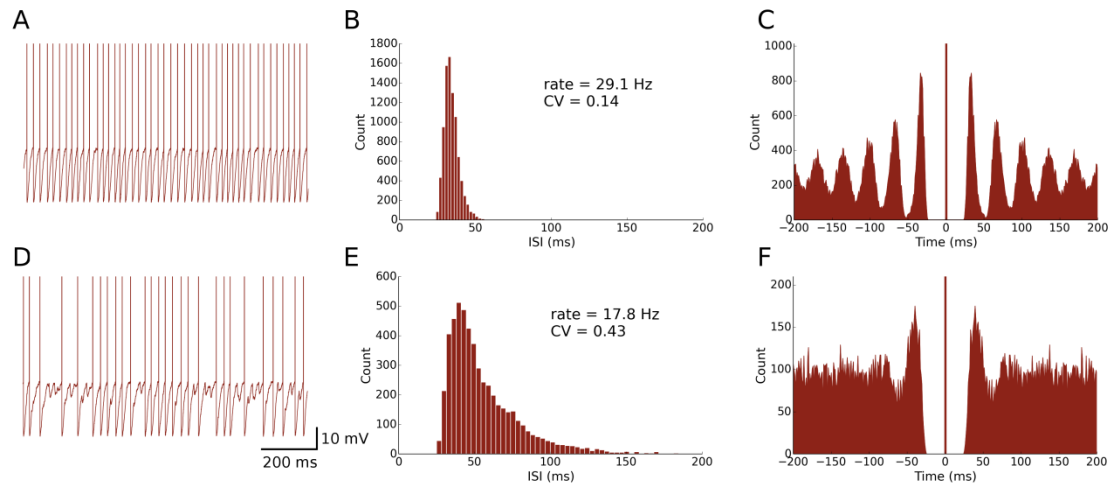
Figure 3.2 Spontaneously active MLI neuron models reproduce similar firing patterns as observed *in vitro.* A.) Trace of an isolated MLI membrane potential with spikes artificially drawn. The neuron appears to fire regularly in absence of inhibitory synaptic currents. B.) Inter-spike interval (ISI) histogram of the isolated MLI. The parameters for the gamma distribution governing the random depolarizing current injected into the neuron were chosen such that the mean firing rate and ISI coefficient of variation (CV) were similar to the example neuron shown in Häusser and Clark (1997). All simulations were run for 300 seconds. C.) A spike autocorrelogram of the isolated MLI showing regularity in trains of spikes. D.) Membrane potential trace of one MLI selected from the intact network of MLIs and PKJs where inhibitory synaptic currents a present. From the trace, the neuron visibly fires irregularly compared to the isolated case. E.) An inter-spike interval histogram of the same MLI. The distribution shifts rightward and becomes broader, suggesting a slower and more irregular firing pattern. F.) A spike autocorrelogram of the same MLI showing the regularity in spike trains has disappeared.
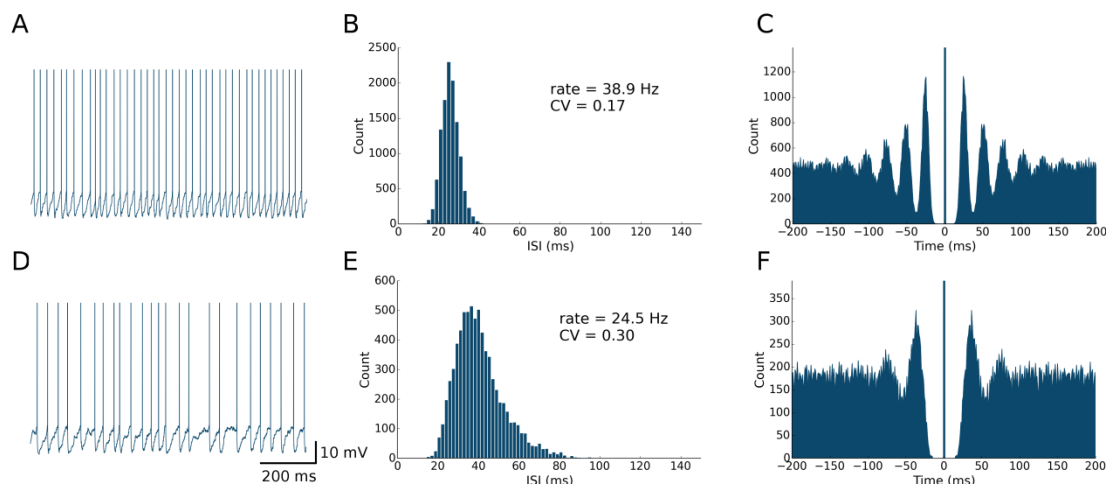
Figure 3.3 Spontaneously active PKJ neuron models reproduce similar firing dynamics as observed *in vitro.* Conventions are as in Figure 3.2

3.3.2 Model PKJs and MLIs in the network exhibit irregular firing

Next, we examined the spike patterns of interconnected, spontaneously active MLI and PKJ neurons in a network (Figure 3.1). We used the same neuron models for MLI and PKJ neurons, respectively, with dynamics depicted in the top panels of Figures 3.2 and 3.3, to form the network. Despite the same prototypical MLI and PKJ being used repeatedly, the random connectivity and random synaptic weight assigned when constructing the network resulted in a diversity of neuron responses (Figure 3.4) with MLI mean firing rates of 13.1 ± 8.0 Hz (n = 160, range: 0.2 - 29.2 Hz) and PKJ mean firing rates of 25.9 ± 3.5 Hz (n = 16, range: 19.1 - 33.1 Hz). The firing patterns of MLIs and PKJs in the network changed substantially due to the constant bombardment by inhibitory postsynaptic currents (IPSCs) from presynaptic neurons. The decreased firing rate and irregular spiking of these neurons is apparent in a trace of the membrane potential (Figures 3.2, 3.3D). The ISI histogram becomes significantly skewed favoring longer and more irregular ISIs (Figures

3.2, 3.3E). MLI ISI coefficients of variation increased markedly from the isolated case to 0.61 ± .24 (range: .14 - 1.04; n=160), as did the PKJ ISI CVs 0.28 ± .04 (range: .21 - .39; n=16). (Hausser and Clark, 1997) reported ISI coefficients in control conditions of 0.51 ± .024 (range: .19 - .85; n=43) for MLIs and 0.28 ± .038 (n=160, range: .05 - 1.13; n=68) for PKJs. We also found examples of both MLIs and PKJs in the model network that closely matched exemplar neurons reported *in vitro* data in control conditions. A model PKJ found in the network produces a mean firing rate of 24.5 Hz and an ISI coefficient of variation (CV) of 0.30 compared to 35 Hz and 0.49, respectively, for an exemplar neuron *in vitro* (Hausser and Clark, 1997). A model MLI found in the network produces a mean firing rate of 17.8 Hz and an ISI CV of 0.43 compared to 15 Hz and 0.40, respectively, for an exemplar neuron *in vitro* (Hausser and Clark, 1997). It should be noted that the background activity of parallel fiber input is present in control conditions reported for *in vitro* data but was shown to contribute only a modest increase in MLI and PKJ firing rates in a separate experiment of the same study. No parallel fiber background activity is present in this model. A significant correlation between mean firing rate and CV was found in both MLIs (Spearman rank-order coefficient r = -0.996, p < 10^{-167}) and PKJs (Spearman rank-order coefficient r = -0.991, p < 10^{-12}). Many of the peaks in the spike autocorrelogram disappeared suggesting that trains of spikes are no longer regularly spaced. These results suggest that a simple neuron model of spontaneously active MLIs and PKJs when interconnected in accordance with known anatomy is capable of reproducing the irregular firing patterns of MLIs

and PKJs observed *in vitro*. Finally, analyses of the consistency of the model results among different random instantiations of the network constrained by the same parameters and of the robustness of the model to random perturbations in the parameters of up to 10% of the original values were performed (Supplementary Figures 3.7-3.9). These results suggest the model reproduces similar results under different random instantiations of the network (Supplementary Figures 3.7-3.8) and is robust to small changes in the parameters (Supplementary Figure 3.9).
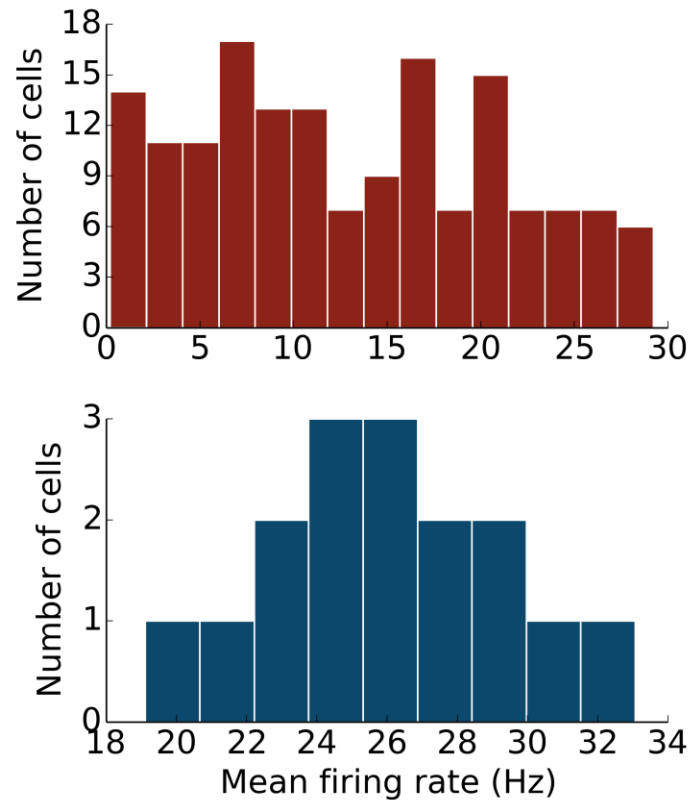
Figure 3.4 The network of MLIs and PKJs exhibits a diversity of responses. A.) A histogram of mean firing rates of MLIs from the network during one simulation. B.) A histogram of mean firing rates of PKJs from the network during one simulation.

3.3.3 Feedforward inhibition produces variable delays in the postsynaptic neuron

Next, we ran simulations to illustrate the effect of feedforward inhibition on the membrane potential of PKJs between successive spikes. Multiple traces of the membrane potential of an isolated PKJ showing two successive spikes are aligned to the first spike and overlaid (Figure 5A). Action potential waveforms have been artificially drawn since the leaky integrate-and-fire model does not explicitly model the membrane potential during action potentials. The random spontaneous current resulted in variable delays between spikes. A model MLI was then synaptically connected providing feedforward inhibition onto the PKJ with a peak IPSC of 4 nS. The MLI was triggered to fire 12 ms after the PKJ's first spike. The effect of feedforward inhibition from the MLI to the PKJ delays the time of the second PKJ spike (Figure 5B). The mean delay with feedforward inhibition is significant (Mann-Whitney U test, $p < 10^{-96}$, $n = 500$) (Figure 5C). Moreover, a linear relationship between the peak IPSC and the ISI can be seen (Figure 5D). This suggests the mean ISI is a function of the total synaptic conductance during the interval preceding the second spike. More elaborate methods for characterizing the response of neurons to synaptic input, such as measuring the phase response curves (PRC) of PKJs (Phoka et al., 2010), can be straightforwardly applied to this model in future work.
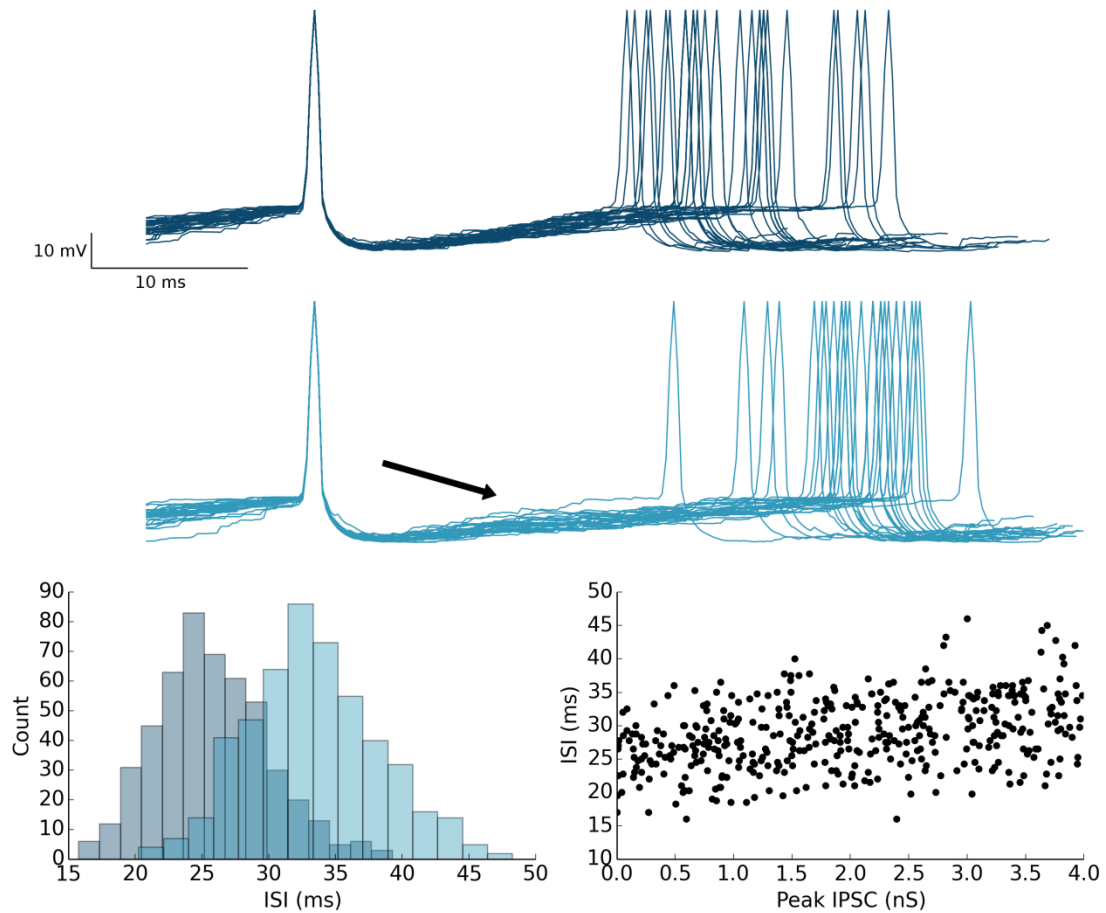
Figure 3.5 Feedforward inhibition causes prolonged inter-spike intervals in the target neuron. A.) 30 membrane potential traces overlaid with first spike aligned from a single isolated PKJ. Spikes are artificially drawn. The variable ISI can be seen. B.) A model MLI was then synaptically connected to the PKJ providing feedforward inhibition and caused to fire 12 ms (marked by the black arrowhead) after the first PKJ spike. 30 membrane potential traces with the first spike aligned from the PKJ are shown. The effect of the IPSC (4 nS peak in this simulation) can be shown to increase the average ISI. C.) Histograms of ISIs in the case without feedforward inhibition (as in A) (darker shade, left histogram) and with feedforward inhibition (as in B) (lighter shade, right histogram). D.) The relationship between IPSC and ISI can be seen by varying the synaptic conductance randomly in separate trials and measuring the resulting ISI.

3.3.4 The effects of removing MLI-MLI or PKJ-MLI synapses

Finally, to explore the effects of MLI-MLI and PKJ-MLI connections on the baseline activity of the network, we simulated the network activity when a random subset of synapses from one connection type or the other were

randomly pruned (i.e. removed). We simulated scenarios where a random subset of 25%, 50% or 75% of the original MLI-MLI or PKJ-MLI synapses were pruned, as well as when the network is fully intact (0%) or all synapses of that connection type are removed (100%) (Figure 6). The activity of each neuron was recorded for 60 seconds and a mean firing rate and mean ISI CV were calculated for each neuron in each neuron-type population. The median (i.e. second quartile) of each population for both measures was computed and is depicted with filled circles. The first and third quartiles for each measure was also computed and is depicted with bars -- where the lower bar is the first quartile and the upper bar is the third quartile -- to show the distribution of values across the population. The population mean was also computed and is depicted by a cross in a contrasting color. As more MLI-MLI synapses are pruned, the MLI firing rates (Figure 6, top-left panel, dark red line) increase due to decreased mutual inhibition. The MLI ISI CVs (light red) decrease due to increased regularity in firing. The result of increased MLI firing is increased inhibition onto PKJs, resulting in decreased PKJ firing rates (Figure 6, lower-left panel) and increased PKJ ISI CVs. In contrast to the significant changes in MLI and PKJ firing rates and ISI CVs when MLI-MLI synapses are pruned, pruning PKJ-MLI synapses has only a subtle effect on the activity of MLIs (Figure 6, top-right) and PKJs (Figure 6, bottom-right). Statistical tests show that the difference between population firing rates in the fully intact network (0%) and the fully pruned PKJ-MLI connections (100%) is not significant for MLIs (Mann-Whitney U test, p<.13, n=160) or PKJs (Mann-Whitney U test, p <.19, n=16). These results show that MLI-MLI mutual inhibition has a significant influence on the baseline activity of the network by governing the

average firing rate and variability of spike timing of MLIs and PKJs whereas the effect of PKJ-MLI connections on the baseline activity of the network is more subtle.
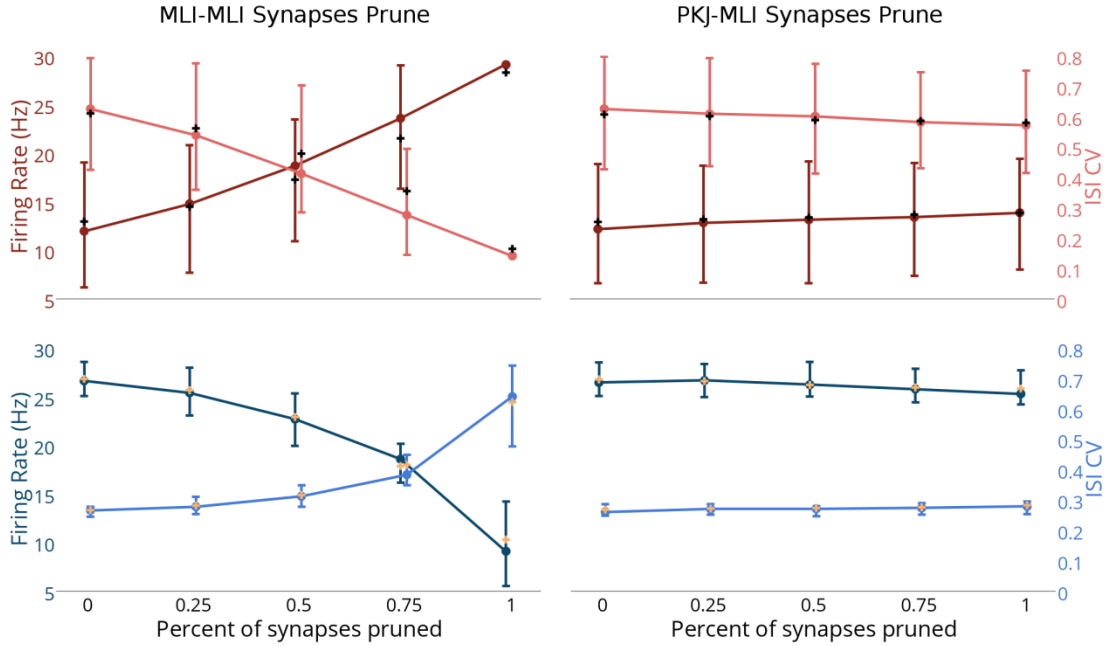
Figure 3.6 Changes in network activity by pruning MLI-MLI or PKJ-MLI synapses. Simulations were performed where a random set of synapses of either MLI-MLI or PKJ-MLI connections were removed from the model network to investigate the effect of these connection types on the activity of the network. Left column: measurements of MLI population (top row, in red) and PKJ population (bottom row, in blue) firing rates (darker shade) and ISI CVs (lighter shade) when MLI-MLI synapses are randomly pruned by 25%, 50% and 75% as well as fully intact (0%) and fully pruned (100%, i.e. no MLI-MLI left synapses at all). Each neuron's mean firing rate and ISI CV was measured over a 60 second simulation of the operation of the network. Solid circles denote the median of the population for each of these statistics. Bars show the first and third quartile to depict the distribution of values across the population. The cross mark denotes the population mean. Right column: similar measurements in the case of PKJ-MLI synapses pruned. Top-left panel: As more MLI-MLI synapses are pruned, the median firing rate of the population of MLIs (dark red) increases due to decreased mutual inhibition. When the synapses are completely pruned, there is very little variance in the population response and quartile bars overlap with the filled circle and are not visible. Additionally, the median ISI CV decreases as more MLI-MLI synapses are pruned (light pink). Bottom-left: As more MLI-MLI synapses are pruned, inhibition onto PKJs from MLIs increases, thus decreasing the median PKJ population firing rate (dark blue) and increases the median PKJ ISI CV (light blue). Top-right: pruning PKJ-MLI synapses has only a subtle effect on the MLI population median firing right and ISI CV. Bottom right: similarly, pruning PKJ-MLI synapses has only a subtle effect on the PKJ population median firing right and ISI CV.

3.4 Discussion

In this study, we demonstrate that a network composed of simple neuron models of MLIs and PKJs is sufficient to reproduce the irregular firing patterns of their biological counterparts as observed *in vitro*. The key elements to the model are neurons with endogenous depolarizing currents that are interconnected via inhibitory synapses in accordance with known anatomy. The random endogenous current drives each neuron to spike in the absence of all input to the neuron in a regular but still variable way. In the event of an inhibitory input from another neuron, the membrane potential of the target neuron is temporarily decreased, requiring more spontaneous depolarizing current and thereby more time to reach threshold, resulting in a longer inter-spike interval. The time between two spikes is dependent on the amount of the endogenous current and the amount of inhibitory post synaptic conductance. The results suggest that a more elaborate neuron model is not necessary to reproduce these phenomena. In addition, simulations investigating the relative importance of MLI-MLI and PKJ-MLI connections on regulating the baseline activity of the network revealed the significant role of MLI mutual inhibition to achieve results matching *in vitro* data and relatively subtle role of MLI-PKJ synapses. Finally, this network model provides a substrate for additional experimental investigation into the role of MLIs in cerebellar learning and function.

3.4.1 Implications of irregular firing

Whether irregular firing has a functional role or is simply a consequence of interconnected spontaneously active neurons is not clear. Some evidence suggests a functional role for these firing patterns. (Wulff et al., 2009) found

that genetically modified mice lacking PKJ $GABA_A$ receptors exhibited normal motor performance but were unable to consolidate motor learning following VOR gain down training. Interestingly, while the ISIs of PKJs were more regular in the genetically modified mice compared to control, the mean firing rate was nearly the same. Motor learning in the cerebellum may initially take place in the cortex and then be partially transferred to the deep cerebellar nuclei/vestibular nuclei (DCN/VN) where it is consolidated for long term storage (Kassardjian et al., 2005;Shutoh et al., 2006). While the overall quantity of PKJ inhibition onto their targets in the DCN/VN is unchanged in knockout mice, the quality of PKJ firing patterns may be enough to disrupt consolidation of memory to the DCN/VN and could explain the failure of knockout mice to consolidate VOR gain down learning. This is consistent with electrophysiological results showing that PKJ inhibition onto DCN/VN targets controls learning at mossy fiber (MF) to DCN/VN synapses (McElvain et al., 2010;Person and Raman, 2010), a putative location for memory consolidation. Mechanistically, irregular PKJ firing may favor rebound depolarizations (RDs) occurring in PKJ targets in DCN/VN (Aizenman and Linden, 1999) by providing a period of intense inhibition followed by a period of relative relief, which in turn may control learning at DCN/VN synapses (Pugh and Raman, 2008). In the absence of spontaneous feedforward inhibition provided by MLIs, the PKJs fire more regularly and prevent DCN/VN targets from firing appropriately, possibly resulting in impaired memory transfer. However, too much feedforward inhibition leads to more irregular PKJ firing (Figure 6), which might also interfere with learning or motor performance. Episodic ataxia type-2 is a condition caused by mutations to P/Q-type voltage-gated calcium channels expressed in PKJs which leads to increased irregularity in PKJ firing

and impaired motor performance (Walter et al., 2006). Thus, feedforward inhibition onto PKJs must be carefully balanced to achieve stable learning and motor performance.

The irregular firing of PKJs may also be a means of preventing synchronous PKJ activity during periods of rest when the cerebellar cortex is not actively emitting control signals. If many PKJs did synchronize their firing in response to input stimulus, then the summed activity could encode a sequence of ON periods, when most PKJs are firing, and OFF periods, when most PKJs are silent. (Maex and De Schutter, 2003) showed computationally that the synaptic conductance delay in a homogeneous network of inhibitory neurons is the primary parameter controlling the frequency of synchronicity among these neurons. While this model does not implement spike propagation or synaptic transmission delays, this could be one way of evoking synchronized activity among MLIs and PKJs. This ON-OFF pattern might be a means of implementing Pulse Width Modulation (PWM), a digital control signal used to represent analog values. (Person and Raman, 2012) found that many synchronous inhibitory inputs to a neuron in the DCN/VN can entrain the neuron to fire at a high and regular rate. This firing rate could be the analog value desired by the PWM control scheme. On the other hand, if irregular firing prevents PKJ synchrony during behavior as well, then the summed activity of asynchronous PKJs could represent an analog value for control of the DCN/VN targets. It is also possible that PKJs can switch between operating modes to convey the most appropriate control signal.

3.4.2 Function of MLI-PKJ network

A more general inquiry is into the functional role of spontaneously active PKJs and MLIs. One advantage of spontaneously active neurons is that their firing rates can be both increased and decreased, by excitation and inhibition, respectively. Presumably, PKJs need to actively inhibit their DCN/VN targets which are spontaneously active and exhibit rebound depolarizations (Aizenman and Linden, 1999). Tonic inhibition by PKJs can be increased and possibly synchronized by excitatory PF inputs which could hyperpolarize or entrain DCN/VN targets. A decrease in PKJ tonic activity, via MLI feedforward inhibition, disinhibits DCN/VN targets. Such a scheme would allow for several modes of control and a similar argument can be made for the spontaneously active MLIs.

A key feature present in this model is MLI-MLI and PKJ-MLI inhibition. In the model, MLI-MLI inhibition is shown to have a significant effect on regulating the baseline firing rate and spike regularity in both MLIs and PKJs (Figure 6). As discussed, a careful balance between these two properties may be needed to ensure effective motor performance and learning. The presence of MLI-MLI inhibition also theoretically allows for competition among MLIs to take place in response to PF stimuli. Electrophysiological evidence suggests an activity dependent form of learning at PF-MLI synapses may exist (Liu and Cull-Candy, 2000;Rancillac and Crepel, 2004;Smith and Otis, 2005), but see also (Jorntell and Ekerot, 2002). If this is correct, a diverse set of MLI receptive fields and responses could emerge from this competition. Plasticity at MLI-PKJ synapses (Gao et al., 2012) could enable PKJs to learn the most appropriate set of inhibitory inputs to achieve the desired output response. While the anatomical data on MLI-PKJ convergence

between cat and rat differs (Eccles et al., 1967;Palay and Chan-Palay, 1974), plasticity at these synapses could also tune the total inhibitory conductance onto a PKJ to ensure that the baseline PKJ activity is appropriate. In the present model, this would be achieved by altering the synaptic weights. In another computer model, PKJ-PKJ feedback inhibition enables PKJs in a network with MLIs to perform temporal integration on a time-scale of seconds (Maex and Steuber, 2013); the role of MLI-MLI and PKJ-MLI inhibition may serve a similar function. In contrast, PKJ-MLI connections appear to have only a small effect on the resting activity of the network (Figure 6). Taken together, these ideas suggest the information storage capacity and expressiveness of the PKJ-MLI network is even greater than previous theories describe (Brunel et al., 2004;Clopath et al., 2012). The model proposed here provides an initial step towards carrying out further computational investigations into these questions.

3.4.3 Comparison with Other Models

De Schutter and Bower (1994b) model a Purkinje cell as a Hodgkin-Huxley-type, multi-compartmental model that reproduces asymmetric ISI distributions in response to PF and MLI inputs. However, in these experiments the model PKJ relies exclusively on PF inputs to drive spiking and not an endogenous depolarizing current. Further the influence of MLIs is modeled indirectly as Poisson spike trains which assumes the ISI distribution is exponential, whereas our model generates MLI spikes by simulating MLI dynamics directly and results in an appropriate ISI distribution. Finally, by simulating the network of MLIs and PKJs, our model enables simulating the response of the MLI-PKJ network to PF input to investigate cerebellar

function. Previous computational network models of the cerebellum that include MLIs typically ignore a number of anatomical or physiological facts. For example, models do not include the spontaneous activity of MLIs (Yamazaki and Nagao, 2012) or MLI-MLI and PKJ-MLI connectivity (Contreras-Vidal et al., 1997;Schweighofer et al., 1998;Medina et al., 2000;Maex and Steuber, 2013). Adaptive filter models implicitly model the inhibitory effect of MLIs by allowing the PF-PKJ filter weights to be negative (Fujita, 1982;Dean et al., 2010). While our network models a parasagittal strip of cerebellar cortex, other work has modeled a medio-lateral strip to investigate the effects of spontaneously active MLIs on PKJs along a beam of PF inputs (Santamaria et al., 2007). Further effort to extend the model proposed in our study to include the medio-lateral axis would be worthwhile.

3.5 Acknowledgements

Chapter 3, in full, is a reprint with minor revisions of the material as it appears in *Frontiers in Computational Neuroscience*. William Lennon, Robert Hecht-Nielsen, Tadashi Yamazaki. "A spiking network model of the cerebellar Purkinje cells and molecular layer interneurons exhibiting irregular firing". Vol. 8, pp. 1-10, 2014. The dissertation author is the primary investigator and author of this material.

3.6   Supplementary Figures
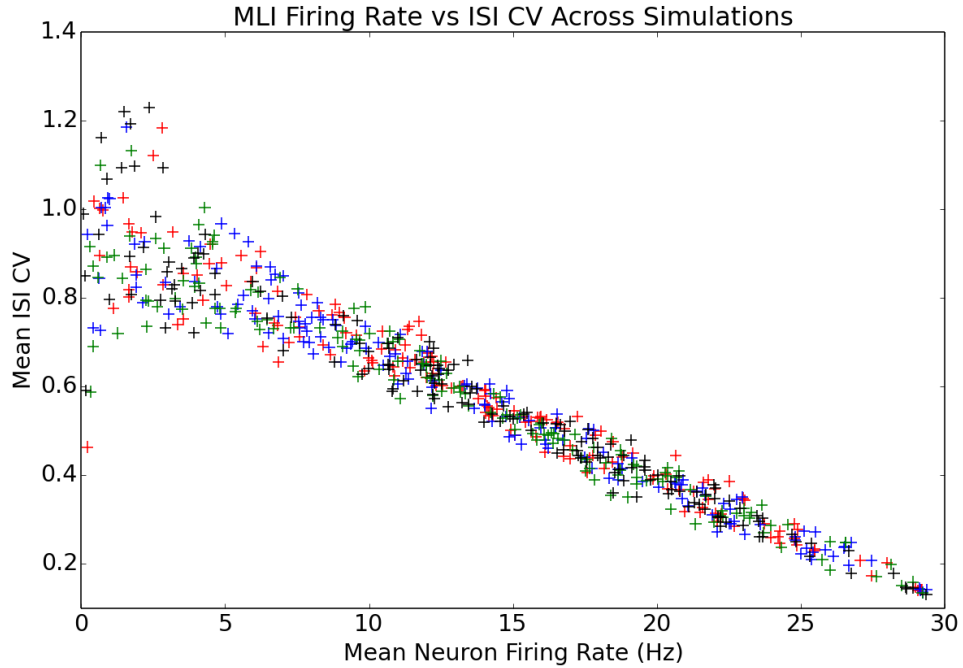
Figure 3.7 Consistency analysis of the model: MLI responses. To test whether different random instantiations of the model governed by fixed parameters (synapse probabilities, axon lengths, and spontaneous current parameters) will produce consistent (similar) results, we simulated 100 different random networks constrained by the parameters described in the Methods section. From these 100 simulations, four were chosen randomly to be visualized. The mean firing rates and ISI CVs of MLIs were measured during each simulation lasting 30 seconds. A scatter plot of mean firing rate and ISI CV was plotted for each neuron (denoted with a plus sign). Each of the four randomly chosen simulation results was assigned a different color. The clouds of points generated by each simulation overlap extensively suggesting the model network consistently produces results similar to those presented in Figures 3.2-3.5 and that they are not the result of selection bias by the experimenter.
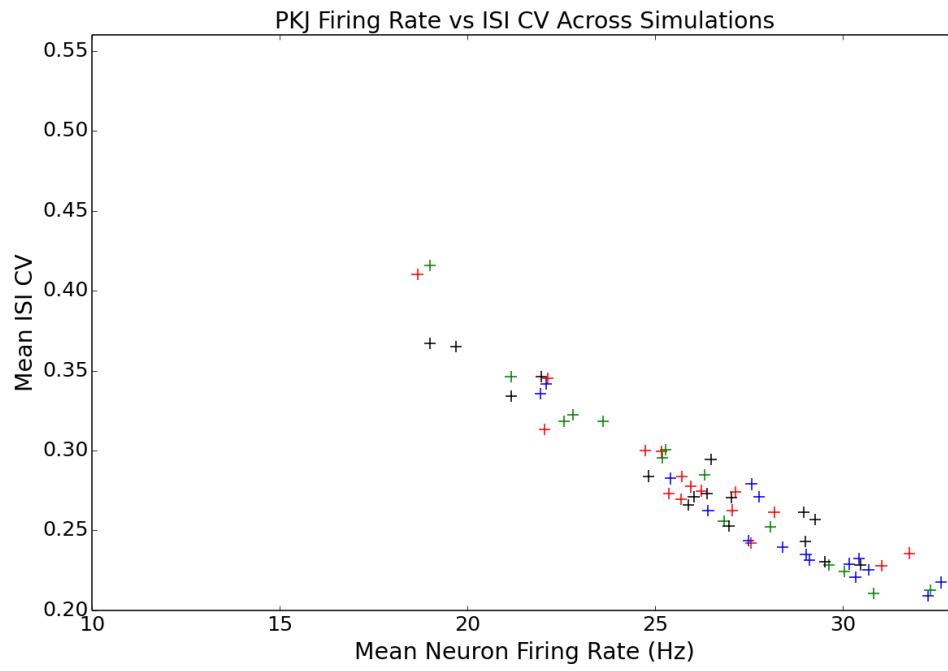
Figure 3.8 Consistency analysis of the model: PKJ responses. Similar to Figure S1 but for PKJs.
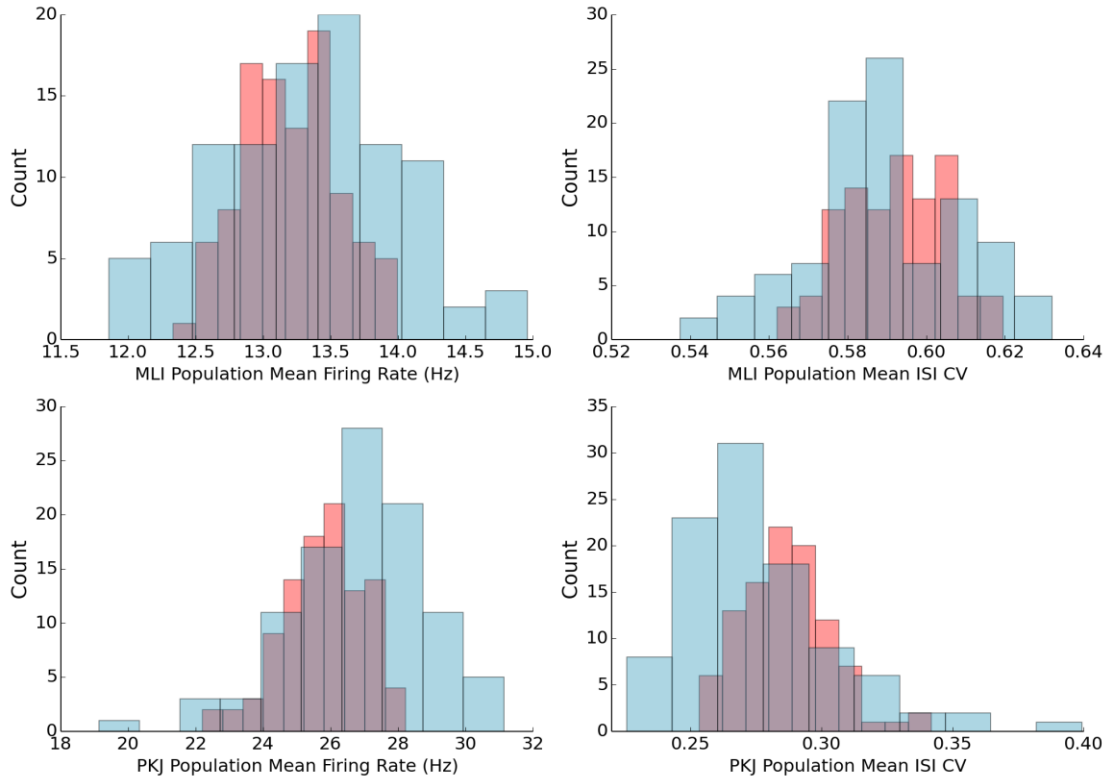
Figure 3.9 Robustness analysis of the model to random perturbations in the parameters. To test the robustness of the model to changes in the parameters, 100 simulations were performed where all parameters (synapse probabilities, axon lengths, and spontaneous current parameters) were randomly perturbed by up to 10% of their original value (drawn from a uniform random distribution). Population mean firing rates and ISI CVs are computed and histograms of these values across trials are plotted. Blue histograms show the responses from the perturbed networks. Red histograms show the responses from 100 randomly instantiated networks with the original (fixed) parameters. There is significant overlap in network activity across simulations in the perturbed and unperturbed cases indicating that the network produces similar activity that is robust to small changes in the model parameters.

Chapter 4 A model of learning at the parallel fiber - molecular layer interneuron synapses

Theoretical and computational models of the cerebellum typically focus on the role of parallel fiber (PF) - Purkinje cell (PKJ) synapses for learned behavior, but few emphasize the role of the molecular layer interneurons (MLIs) -- the stellate and basket cells. A number of recent experimental results suggests the role of MLIs is more important than previous models suggest. We investigate learning at PF - MLI synapses and propose a mathematical model to describe plasticity at this synapse. We perform computer simulations with this form of learning using a spiking neuron model of the MLI and show that it reproduces several *in vitro* experimental results. Further, we show how this model can predict the results of other experimental protocols that are not simulated and describe how the model could be extended to reproduce the receptive field changes of MLIs observed *in vivo.* Finally, we hypothesize what the biological mechanisms are for changes in synaptic efficacy that embody the phenomenological model proposed here.

4.1 Introduction

The parallel fiber (PF) - Purkinje cell (PKJ) excitatory synapse has historically been considered the locus of learning and memory in the cerebellar cortex, driven by climbing fiber (CF) inputs (Grossberg, 1969;Marr,

1969;Albus, 1971;Ito et al., 2014). While the number of PF-PKJ synapses formed and capacity for information storage is massive (Brunel et al., 2004;Ito, 2006), excitatory inputs to PKJs alone do not explain the bidirectional changes in PKJ activity observed during behavior (Miyashita and Nagao, 1984;Jirenhed et al., 2007) since PKJs fire spontaneously in absence of excitatory inputs (Hausser and Clark, 1997;Cerminara and Rawson, 2004). The molecular layer interneurons (MLI) -- stellate and basket cells -- also receive PF inputs and provide feedforward inhibitory inputs to the PKJs in addition to the recurrent inhibitory inputs they form with other MLIs (Eccles et al., 1967;Palay and Chan-Palay, 1974). Learned changes to PF-MLI and MLI-PKJ synapses are postulated to increase the information capacity of the MLI-PKJ network and richness of PKJ output dynamics (Albus, 1971;Dean et al., 2010), however relatively little is known about plasticity at these synapses.

There is mounting experimental evidence that MLIs play an important role in cerebellar function. Genetically modified mice lacking PKJ gamma-aminobutyric acid A (GABA$_A$) receptors exhibit significant motor learning deficits (Wulff et al., 2009), suggesting a significant functional role for MLI feedforward inhibition in motor learning. Further, using optogenetics to selectively modulate the firing rates of MLIs via photostimulation elicits movement and controls movement kinematics in awake mice (Heiney et al., 2014). Thus, orchestrated MLI activity is functionally capable of controlling the gain and timing of movement components. Understanding the learned changes in MLI feedforward inhibition onto PKJs is crucial to understanding the learned output of the cerebellar cortex.

PF-MLI synapses are one such locus of learned changes in MLI-PKJ inhibition. Previous *in vivo* studies showing CF driven changes to the MLI PF

receptive fields (RF) led to the hypothesis that concomitant PF and CF activation strengthens PF-MLI synapses and PF stimulation alone weakens them (Jorntell and Ekerot, 2002;2003;2011). Thus, this form of learning is said to be complementary and synergistic to PF-PKJ learning (Gao et al., 2012). However, *in vitro* experimental evidence suggests that bidirectional changes in synaptic efficacy can occur in absence of CF activity (Rancillac and Crepel, 2004;Smith and Otis, 2005;Kelly et al., 2009).

In this study, we propose a mathematical model of learning at PF-MLI synapses that is consistent with *in vitro* experimental findings. We perform computer simulations with spiking neuron models and reproduce a number of these *in vitro* experimental results. Finally, we speculate on the biological mechanisms underlying this model and describe future work for extending the model to reproduce the receptive field changes seen *in vivo*.

4.2 Methods

4.2.1 Neuron Model

The MLI neuron model is similar to the neuron model we used in our previous simulations (Lennon et al., 2014) except that it excludes inhibitory synaptic conductances and includes excitatory synaptic conductances described below. Briefly, the MLI is modeled as a conductance-based leaky integrate-and-fire neuron model (Gerstner and Kistler, 2002) with α-Amino-3-hydroxy-5-methyl-4-isoxazolepropionic acid (AMPA) and N-Methyl-D-aspartic acid (NMDA) conductances and an intrinsic depolarizing current which is drawn from a gamma distribution, $I_{spont}(t) \sim \Gamma(\kappa, \beta)$ (in units nA), that causes the

neuron to fire spontaneously. Actual parameters used are summarized in Table 4.1.

$$C\frac{dV}{dt} = -g_{leak}(V(t) - E_{leak}) - g_{ahp}(t)(V(t) - E_{ahp}) - (g_{AMPA}(t) + g_{NMDA}(t))(V(t) - E_{exc}) + I_{spont}(t) \quad (4.1)$$

Granule cells were not modeled directly and instead we simulated the arrival of PF spikes to PF-MLI synapses according to Poisson statistics with variable rate $\lambda(t)$ which is controlled during simulations.

Table 4.1 Summary of simulation parameters. MLI biophysical parameters (Midtgaard, 1992;Hausser and Clark, 1997;Carter and Regehr, 2002;Lachamp et al., 2009) AMPA receptor parameters (Carter and Regehr, 2002;Satake et al., 2012); NMDA receptor parameters (Gabbiani et al., 1994); τ_n derived by hand to match (Carter and Regehr, 2002); κ, β from (Lennon et al., 2014)

MLI Neuron Parameters	Value
$V_{threshold}$ (mV)	-53.0
C (pF)	14.6
$\bar{g}_{leak}$ (nS)	1.6
E_{leak} (mV)	-68.0
$\bar{g}_{AMPA}$ (nS)	3.0
E_{exc} (mV)	0.0
τ_{fast} (ms)	0.8
τ_{slow} (ms)	18.0
α_{fast}	0.8
α_{slow}	0.2
$\bar{g}_{NMDA}$ (nS)	1.0
τ_{rise} (ms)	3.0
τ_{decay} (ms)	40.0
τ_n (ms)	10.0
$\bar{g}_{AHP}$ (nS)	50.0
E_{AHP} (mV)	-82.0
τ_{AHP} (msec)	2.5
κ	3.966333
β	0.006653

Table 4.2 Learning Rule Parameters

Neuron trace and weight update parameters	MLI	PF
τ_ψ (ms)	60.0	10.0
ν_ψ (ms)	15.0	2.0
f_{max} (Hz)	150	300
η	.001	
w_0	0.2	

4.2.2 Synaptic conductances

Model PF-MLI synapses contain both AMPA and NMDA receptor conductances. Total AMPA synaptic conductances are computed according to Equation 4.2, where $\overline{g}_{syn}$ is the maximal synaptic conductance, w_i is the synaptic weight, $\alpha(t)$ is the synaptic conductance kinetics function, and $\delta_i(t)$ is a Dirac delta function for the ith synapse onto the target neuron, indicating whether the presynaptic neuron has spiked at time t. We use the terms "synaptic weight", "synaptic efficacy" and "synaptic strength" interchangeably. PF-MLI AMPAR conductance rise times are modeled as instantaneous increases whereas decay times are modeled as double exponentials to approximately fit the prolonged conductances at these synapses (Carter and Regehr, 2000) (Equation 4.3).

$$g_{AMPA}(t) = \overline{g}_{AMPA} \sum_i w_i \int_{-\infty}^{t} \alpha_{AMPA}(t-s)\delta_i(s)ds \qquad (4.2)$$

$$\alpha_{AMPA}(t) = \alpha_{fast} \exp\left(-\frac{t}{\tau_{fast}}\right) + \alpha_{slow} \exp\left(-\frac{t}{\tau_{slow}}\right) \qquad (4.3)$$

PF-MLI synaptic weights are modeled with a fixed minimum value, $w_0 \in (0,1)$, and a variable component, $\widehat{w}_i \in [0,1]$ that changes according to the

weight update equation described in the next section. Equation 4.4 ensures the effective synaptic weight, w_i, lies within the range $[w_0, 1]$.

$$w_i = w_0 + (1 - w_0)\widehat{w}_i \qquad (4.4)$$

Voltage sensitive NMDAR conductances are modeled in accordance with Equations 5-7 which roughly capture the neurotransmitter availability in the synaptic cleft and the opening and closing kinetics of NMDA receptors, respectively. Where $\rho = (3.57\,\text{mM})^{-1}$, $[\text{Mg}^{2+}]_0 = 1.2\,\text{mM}$ is the extracellular magnesium concentration, and $\sigma = (-0.062\,\text{mV})^{-1}$ (McCormick et al., 1993;Gabbiani et al., 1994). The logarithm of $n(t)$ in Equation 4.6 is used for numerical stability.

$$n(t) = \int_{-\infty}^{t} \exp\left(-\frac{t-s}{\tau_n}\right)\delta(s)ds \qquad (4.5)$$

$$\frac{dR}{dt} = \frac{\log(n(t)+1)\,(1-R)}{\tau_{rise}} - R/\tau_{decay} \qquad (4.6)$$

$$g_{NMDA}(t) = \bar{g}_{NMDA}R(1 + \rho[\text{Mg}^{2+}]_0 e^{\sigma V})^{-1} \qquad (4.7)$$

4.2.3 Neuron Traces

A trace of the neuron spiking activity is calculated every time step of the simulation and used to compute a smooth measure of the instantaneous neuron firing rate that is normalized using a neuron specific maximum firing rate, f_{max}. If the actual firing rate of the neuron exceeded f_{max}, the trace is truncated to f_{max}. This results in a unitless measure of the neuron firing activity bounded by zero and one, i.e. $\bar{x}_i(t) \in [0,1]$. Throughout the paper we

refer to this as the neuron "activity trace" or "firing trace". In several figures we plot the non-normalized "firing rate trace" (in units Hz) as well.

$$\psi(t) := \frac{e^{\frac{-t}{\tau_\psi}} - e^{\frac{-t}{\nu_\psi}}}{\tau_\psi - \nu_\psi} \tag{4.8}$$

$$\bar{x}_i(t) = \frac{1}{f_{max}} \int_{-\infty}^{t} \psi(t-s)\delta_i(s)ds \tag{4.9}$$

4.2.4 Synapse learning rule

Synapses are updated according to the *gated steepest descent* learning rule (Chen, 2007). The weight update is correlative based on the activity of the presynaptic neuron, $\overline{PF_i}(t)$, and the difference between the post-synaptic activity, $\overline{MLI_j}(t)$, and a measure of the synaptic strength, $w_{i,j}$. η is the learning rate parameter, and γ is a free parameter that is adjusted during certain experiments, but is otherwise set to one. A biological interpretation of the learning rule can be found in the Discussion.

$$\frac{d\widehat{w}_{i,j}}{dt} = \eta\overline{PF_i}(t)[\overline{MLI_j}(t) - \gamma\widehat{w}_{i,j}] \tag{4.10}$$

4.2.5 Software and Data Analysis

Simulations were performed in Python using BRIAN simulator -- a spiking neural network framework (Goodman and Brette, 2009). All simulations are performed with a time step of .25 ms using Euler's method for integration of differential equations to ensure numerical stability. Data was analyzed and plotted using BRIAN Simulator, SciPy, Numpy, Matplotlib, Seaborn and homemade software written in Python. Action potentials are

drawn in plots by inserting a value of 0 mV in recordings of neuron model membrane potentials immediately after the model neuron reaches threshold. The source code for all experiments will be made freely available online upon publication.

4.3 Results

4.3.1 Model of Synaptic Plasticity

Plasticity at the PF-MLI synapses involves several mechanisms that produce both pre- and post-synaptic changes (Liu and Cull-Candy, 2000;Rancillac and Crepel, 2004;Smith and Otis, 2005;Soler-Llavina and Sabatini, 2006;Sun and June Liu, 2007;Bender et al., 2009;Kelly et al., 2009). Here, we present a *phenomenological* model of PF-MLI plasticity that is a function of PF and MLI activity and a measure of the synaptic efficacy, *w*. While we mainly focus on evidence for post-synaptic plasticity, it is expected that this model also accounts for pre-synaptic changes in synaptic efficacy in physiologically realistic conditions. Post-synaptic plasticity involves changes in the AMPA receptor phenotype composition (Liu and Cull-Candy, 2000;Liu and Cull-Candy, 2002;Liu and Savtchouk, 2012). Both LTP and LTD are observed and dependent on post-synaptic calcium signaling (Liu and Cull-Candy, 2000;Rancillac and Crepel, 2004;Smith and Otis, 2005).

We hypothesize that activity-dependent post-synaptic Ca^{2+} transients induce changes in post-synaptic plasticity. These transients can induce both LTD and LTP, dependent on a dynamic cytosolic Ca^{2+} threshold. We roughly capture the effects of activity dependent calcium transients as unit-less traces of the pre- ($\overline{PF}(t)$) and post-synaptic activities ($\overline{MLI}(t)$), and the dynamic

threshold as a variable synaptic strength, w, multiplied by a variable scaling factor γ. For the purpose of these simulations, $\gamma = 1$ unless otherwise stated. η serves as a learning rate and is typically small, $\eta = .001$. This learning rule is also known as *gated steepest descent* (Chen, 2007) and is similar to the BCM learning rule (Bienenstock et al., 1982) and mechanistic models of calcium-dependent synaptic plasticity (Shouval et al., 2002).

$$\frac{dw}{dt} = \eta \overline{PF}(t)[\overline{MLI}(t) - \gamma w] \tag{4.11}$$

Due to w serving as a dynamic threshold for plasticity, this learning rule exhibits LTP when $\overline{PF}(t) > 0$ and $\overline{MLI}(t) > \gamma w$, and LTD when $\overline{PF}(t) > 0$ and $\overline{MLI}(t) < \gamma w$ and is self-stabilizing so that synaptic weights do not "blow up". The effect of this learning rule can be seen as w "chasing" the value of $\overline{MLI}(t)$, when the presynaptic activity is non-zero, i.e. $\overline{PF}(t) > 0$, and the pre-synaptic activity serves as a dynamic learning rate. The learning rule is Hebbian in the sense that it is the sum of a correlative term, $\overline{PF}(t)\overline{MLI}(t)$, and a weight decay term, $-\gamma \overline{PF}(t)w$, which can be seen by multiplying the pre-synaptic activity term through. The model of synaptic efficacy implemented for the simulations described next has a fixed component to simulate a minimal synaptic efficacy and a variable component that is governed by Equation 4.11.

4.3.2 Simulation Results

In this section, we present the results of computer simulations implementing this learning rule at PF-MLI synapses. The simulations consist

of a single MLI spontaneously firing at about 30 Hz (simulating isolation from all inhibitory synaptic currents) with either a single PF or a bundle of 8 PFs forming synapses onto the MLI. Input spikes from PFs are modeled according to Poisson statistics with a variable rate which is controlled during the simulation. PF spikes produce both AMPA and NMDA conductances (described in Methods) in the MLI. In simulations I-IV, we simulate novel protocols to demonstrate the variety of synaptic weight changes depending on pre- and post- synaptic activities. In these simulations the simulated MLI receives only one PF input. In simulations V-X, we attempt to replicate the plasticity inducing protocols from a number of *in vitro* experiments and show that the simulations reproduce similar changes in synaptic efficacy. Table 4.3 summarizes the simulation protocols and results while Table 4.4 summarizes the corresponding *in vitro* experiments and interpretations in terms of this learning rule.

Table 4.3 Summary of Simulations

Simulation	Simulation Protocol	Result	Figure(s)
I	Single PF bursts at 100 Hz, isolated MLI fires spontaneously at baseline. n=10	LTP	4.1,4.2
II	Single PF fires continuously at 10Hz with a depolarizing current injected into an isolated MLI. n=10	LTP	4.2, S1
III	Single PF fires continuously at 10Hz with a hyperpolarizing current injected into an isolated MLI. n=10	LTD	4.2,S2
IV	Single PF fires continuously at 2Hz, isolated MLI fires spontaneously at baseline. n=10	---	4.2, S3
V	A bundle of 8 PFs fires at 50 Hz while the target MLI is voltage clamped to -60 mV.	LTD	4.3, 4.5
VI	A bundle of 8 PFs fires 100 Hz bursts while the target MLI is current clamped to -80 mV.	LTP	4.4, 4.5
VII	A bundle of 8 PFs fires at 1 Hz while the target MLI is current clamped to -80 mV.	LTD	4.5, S4
VIII	A bundle of 8 PFs fires at 2 Hz while the target MLI is injected with a depolarizing current.	LTP	4.5, S5
IX	A bundle of 8 PFs fires at 1 Hz while the MLI fires spontaneously and the weight update parameter γ is increased to $\gamma = 1.5$.	LTD	4.5,S6
X	A bundle of 8 PFs fires at 1 Hz while the MLI fires spontaneously and the weight update parameter γ is decreased to $\gamma = 0.5$.	LTP	4.5,S7

4.3.2.1 Simulation I: High-frequency PF bursts induce LTP in spontaneously firing MLIs

Simulation I investigates the effects of PF burst stimulation on the firing rate of a spontaneously firing isolated MLI and the consequent changes to synaptic efficacy. The simulation begins with a five second baseline period where the MLI and PF fire spontaneously at their baseline rates of 30 Hz and .33 Hz respectively (Figure 4.1). After five seconds, the PF is then stimulated to fire approximately 100 Hz bursts (according to Poisson statistics) for 100 ms every one second. Each one second period starting after the baseline period constitutes one trial and 60 trials are simulated for a total simulation time of

65 seconds. The simulation is repeated independently ten times (n=10); Figure 4.1 shows the first 10 seconds of an example of one simulation. A recording of the MLI voltage is shown in the top panel (red) and a non-normalized firing rate trace is shown in the middle panel below (red). This firing rate trace is divided by a maximum firing rate parameter to normalize its value between [0,1] yielding $\overline{\text{MLI}}(t)$ which is used in the weight update equation (described in Methods). A non-normalized trace of the PF firing rate is shown in the bottom panel (blue). The value of the synaptic strength, w, starts near its equilibrium value (where $\hat{w} \approx \overline{\text{MLI}}(t)$ when PF stimulation is low but non-zero) and is plotted in the bottom panel (green). PF bursts increase the MLI firing rate above its baseline value. During periods where PF activity is non-zero *and* where the normalized MLI firing activity (not shown) is greater than the variable weight component, $\hat{w}$, the synapse strengthens. The PF activity serves two functions: first to increase the MLI firing rate, and second to *gate* plasticity. The trajectory of the synaptic weight across trials and averaged over independent simulations is shown in Figure 4.2. One important feature of this learning rule is that the synaptic weight asymptotes instead of "blowing up" and is thus stable compared to a purely Hebbian rule. The asymptote is the result of the synaptic weight catching up to the MLI activity -- as it gets closer, the change in synaptic efficacy is smaller.
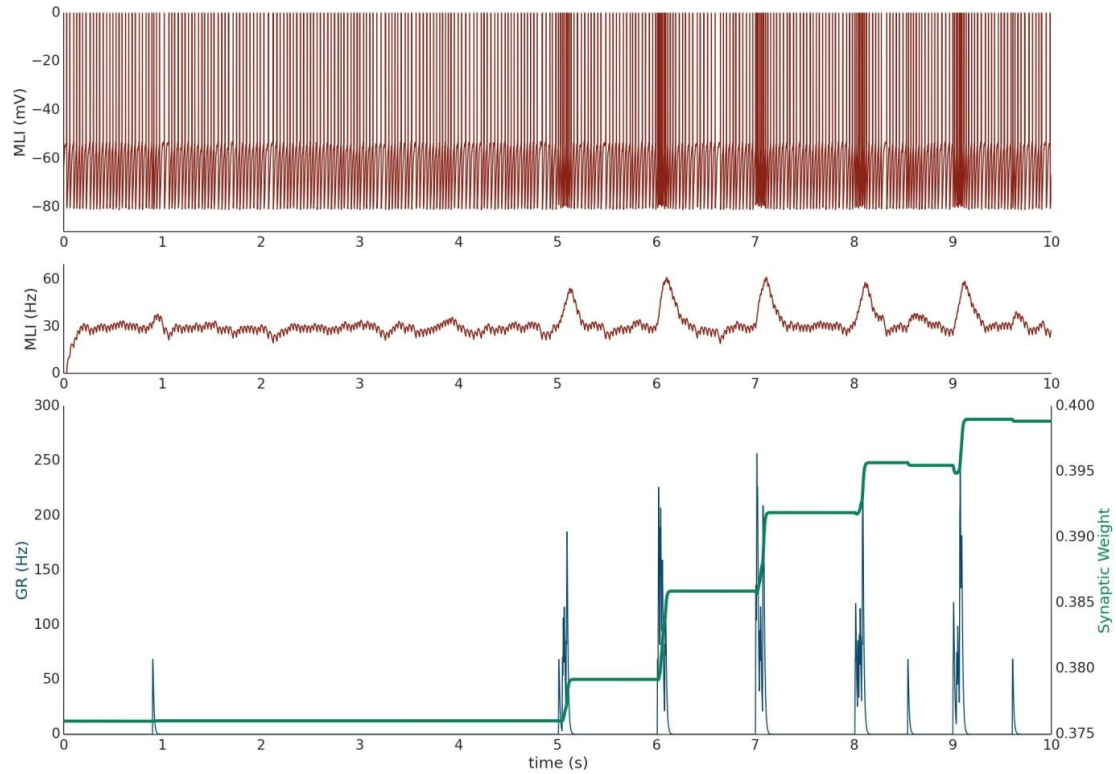
Figure 4.1 Simulation I: PF-driven long term potentiation. An example of one simulation run with an isolated MLI firing spontaneously (red traces; top panel: membrane potential; middle panel: firing rate trace) which receives one PF input (blue trace). Only the first 10 seconds of the simulation are shown. The value of the synaptic strength, w, is shown in green in the lower panel and begins near its equilibrium value. During the first five seconds both PF and MLI firing at baseline at about .33 Hz and 30 Hz, respectively. After five seconds, the PF fires 100 Hz bursts for 100 ms every one second. Starting at five seconds, each one second interval is considered a trial. The increased PF firing causes the MLI to increase its firing rate; at the same time, the synaptic weight, w, increases to compensate for the difference between the normalized MLI firing rate and the current value of w.
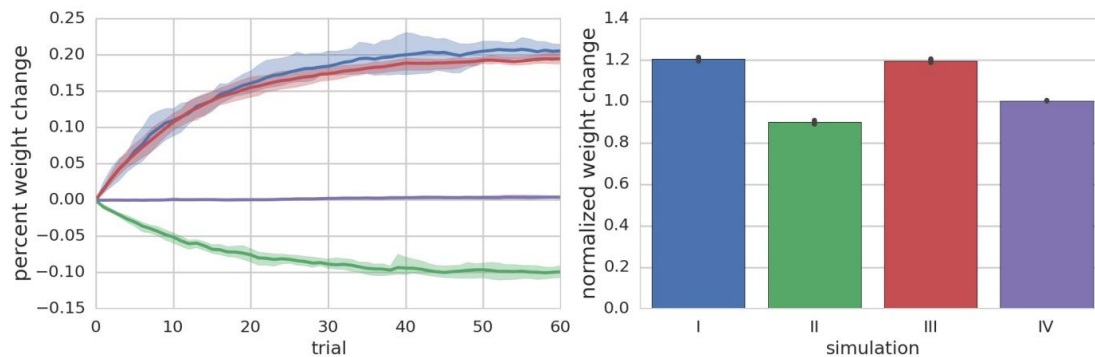
Figure 4.2. Summary of Simulations I-IV. The left panel shows the mean (solid lines) and range (shaded regions) percent change of synapse weight from starting values at the end of each trial across all simulated neurons (n=10) for a particular simulation. For simulation I where the PF is stimulated to fire 100 Hz bursts for 100 ms every one second (i.e. one second trials), the synapse weights reach an equilibrium value of about 20% greater than starting values. The right panel shows the final mean (bar height) and range (black error bar) of weight values normalized to their starting values for each simulation.

4.3.2.2 Simulation II: Continuous 10 Hz PF firing with paired MLI depolarizing current injection induces LTP

Simulation II investigates the effects of a continuous 10 Hz stimulation of the PF with a paired depolarizing current injected into the MLI. Similar to the previous simulation, a 2.5 second baseline period is simulated where both PF and MLI fire spontaneously. Beginning at 2.5 seconds the MLI is injected with a constant depolarizing current sufficient to increase the MLI firing rate to approximately 40 Hz. Beginning at 5 seconds, the PF is continuously stimulated to fire at approximately 10 Hz (according to Poisson statistics) for the remainder of the simulation, 60 seconds (Supplementary Figure 4.6, analogous to Figure 4.1). Thus, the total simulation time is 65 seconds and we again refer to the one second periods beginning at 5 seconds as trials. Because the PF firing rate is non-zero and the MLI firing rate increases above baseline, the synaptic weight increases (Figure 4.2).

4.3.2.3 Simulation III: Continuous 10 Hz PF firing with paired MLI hyperpolarizing current injection induces LTD

Simulation III is identical to simulation II, except that a constant hyperpolarizing current is injected into the MLI to reduce its firing rate to approximately 10 Hz beginning at 2.5 seconds. Again, the PF is stimulated continuously to fire at approximately 10 Hz beginning at 5 seconds and continuing for 60 seconds. During this period, where non-zero PF activity gates plasticity, the synaptic weight decreases since the MLI activity is below the synaptic weight value (Figure 4.2; Supplementary Figure 4.7).

4.3.2.4 Simulation IV: Low-frequency PF stimulation with spontaneous MLI firing results in unremarkable changes in synaptic efficacy

Simulation IV investigates the effect of a constant low frequency stimulation of the PF (2 Hz) while the MLI fires spontaneously at its baseline rate of 30 Hz. Similar to simulation I, a 5 second baseline period is simulated where the PF and MLI fire at .33 Hz and 30 Hz, respectively. After 5 seconds, for another 60 seconds, the PF fires at 2 Hz (according to Poisson statistics). Since this PF firing rate does not sufficiently change the MLI firing rate and the weight value begins near equilibrium for baseline PF and MLI rates, the synaptic weight value does not change remarkably (Figure 4.2; Supplementary Figure 4.8).

4.3.2.5 Simulation V: PF bundle stimulation at 50 Hz with paired MLI voltage clamp induces LTD

Simulation V emulates the experimental conditions from Liu and Cull-Candy (2000) used to induce PF-MLI LTD. Table 4.4 summarizes the experimental protocols. The simulation models a single isolated MLI with eight

PF inputs to emulate the effect of stimulating a bundle of PFs with an electrode *in vitro*. The simulation begins with a 2.5 second baseline period where the PFs and MLI fire at baseline rates of .33 Hz and 30 Hz, respectively (Figure 4.3). At 2.5 seconds, the MLI is then voltage clamped to -60 mV. At 5 seconds, the PFs are stimulated to individually fire at approximately 50 Hz (according to Poisson statistics) which continues for 60 seconds. As before, each one second interval starting at 5 seconds is considered a trial to allow comparison among simulations. Concomitant with the activation of PFs, the synaptic weights decrease since the MLI firing activity is effectively zero, below the value of the synapse weight. Figure 4.3 depicts these changes, where figure conventions are the same as before except that the weight trace is the mean weight of all PF synapses impinging on the MLI and only one example PF trace is shown. The trajectory of the mean and range of synaptic weights onto this MLI is summarized in Figure 4.5. The synaptic weight asymptotically decreases to the minimum weight value, w_0. The synaptic weight decrease in the simulation is consistent with the observed decrease in synaptic efficacy by Liu and Cull-Candy (2000).
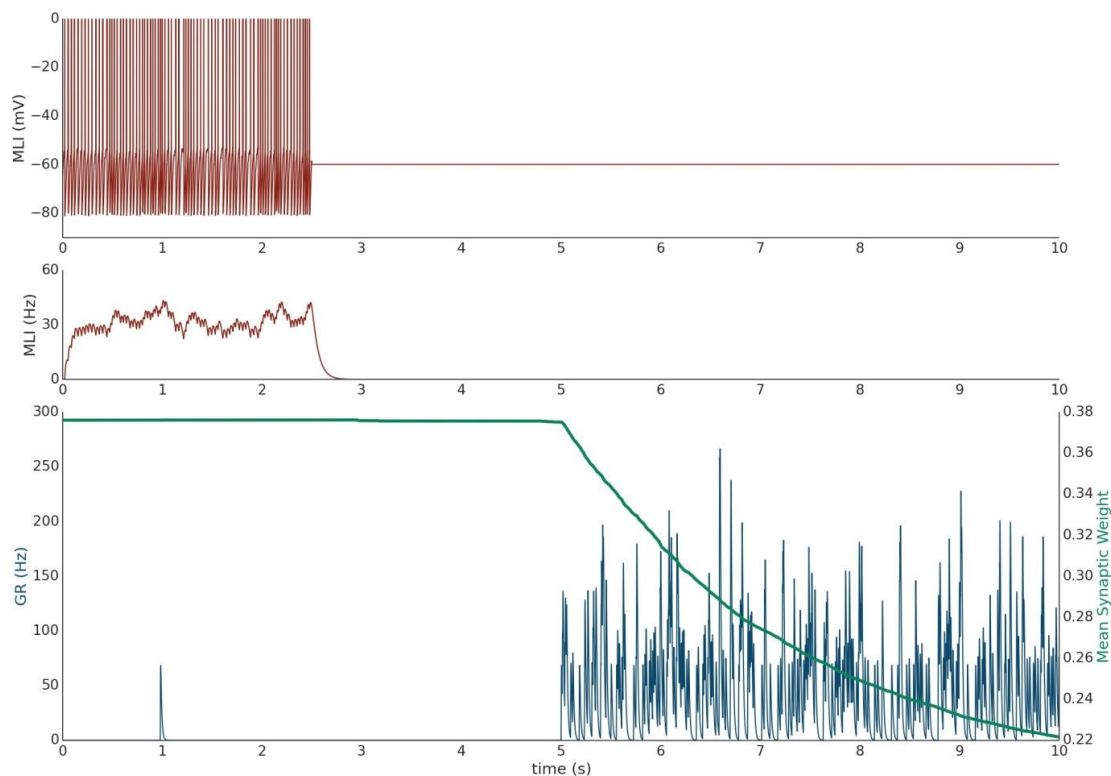
Figure 4.3. Simulation V: Voltage clamping MLI induces PF-MLI LTD. An isolated MLI fires spontaneously for the first 2.5 seconds of the simulation and is then voltage clamped to -60 mV for the remainder of the simulation. Starting at 5 seconds, each PF in the bundle fires at 50 Hz. Figure conventions are the same as Figure 4.1 except that the mean synaptic weight value across all PF synapses converging onto this MLI is shown (green) and only one sample PF trace is shown (blue). Between 2.5 and 5 seconds, the synaptic weights do not change significantly since the PFs are firing at a low .33 Hz. However, once the PFs begin firing at 50 Hz, the synaptic weight decreases rapidly since the normalized value of MLI firing is effectively 0 and below the synaptic weight value. This simulation attempts to reproduce the experimental results of Liu and Cull-Candy (2000).

4.3.2.6 Simulation VI: PF bundle burst stimulation with paired MLI current clamp induces LTP

Simulation VI models the experimental protocol used by Smith and Otis (2005) to induce PF-driven LTP at PF-MLI synapses. A single isolated, spontaneously firing MLI receiving eight PF inputs is simulated. The simulation begins with the MLI and PFs firing at their baseline rates of 30 Hz and .33 Hz, respectively (Figure 4.4). After 2.5 seconds, a constant current is

injected into the MLI to hold it near -80 mV. Beginning at 5 seconds, each PF is stimulated to fire at 100 Hz (according to Poisson statistics) for 100 ms every one second and continues for 60 seconds. Despite being injected with a hyperpolarizing current, the cumulative PF input is sufficient to cause the MLI to depolarize and fire action potentials, raising the MLI activity trace from near zero to above the original weight equilibrium values when both PF and MLI fire spontaneously. Thus, the synaptic weights increase during these periods of PF activity and results in a cumulative LTP (Figure 4.5).
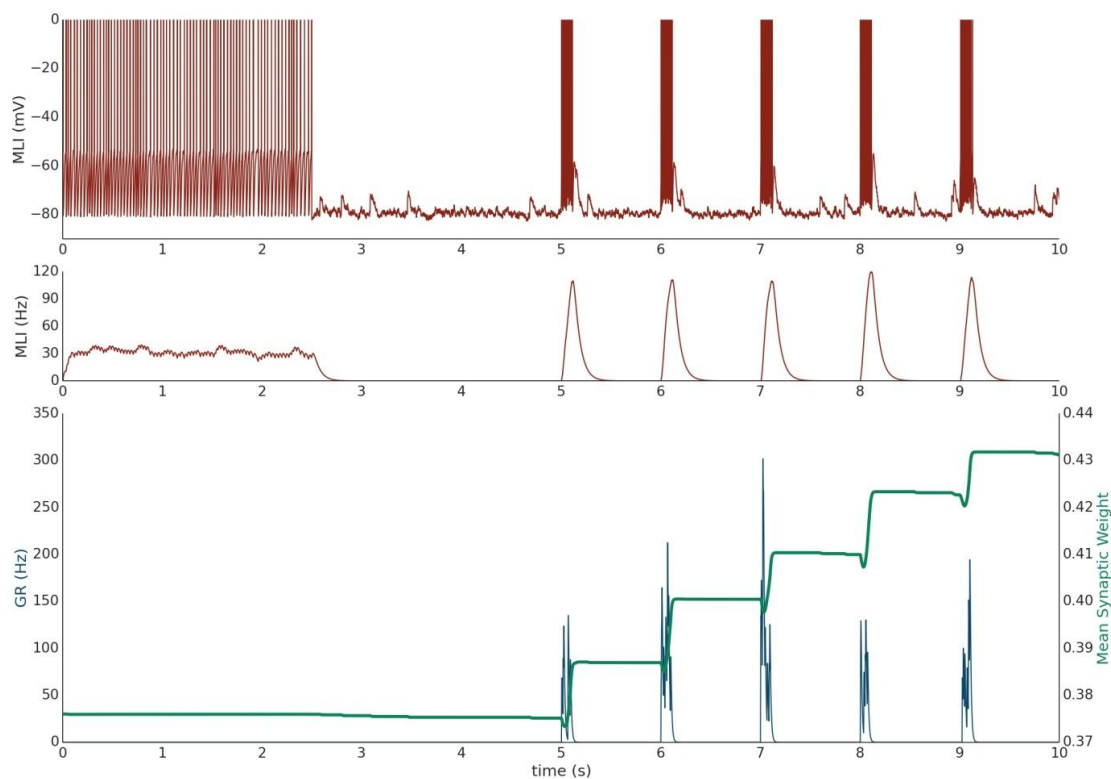
Figure 4.4 Simulation VI: Current clamping MLI with PF bursting results in LTP. An isolated MLI fires spontaneously for the first 2.5 seconds of the simulation and is then injected with a constant current to keep the membrane potential near -80 mV for the remainder of the simulation. Starting at 5 seconds, each PF in the bundle fires 100 Hz bursts for 100 ms every one second. Figure conventions are the same as Figure 4.3. Synchronous PF burst firing is sufficient to depolarize the MLI and cause it to fire. During periods where the PFs are active, the MLI firing rate trace rises above the value of the synaptic weight and thus results in an increase in the synaptic weight, i.e. LTP. This simulation attempts to reproduce the experimental results of Smith and Otis (2005).

4.3.2.7 Simulation VII: PF bundle low-frequency stimulation with paired MLI current clamp induces LTD

Simulation VII models a different experimental protocol used by Smith and Otis (2005) which was shown to induce PF-MLI LTD. The simulation protocol is identical to the one described for simulation VI except that each PF is stimulated to produce 2 Hz firing continuously (Supplementary Figure 4.9) beginning at 5 seconds. The low frequency spike inputs from all 8 simulated PFs is insufficient to regularly depolarize the MLI. Thus, the MLI activity trace remains zero while the PF activity trace is briefly greater than zero for short periods of time. The cumulative effect is a decrease in the mean PF-MLI synaptic strength, i.e. LTD (Figure 4.5).
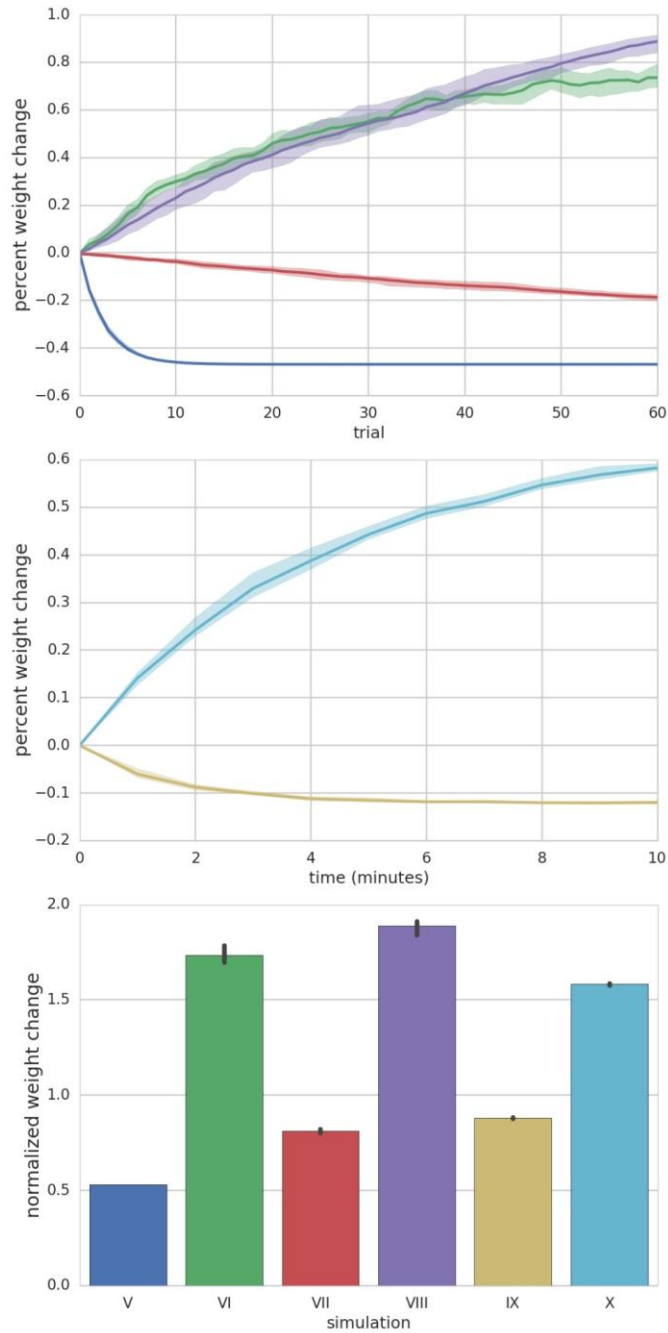
Figure 4.5. Summary of Simulations V-X. Top panel depicts the mean (solid lines) and range (shaded) percent weight change of synaptic weights converging onto the MLI at the end of each trial for simulations V-VIII. Middle panel shows the mean (solid lines) and range (shaded) percent weight change of synaptic weights converging onto the MLI at the end of each minute of simulation time for simulations IX and X. The bottom panel compares the final mean normalized synaptic weights at the end of the simulation for each simulation (bar height) and range of values (black error bars).

4.3.2.8 Simulation VIII: PF bundle low-frequency stimulation with paired MLI depolarizing current injection induces LTP

Simulation VIII attempts to model one of the experimental protocols used by Rancillac and Crepel (2004) which results in PF-MLI LTP. The protocol consists of an induction period of low-frequency (.33 Hz) stimulation of the PF bundle for 8 minutes while simultaneously holding the MLI in voltage clamp at -60 mV. After the induction period, the PFs are stimulated to fire at 2 Hz while the MLI is depolarized to 0 mV for 60 seconds. We hypothesized that during this induction period the synaptic efficacy would decrease from its previous equilibrium value since the PF is somewhat active and the MLI is in voltage clamp. To investigate this in the simulation, we begin the simulation with the MLI in voltage clamp at -60 mV and the synaptic weight at a lower value than previous experiments. The MLI is held in voltage clamp for the first 5 seconds of the simulation while the PFs fire spontaneously around .33 Hz. After 5 seconds, the MLI is injected with current to fire at 50 Hz. Since holding the simulated MLI at 0 mV would not result in spiking and thus a zero value for the activity trace, we chose to inject current to depolarize the neuron to fire at 50 Hz and produce a non-zero activity trace as a surrogate. The result of the simulated protocol is that the MLI activity trace value is greater than the synaptic weight and thus a strengthening of the synapse occurs (Figure 4.5). This is consistent with the result of Rancillac and Crepel (2004).

4.3.2.9 Simulation IX & X: Simulating changes in 'basal tone' induces bidirectional changes in synaptic efficacy

Metabotropic 1 glutamate receptors ($mGluR_1$) and gamma-aminobutyric acid B receptors ($GABA_BR$) found in MLIs are tonically active

and their level of activity sets the 'basal tone' for PF-MLI EPSC amplitude *in vitro* (Kelly et al., 2009). Simulations IX and X reproduce the effects of modulating the activity of these metabotropic receptors *in vitro* using chemical agonists and antagonists by modifying γ in the synaptic weight update rule. By increasing γ, the MLI activity level needed to surpass the γw threshold for LTP is increased. Thus, if w begins near its equilibrium value for baseline PF and MLI activity and γ is increased, w will decrease to reach a new equilibrium. In Simulation IX, 8 PFs connected to a MLI all fire spontaneously at baseline rates of .33 Hz and 30 Hz, respectively, and the synaptic weights begin near their equilibrium values. Starting a five seconds, and continuing for 10 minutes, γ is raised from $\gamma = 1.0$ to $\gamma = 1.5$. The result is a gradual decay in the synaptic weight (Figure 4.5) which is consistent with observed LTD when applying $mGluR_1$ and $GABA_BR$ agonists *in vitro* (Kelly et al., 2009). Conversely, in Simulation X, by decreasing γ from $\gamma = 1.0$ to $\gamma = 0.5$ w increases to reach a new equilibrium, reproducing the effects of applying chemical antagonists of applying $mGluR_1$ and $GABA_BR$ antagonists *in vitro* (Kelly et al., 2009).

4.4 Discussion

In this study, we present a mathematical model of plasticity at PF-MLI synapses that describes bidirectional changes in synaptic efficacy as observed *in vitro*. The current model depends only on the pre- and post-synaptic neuronal activity and a dynamic threshold partly determined by a measure of synaptic efficacy. The dynamic threshold enables bidirectional changes in

efficacy and is inherently self-stabilizing. We show via computer simulations that the model reproduces similar changes in synaptic efficacy as observed in a variety experimental results. In addition, we simulate novel protocols which serve as predictions to be validated by future experimental investigation.

Table 4.4 Summary of Experimental Results

Sim.	Ref.	Experimental Protocol	Result	Interpretation
V	Liu and Cull-Candy (2000)	*In vitro*, MLI voltage clamped at -60 mV. 300 PF stimuli delivered @ 50 Hz. Bicuculline, picrotoxin, D-APV5.	LTD	Holding the MLI in voltage clamp prevents its spontaneous activity and prevents inward Ca^{2+} currents ($\downarrow$MLI). PF stimulation at 50 Hz increases PF activity above baseline ($\uparrow$PF). Δw = $\uparrow$PF($\downarrow$MLI-w) < 0
VI	Smith and Otis (2005)	*In vitro*, MLI current clamped at -80 mV. PFs stimulated (3-10 PFs) with 10 pulses at 100 Hz every 3 seconds for 5 minutes. Picrotoxin in bath.	LTP	Sufficient PF stimulation ($\uparrow$PF) increases MLI activity ($\uparrow$MLI) since current clamp allows the membrane potential to fluctuate. Δw = $\uparrow$PF($\uparrow$MLI-w) > 0
VII	Smith and Otis (2005)	*In vitro*, MLI current clamped at -80 mV. PFs stimulated (3-10 PFs) with at 1 Hz for 5 min. Picrotoxin in bath.	LTD	Low frequency PF stimulation is a slight increase in PF activity ($\uparrow$PF) but insufficient to increase MLI activity which is held in current clamp ($\downarrow$MLI) Δw = $\uparrow$PF($\downarrow$MLI-w) < 0
Similar to IV	Rancillac and Crépel (2004)	*In vitro*, MLI voltage clamp at -60 mV. Bicuculline in bath. Induction protocol of PF stimulation at .33 Hz for 8 minutes, then PF stimulated at 2 Hz for 60 seconds.	LTP/-/LTD	The induction protocol initially shifts $\downarrow$w to a new value w* since $\downarrow$MLI. The plasticity protocol then increases PF activity ($\uparrow$PF). Δw = $\uparrow$PF(MLI-w*) $\approx$ 0

Table 4.4 Summary of Experimental Results......................................, continued

Sim.	Ref.	Experimental Protocol	Result	Interpretation
VIII	Rancil lac and Crépel (2004)	*In vitro*, MLI voltage clamp at -60 mV. Bicuculline in bath. Induction protocol of PF stimulation at .33 Hz for 8 minutes, then PF stimulated at 2 Hz for 60 seconds with a paired MLI depolarization at 0 mV	LTP/-	The induction protocol initially shifts ↓w to a new value w* since ↓MLI. The plasticity protocol then increases PF activity (↑PF) and admits more Ca^{2+} possibly via NMDARs and VGCCs (↑MLI). $\Delta w = ↑PF(↑MLI\text{-}w^*) > 0$
---	Sun and Liu (2007)	*In vitro*, MLI held at -70 mV during stimulation followed by brief depolarization to 0 mV. GYKI in path (AMPAR blocker). PF 4 stimuli @ 50 Hz, 100 sweeps.	LTD	High frequency PF bursts (↑PF) paired with brief MLI depolarization, leads to spillover activation of NMDARs and limited Ca^{2+} influx via NMDARs. Since CP-AMPARs are blocked and MLI spontaneous activity is prevented via voltage clamp, the overall Ca^{2+} transient is below threshold (↓MLI). $\Delta w = ↑PF(↓MLI\text{-}w) < 0$
IX	Kelly et al. (2009)	*In vitro,* MLI voltage clamped at -60 mV. D-APV5, bicuculline in bath. Either DHPG (mGluR1 agonist) or baclofen (GABA$_B$R agonist) added.	LTD	Increasing mGluR Group I activity (↑mGluR) can be interpreted as increasing PF activity (↑PF). Additionally, ↑mGluR may directly increase the intracellular Ca^{2+} threshold required for plasticity (↑w). Increasing GABA$_B$R (↑GABA$_B$R) enhances mGluR activity, and a similar result holds. $\Delta w = ↑PF(MLI\text{-}↑w) < 0$

Table 4.4 Summary of Experimental Results...................................., continued

Sim.	Ref.	Experimental Protocol	Result	Interpretation
X	Kelly et al. (2009)	*In vitro,* MLI voltage clamped at -60 mV. D-APV5, bicuculline in bath. Either LY367385 (mGluR1 antagonist) or CGP62349(GABA$_B$R antagonist) added.	LTP	Decreasing mGluR activity adjusts the 'basal tone' by shifting the intracellular Ca^{2+} threshold for plasticity ($\downarrow$w). Ambient glutamate allows some Ca^{2+} to still flow into the MLI. Since GABA$_B$R enhances mGluR activity, $\downarrow$GABA$_B$R causes $\downarrow$mGluR, thus $\downarrow$w. Δw = PF(MLI-$\downarrow$w) > 0

4.4.1 Biological mechanisms of the model

The model presented in this study is a *phenomenological* description of plasticity that is a function of PF and MLI spiking activity and a measure of synaptic efficacy. This model serves as a high-level surrogate for describing plasticity until the detailed biological mechanisms are modeled directly. In this section, we speculate on what the underlying mechanisms are which give rise to this phenomenological description.

Plasticity at the PF-MLI synapses involves several mechanisms that produce both pre- and post-synaptic changes (Liu and Cull-Candy, 2000;Rancillac and Crepel, 2004;Bender et al., 2009). While we mainly focus on evidence for post-synaptic plasticity, it is expected that this model also accounts for pre-synaptic changes in synaptic efficacy in physiologically realistic conditions. Post-synaptic PF-MLI plasticity involves changes in the AMPA receptor (AMPAR) phenotype composition (Liu and Cull-Candy, 2000). Stellate-type MLIs, and presumably basket-type MLIs, express

glutamate receptor 2 (GluR2) lacking calcium-permeable AMPARs (CP-AMPARS) and GluR2-containing calcium-impermeable AMPARs (CI-AMPAR) and have been shown to make an activity dependent switch from CP- to CI-AMPARs (Liu and Cull-Candy, 2000, 2002; Kelly et al., 2009). CP-AMPARs admit more charge at negative potentials (Liu and Cull-Candy, 2000) so a switch from CP- to CI-AMPARs results in a functional decrease in the strength of this synapse. Thus, the mixture of CP/CI-AMPARs at the post-synaptic density determines the excitatory post-synaptic potential (EPSC) amplitude, or 'basal tone', of the synapse. Additionally, the level of tonic activation of mGluR$_1$ and GABA$_B$ receptors influence the basal tone of the synapse (Kelly et al., 2009). Both activity dependent LTP and LTD at this synapse are observed and are post-synaptic calcium signaling dependent (Liu and Cull-Candy, 2000;Rancillac and Crepel, 2004;Smith and Otis, 2005;Sun and June Liu, 2007).

We hypothesize that activity-dependent post-synaptic Ca^{2+} transients initiate changes in synaptic efficacy. These transients could induce both LTD and LTP dependent on a dynamic cytosolic Ca^{2+} threshold which could be reflected in the level of intracellular calcium stores. In the model proposed here, the dynamic threshold is captured by γw, where w captures the strength of the synapse in terms of CP- and CI-AMPAR makeup, and γ captures the effects of basal activity levels of metabotropic receptors involved in AMPAR phenotype composition. CP-AMPARs are one source of calcium influx. Indeed, the change in AMPAR phenotype composition could provide one mechanism for governing bidirectional changes in plasticity. The upper limit on synaptic efficacy could be governed by the dependence on sufficient amounts of calcium

influx simply to maintain the phenotype composition of the synapse since stronger synapses may require increasingly greater post-synaptic calcium concentrations simply to maintain or increase the strength of the synapse during periods of PF activation. This limit may be further enhanced by partial block of calcium influx through CP-AMPARs during physiologic activation due to intracellular polyamines (Bats et al., 2013). The lower limit on synaptic efficacy could be governed by the dependence of the CP- to CI-AMPAR switch on calcium influx through CP-AMPARs (Liu and Cull-Candy, 2000;Gardner et al., 2005;Liu and Cull-Candy, 2005).

NMDARs are another source of calcium influx for signaling changes in plasticity which are MLI activity dependent. Indeed, blocking NMDARs prevents LTP and even uncovers some LTD during PF stimulation *in vitro* (Rancillac and Crepel, 2004;Smith and Otis, 2005). MLI NMDARs are located extrasynaptically (Clark and Cull-Candy, 2002) and can be activated by a single PF firing at a sufficiently high frequency (Nahir and Jahr, 2013). Since PFs fire high-frequency bursts in physiologically realistic conditions (Chadderton et al., 2004;van Beugen et al., 2013), PFs likely activity NMDARs *in vivo* when firing bursts. Furthermore, climbing fibers (CFs) activate MLIs exclusively via glutamate spillover (Szapiro and Barbour, 2007) and CF mediated EPSCs have a significant NMDAR-mediated component (Coddington et al., 2013). Thus, CFs may play a special role in gating calcium influx and biasing plasticity towards LTP *in vivo*. This is consistent with adaptive filter models of cerebellar learning which require correlated PF and CF firing to induce LTP at these synapses (Dean et al., 2010).

The proposed model is also a function of PF and MLI activity which is a normalized, unit-less trace of the spiking activity of these neurons. Calcium

signals could be the common mechanism of conveying this activity. MLI somatic calcium concentrations change slowly as a function of the firing rate of these neurons (Franconville et al., 2011) and dendritic calcium concentrations are regulated by somatic spikes (Myoga et al., 2009). Thus, the firing rate of MLIs could produce a global time-varying calcium concentration in the dendrites of MLIs. Similarly, PF traces could be implemented using calcium signals since physiological PF firing results in prolonged glutamate conductances, and thus calcium influx, at MLI synapses (Carter and Regehr, 2000). Furthermore, changes in PF-MLI synapses are input-specific due to localized synaptic Ca^{2+} signaling in MLI dendrites (Soler-Llavina and Sabatini, 2006). Thus, a synapse specific trace of PF activity may use a sustained level of glutamate at the synapse and local calcium concentrations in the post-synaptic membrane.

4.4.2 Limitations of the model

The model is limited to describing plasticity at the level of pre- and post-synaptic activities and is thus unable to simulate certain physiological conditions from past experimental protocols (Table 4.4). In particular, calcium currents from AMPARs and NMDARs are not directly accounted for in this model and their influence is based on their collective ability to depolarize the MLI. This makes simulating chemical NMDA channel block and voltage-dependent calcium conductances, such as holding the MLI in voltage clamp at 0 mV, (as in Simulation VIII) impossible. In addition, the effect of modulating metabotropic receptor activities and their downstream effects cannot be modeled directly. The model is also unrealistic in that changes in synaptic efficacy happen instantaneously whereas changes *in vitro* and *in vivo*

continue to take place for several minutes after stimulation (Rancillac and Crepel, 2004;Smith and Otis, 2005).

4.4.3 Related models of plasticity

BCM theory (Bienenstock et al., 1982) is a model of plasticity used to describe activity dependent synaptic changes in the visual cortex which also employs a dynamic threshold to induce bidirectional changes in synaptic efficacy. Using the BCM model in lieu of the gated steepest descent model would not reproduce all of the experimental results described here. This can be seen using Simulation V as an example. Using a trace of MLI spiking for the post-synaptic activity in the BCM weight update equation would result in no weight change when the MLI is held in current clamp since this trace is effectively zero and all other terms of the weight update equation are multiplied by this term.

A number of other models of cerebellar learning have either explicitly or implicitly modeled learning at PF-MLI synapses, but most of these models were proposed before any experimental evidence describing plasticity at this synapse existed. Kenyon (1997) proposed a model where changes in PF-PKJ synapses are consolidated into long-term memories at PF-MLI synapses, but the weight update equation used doesn't appear to be consistent with experimental evidence. Albus (1971) also predicted learned changes to PF-MLI synapses but suggested that CF inputs act to weaken PF-MLI synapses, similar to PF-PKJ synapses. Adaptive filter models of cerebellar learning have been proposed that use positive and negative values for adaptive weights which implicitly defines plasticity at MLI synapses that is complementary and synergistic to PF-PKJ learning (Dean et al., 2010).

Finally, a modified gated steepest descent learning rule has also been used to model plasticity at the synapses formed by mossy fibers onto neurons in the deep cerebellar nuclei/vestibular (Yamazaki et al., 2015). Simulations using this model reproduce post-training memory consolidation in learned gain changes of the optokinetic response.

4.4.4 Extending the model

Concomitant PF and climbing fiber (CF) activation leads to a drastic increase in the PF-MLI receptive field (RF) and subsequent PF stimulation alone leads to a decrease in the MLI RF (Jorntell and Ekerot, 2002;2003;2011). The increased RF could be due to activation of electrically silent synapses, however the mechanisms governing this process are not understood. One way to augment the current model is to include a separate equation for plasticity at electrically silent synapses that requires concomitant activation of PF and CF input in order for a synapse to become electrically active. In simulations, this would result in an increase in the number of synapses that depolarize the target MLI and an effective increase in the RF size.

CFs may also influence plasticity at active synapses in two ways: indirectly, by increasing MLI firing rates thus favoring LTP, and directly, by modulating the threshold for plasticity through γ − capturing the effects of glutamate spillover and changes in post-synaptic calcium concentration due to activation of NMDARs and CP-AMPARs. Note that this would be a separate mechanism than modulating metabotropic receptors to modulate γ. This could be implemented where γ is a function of the activity of CFs or the spillover of glutamate from CF inputs to the MLI. When CFs are inactive (active) or the

volume of glutamate spillover is low (high), γ would be high (low). This mechanism would bias PF-MLI synapses with concomitant PF and CF activation towards potentiation by lowering the threshold in favor of LTP. Subsequently, if the PF were active without concomitant CF activation, the synapse might weaken since γ and thus γw is higher than before. This could be one mechanism for observing decreases in PF receptive field sizes with PF stimulation subsequent to a PF+CF protocol which results in PF receptive field increases (Jorntell and Ekerot, 2002). Homeostatic plasticity (Turrigiano, 2012) such as synaptic scaling may be another mechanism that reduces receptive field sizes over time or causes electrically active synapses to become inactive.

The model can also be extended to model calcium concentrations directly. Similar models based on BCM theory (Bienenstock et al., 1982) have been extended to model plasticity as a function of calcium concentrations which include influences from both AMPARs, NMDARs and action potentials (Shouval et al., 2002;Yeung et al., 2004). Indeed, the form of the equations governing plasticity as a function of calcium concentrations in these models is similar to the model presented here.

4.4.5 Interpretation of experimental results

A number of *in vitro* experimental protocols used to induce plasticity at PF-MLI synapses can be described in terms of the model presented in this study which also correctly predicts the experimental results. We present this interpretation and speculate on some of the biological mechanisms responsible for plasticity in each case. Table 4.4 summarizes selected experiments and their interpretations in terms of this model.

Early on, it was shown that high frequency stimulation of PFs while holding the MLI in voltage clamp at -60 mV induces a switch from CP- to CI-AMPARs (Liu and Cull-Candy, 2000), i.e. LTD. This result is predicted by the model since holding the MLI in voltage clamp decreases its activity relative to baseline ($\downarrow MLI(t)$), and stimulating PFs increases their activity relative to baseline ($\uparrow PF(t)$); i.e. $\Delta w \propto \uparrow PF(t)[\downarrow MLI(t) - \gamma w] < 0$ where $MLI(t) < \gamma w$. Chelating post-synaptic Ca^{2+} prevented the switch in AMPAR phenotype and resulted in no change in synaptic efficacy, supporting the idea that the mechanism of plasticity is calcium signaling dependent. Similarly, a separate study showed that a 30 Hz PF stimulation with the MLI held in voltage clamp leads to pre-synaptic LTD that is also dependent on post-synaptic Ca^{2+} influx (Soler-Llavina and Sabatini, 2006), suggesting a complementary form of LTD. While this is a different mechanism, it is consistent with the model prediction by the same reasoning.

In somewhat more realistic physiological conditions, high frequency PF burst stimulation was shown to induce LTP *in vitro* (Smith and Otis, 2005). This was demonstrated in two ways. In the first method, MLIs were held in current clamp at -80 mV while PFs were stimulated to fire brief high frequency bursts at 100 Hz. The bath contained picrotoxin to block inhibitory currents into the MLI. Following the plasticity protocol, LTP was measured directly by observing an increase in MLI spike firing in response to PF input compared to control conditions. In the second method, synaptic changes were induced indirectly by stimulating the PFs according to the same protocol but in a bath without picrotoxin and then recording responses from PKJs. After the protocol, PKJs initially had a higher firing rate due to PF-PKJ LTP,

followed by a period of spike depression caused by inhibition, presumably from increased MLI feedforward inhibition. Additional experimental evidence suggests increased depression appears to be due to PF-MLI potentiation and not from MLI-PKJ potentiation. The model predicts LTP in these experiments by $\Delta w \propto \uparrow PF(t)[\uparrow MLI(t) - \gamma w] > 0$ with $MLI(t) > \gamma w$ since the membrane potential of the MLI is able to fluctuate during PF stimulation in contrast to the protocol used in (Liu and Cull-Candy, 2000) where it is voltage clamped. Using the same LTP-inducing protocol in the presence of NMDAR antagonists, LTP is abolished and some LTD is uncovered (Smith and Otis, 2005). NMDARs are located extrasynaptically and can be activated by a high frequency train of PF stimulation (Carter and Regehr, 2000;Clark and Cull-Candy, 2002). This suggests the 100 Hz stimulation caused spillover activation of NMDARs and that this is important for LTP, presumably due to Ca^{2+} influx since chelating post-synaptic Ca^{2+} also blocked LTP (Smith and Otis, 2005). Using a low frequency stimulation protocol consisting of PF stimulation at 1 Hz for 5 minutes, PF-MLI LTD is observed both directly and indirectly (Smith and Otis, 2005). In the indirect case when the MLI is held in current clamp, the stimulus may be insufficient to perturb the MLI membrane potential significantly or to activate extrasynaptic NMDARs, thus the current clamp acts similar to voltage clamp as in previous experiments. The model also predicts LTD, i.e. $\Delta w \propto \uparrow PF(t)[\downarrow MLI(t) - \gamma w] < 0$.

Sun and June Liu (2007) investigated the role of NMDARs in the CP-to CI-AMPAR switch. To induce this change, MLIs were held in voltage clamp at -60 mV while chemically blocking AMPARs; PFs were stimulated to produce high frequency bursts that activated NMDARs and were paired with

fast, 1 ms, MLI depolarizations to 0 mV to release NMDAR Mg^{2+} block. A Ca^{2+} dependent CP- to CI-AMPAR switch was observed, suggesting that Ca^{2+} entry through NMDARs provide an additional pathway to induce plasticity at the synapse. While Ca^{2+} enters through NMDARs during the brief depolarization, it is insufficient to signal LTP since the normal spiking activity of the MLI, and thus cytosolic calcium concentration, is reduced by voltage clamp. The model would reflect this as $\Delta w \propto \uparrow PF(t)[\downarrow MLI(t) - \gamma w] < 0$ where $MLI(t) < \gamma w$.

Rancillac and Crepel (2004) found that holding the MLI in voltage clamp at -60 mV and stimulating PFs at 2 Hz resulted in a mix of LTP and LTD at the PF-MLI synapse. One explanation for the mix of LTP/LTD may be the result of the induction protocol used which held the MLI in voltage clamp at -60 mV while stimulating the PFs at .33 Hz for several minutes; this could decrease the synaptic strength and/or the dynamic threshold down during this period. During the experiment, the MLI activity is compared to the threshold for synaptic plasticity -- for some synapses, the low activation could be sufficient to surpass the threshold $(MLI(t) > \gamma w)$ and not for others $(MLI(t) < \gamma w)$. Thus, on average $\Delta w \propto \uparrow PF(t)[MLI(t) - \gamma w] \approx 0$. In contrast, when repeating this stimulation and pairing it with MLI depolarization at 0 mV more cells underwent LTP, indicating that post-synaptic activity plays a role in plasticity, i.e. $\Delta w \propto \uparrow PF(t)[\uparrow MLI(t) - \gamma w] > 0$. This form of LTP was independent of cAMP but required NO production. In another experiment stimulating PFs at 8Hz while holding the MLI in voltage clamp induced a mix of LTP or no change in tested synapses, but part of the LTP was cAMP dependent (Rancillac and Crepel, 2004). This last result in consistent with

(Bender et al., 2009) which showed pre-synaptic LTP dependent on cAMP through a similar induction protocol. These results reveal the complexity of synaptic plasticity at the PF-MLI synapse consisting of both pre- and post-synaptic mechanisms induced under artificial physiological conditions.

Kelly et al. (2009) found that activation of both mGluRs and CP-AMPARs is necessary and sufficient to drive the CP- to CI-AMPAR subunit switch and that activation of $GABA_BR$ enhances mGluR activity. Adding $mGluR_1$ agonists to the *in vitro* preparation results in LTD at the synapse. A similar effect is seen when adding $GABA_BR$ agonists to the bath. Assuming metabotropic receptors act to directly modulate the post-synaptic cytosolic calcium threshold used for bidirectional changes in plasticity, the effects of up-regulating these metabotropic receptor activities can be seen as increasing γ in the model, i.e. $\Delta w \propto PF(t)[MLI(t) - \uparrow \gamma w] < 0$. Similarly, adding $mGluR_1$and $GABA_BR$ antagonists results in LTP which can be interpreted as $\downarrow \gamma$.

4.5 Acknowledgements

Chapter 4, in part, has been submitted for publication of the material. William Lennon, Tadashi Yamazaki, Robert Hecht-Nielsen. The dissertation author is the primary investigator and author of this material.

4.6 Supplementary Figures
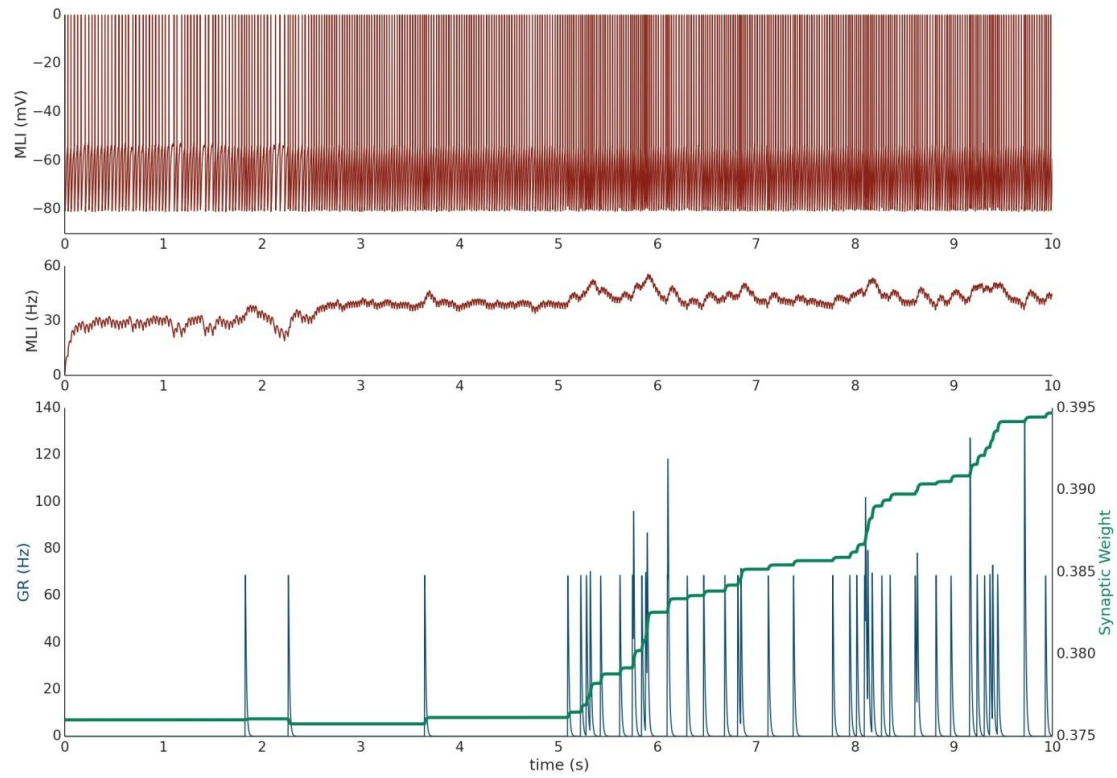
Figure 4.6 Simulation II. Conventions similar to Figure 4.1. See text for description.
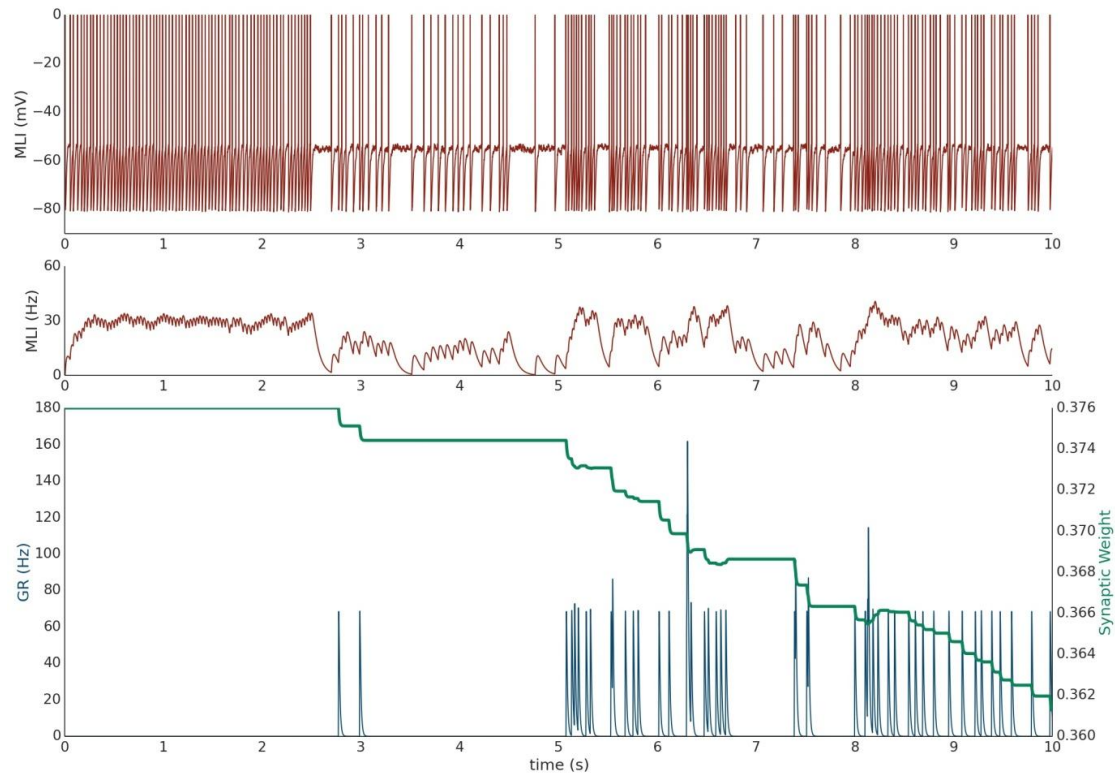
Figure 4.7 Simulation III. Conventions similar to Figure 4.1. See text for description.
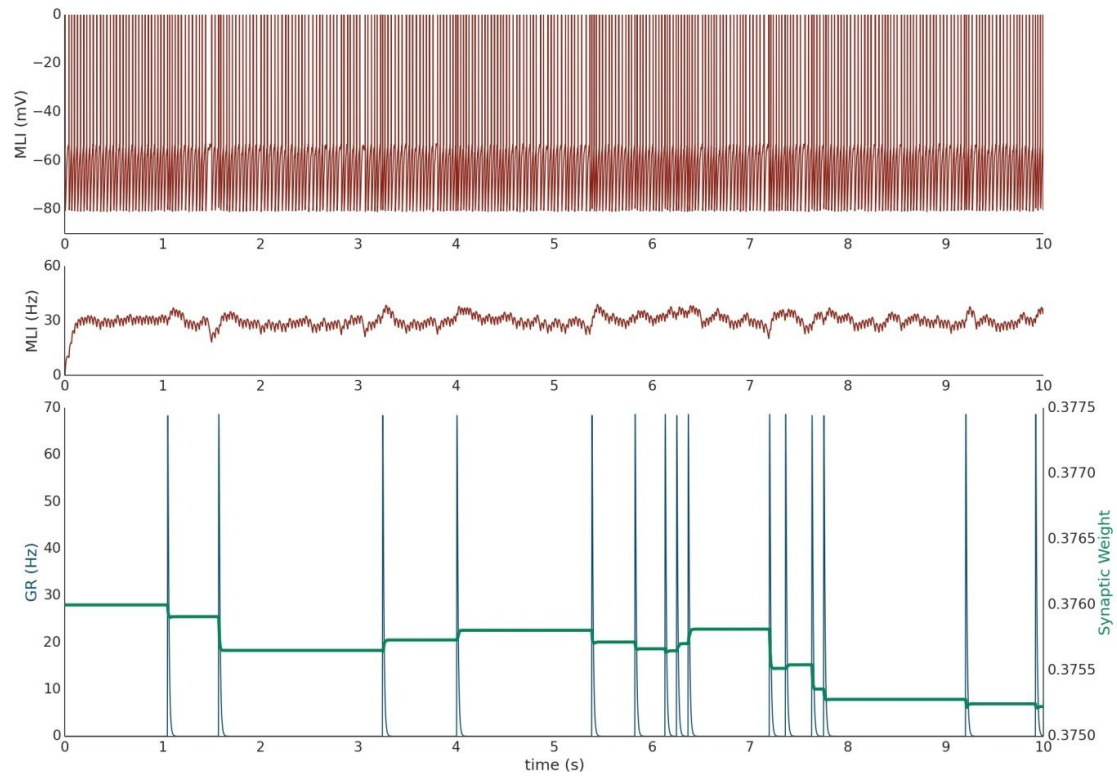
Figure 4.8 Simulation IV. Conventions similar to Figure 4.1. See text for description.

Figure 4.9 Simulation VII. Conventions similar to Figure 4.3. See text for description.

Figure 4.10 Simulation VIII. Conventions similar to Figure 4.3. See text for description.
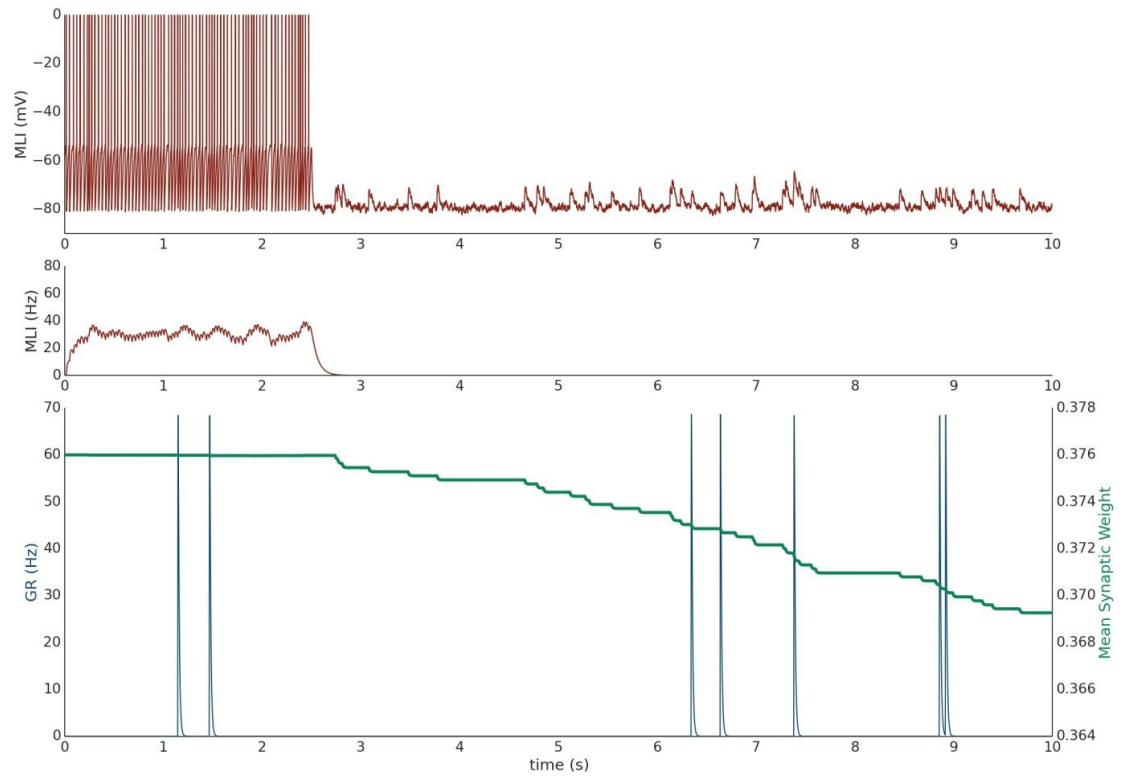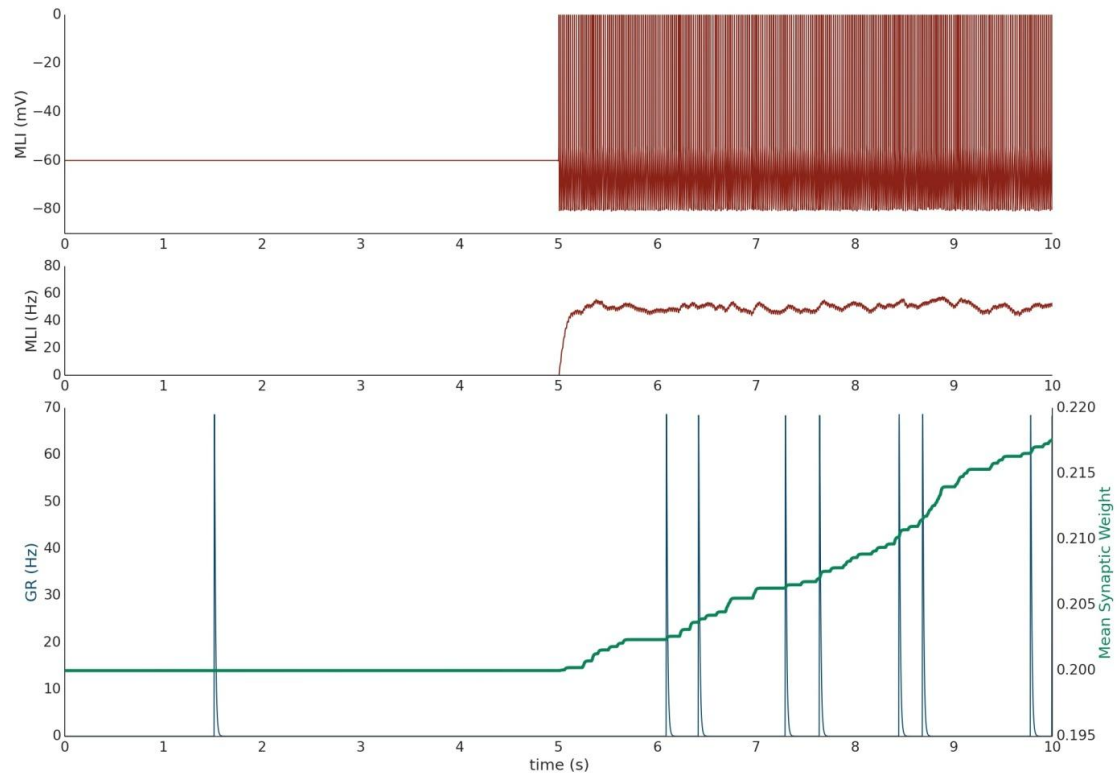
Figure 4.11 Simulation IX. Conventions similar to Figure 4.3. See text for description.
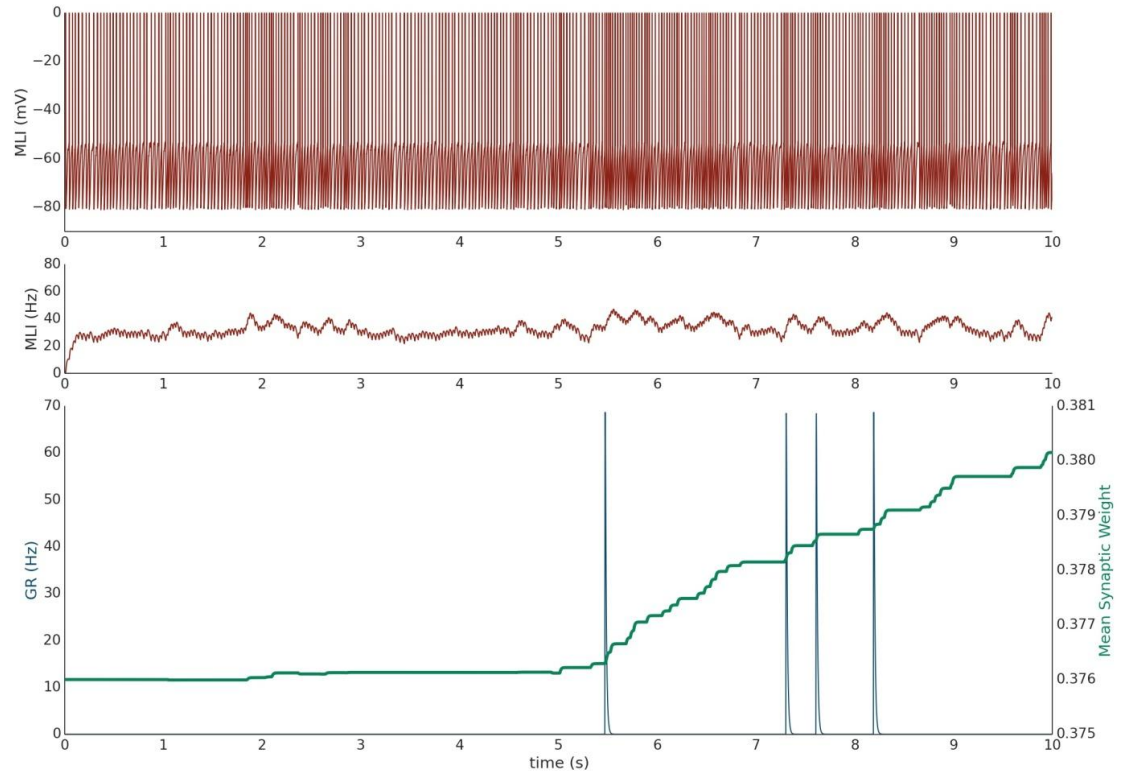
Figure 4.12 Simulation X. Conventions similar to Figure 4.3. See text for description.
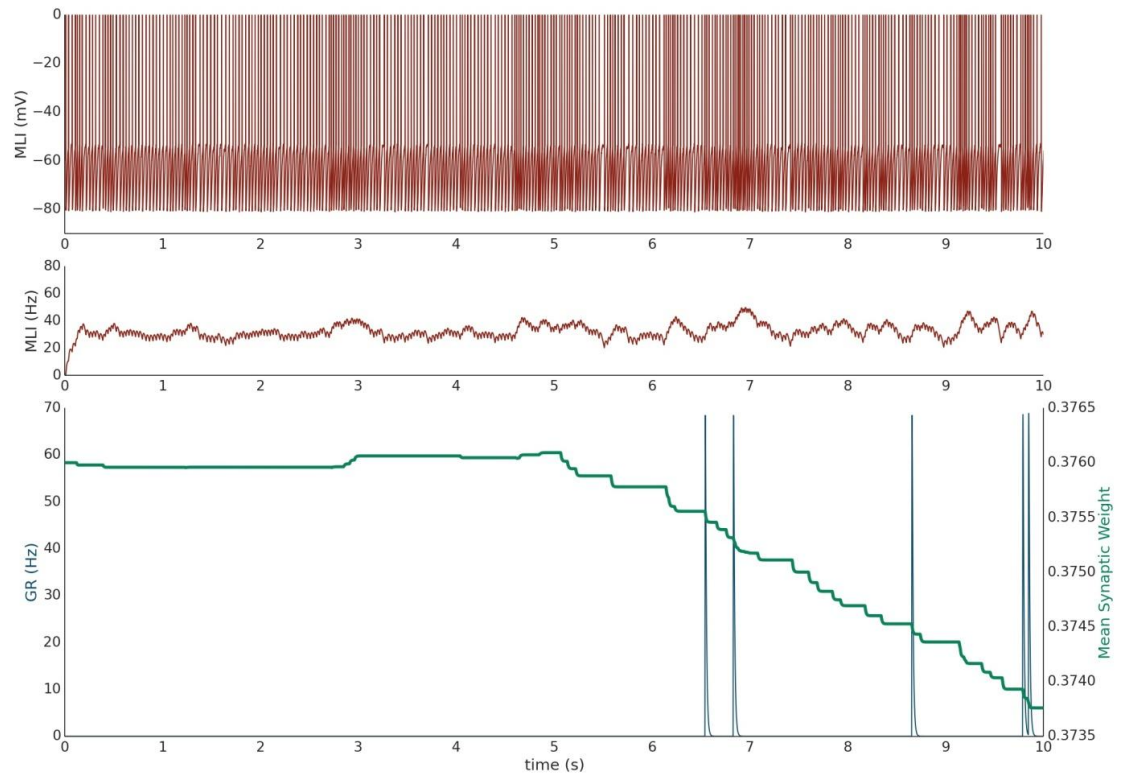
Chapter 5 Temporal difference learning at parallel fiber - molecular layer interneuron synapses

5.1 Introduction

The cerebellum is involved in producing smooth and coordinated movements to achieve the behavioral goals of an organism (Itō, 2012), but how the cerebellar circuitry achieves this is not understood. Achieving this performance requires repeated practice with sensory feedback for learning. Climbing fibers (CFs) are postulated to be a source of feedback motor error signals that enable learning in the cerebellar cortex (Bloedel and Bracha, 1998), however the *method* of learning in the cerebellar cortex is still under debate. One proposed paradigm is supervised learning (Doya, 1999) where climbing fibers convey directional error vectors and synaptic weights change to minimize this error signal. Another proposed paradigm is reinforcement learning (Swain et al., 2011;Magal, 2013) where climbing fibers convey scalar reinforcement or reward signals and synaptic weights change to maximize positive rewards or, equivalently, minimize negative rewards. In this study, we analytically show that a recently proposed mathematical model of parallel fiber (PF) - molecular layer interneuron (MLI) synaptic plasticity can be used to

show analytically that these synapses implement *temporal difference learning*, a type of learning used in reinforcement learning systems.

PF − Purkinje cell (PKJ) synapses are one location for CF-driven learning and memory in the cerebellum (Ito et al., 2014). Another, less well-studied location, is the PF-MLI synapse, where learning adjusts the amount of feedforward inhibition onto the PKJs by MLIs (Gao et al., 2012). Previously, we proposed a mathematical model of plasticity at the PF-MLI synapse (Chapter 4) which reproduces a number of experimental results of plasticity at this synapse via computer simulation. The mathematical model for learning at electrically active synapses takes the form of the *gated steepest descent* learning rule, a correlative, activity-dependent learning rule that allows for bidirectional changes in synaptic efficacy. Using this learning rule, and interpreting climbing fiber signals as reinforcement signals, we analytically show that PF-MLI synapses can be seen to implement *temporal difference learning* (TD-learning) (Barto et al., 1983;Sutton, 1988). Further, we show that the structure cerebellar cortical circuitry can be interpreted as a derivative of the Actor-Critic framework proposed by (Barto et al., 1983).

5.2 Background

TD-learning is a learning paradigm for iteratively updating an estimate of a value that depends on some future value of a signal (Barto, 2007). It is used in reinforcement learning to predict the expected value that being in some state will lead to a future reward (the signal). Since rewarding signals are typically temporally sparse, this paradigm learns to temporally backpropagate expectations of the reward to states which likely lead to the reward. Thus, an expected reward signal is created that is a function of state and is not

temporally sparse. In reinforcement learning, this new expected reward signal can be used to learn actions which lead to states with even higher expected rewards and ultimately to states with the actual reward. Barto et al. (1983) proposed the *Actor-Critic Framework* to achieve just this. The Actor-Critic framework consists of a *decoder* which receives *state* (i.e. sensory) information about a *controlled object* as input and transforms it into usable signals, $x(t) \in \mathbb{R}^n$, by the *controller*. The controller consists of an *actor* and a *critic*. The actor chooses actions or control signals based on the current state of the system, $x(t)$, which are most likely to lead to reward/reinforcement signals, $r(t) \in [-1,1]$. The *critic* receives the actual reinforcement signal and the current state information and learns to predict an expected value of reward for being in the current state, $p(t) = \sum_i x(t)_i z_i$, by modifying weights $z_i \in [0,1]$. The critic provides as output to the actor an *internal reinforcement signal,* $\hat{r}(t)$ (Equation 5.1), used for choosing the optimal actions, where $0 < \gamma < 1$ is a *discount factor*. The internal reinforcement signal consists of the actual reinforcement signal, a *discounted* current value estimate, and the value estimate from the moment immediately prior.

$$\hat{r}(t) = r(t) + \gamma p(t) - p(t-1) \tag{5.1}$$

The critic learns to predict as early as possible indications of future reward using TD-learning (Equation 5.2). $\bar{x}_i$ is a moving average trace of the ith input to the critic and β is a constant learning rate.

$$\Delta z_i = \beta \bar{x}_i(t)[r(t) + \gamma p(t) - p(t-1)] \tag{5.2}$$

The key insight into TD-learning is that by learning to predict future predictions of reward, i.e. $\gamma p(t) - p(t-1)$, the system learns to predict as early as possible any indication of future reward. This can be thought of as backpropagating the reward signal across states that likely lead to reward. The parameter γ results in an extinction of predicted value when external reinforcement disappears for a long time. Systems that implement this form of learning solve the temporal credit assignment problem of reinforcement learning.

5.3 Results

To begin, we introduce a model of the activity of MLIs. The firing rate of the kth MLI is modeled as a linear function of its inputs from a single CF, multiple PFs and laterally connected MLIs (Equation 5.3). $w_{k,i}$ is the synaptic weight from the ith PF to the kth MLI; $v_{k,j}$ is the synaptic weight of the jth MLI to the kth MLI. MLIs have been shown to form autapses and these are included in this formulation (Pouzat and Marty, 1998). MLIs also form gap junctions with other MLIs (Rieubland et al., 2014) which are not explicitly modeled here but could result in ensembles of MLIs acting in unison. If this were the case, we can consider $MLI_k(t)$ to be the kth MLI ensemble.

$$MLI_k(t) \stackrel{\text{def}}{=} CF(t) + \sum_i PF_i(t)w_{k,i} - \sum_j MLI_j(t-1)v_{k,j} \qquad (5.3)$$

A connection can be made to reinforcement learning by drawing an isomorphism between the components of the Actor-Critic framework and cerebellar circuitry. First, the climbing fiber can be interpreted as the

reinforcement signal, since it is known to convey motor error signals (a negative reward), is temporally sparse, and involved in learning and memory, i.e. $r(t) = CF(t)$. The granule cell - Golgi cell circuit acts as the decoder, receiving sensory information in the form of mossy fibers and passing a state signal along as PFs. The PF-MLI synapses learn to compute the discounted value estimate, i.e. $\gamma p_k(t) = \sum_i PF_i(t)w_{k,i}$. The recurrent inhibitory conductances from other MLIs provide the previous value estimate, i.e. $p_k(t-1) = \sum_j MLI_j(t-1)v_{k,j}$. Thus, the MLIs can be seen to act as the critic and through MLI-PKJ connections provide the internal reinforcement signal to PKJs -- the actor.

$$\hat{r}_k(t) = r_k(t) + \gamma p_k(t) - p_k(t-1)$$

$$\cong CF_k(t) + \sum_i PF_i(t)w_{k,i} - \sum_j MLI_j(t-1)v_{k,j} = MLI_k(t)$$

Equation 5.4 describes the learning law we proposed previously (Chapter 4), where β is a constant learning rate parameter, $\overline{PF}_l(t)$ is a trace of the lth PF input, $\overline{MLI}_k(t)$ is a trace of the kth MLI neuron in the target population, and $w_{k,l}$ is the value of the synaptic weight undergoing plasticity and it is implicit that this is $w_{k,l}(t-1)$.

$$\Delta w_{k,l} = \beta\overline{PF}_l(t)[\overline{MLI}_k(t) - w_{k,l}] \tag{5.4}$$

If we substitute $\hat{r}_k(t) \cong \overline{MLI}_k(t)$, as described previously,

$$\Delta w_{k,l} \cong \beta\overline{PF}_l(t)\left[r_k(t) + \gamma p_k(t) - p_k(t-1) - w_{k,l}\right]$$

$$= \beta \overline{PF_l}(t) \left[r_k(t) + \sum_i PF_i(t)w_{k,i} - p_k(t-1) - w_{k,l} \right]$$

$$= \beta \overline{PF_l}(t) \left[r_k(t) + \sum_{i \neq l} PF_i(t)w_{k,i} - \left(1 - PF_l(t)\right)w_{k,l} - p_k(t-1) \right]$$

Letting $\gamma \hat{p}_k(t) = \sum_{i \neq l} PF_i(t)w_{k,i} - \left(1 - PF_l(t)\right)w_{k,l}$,

$$= \beta \overline{PF_l}(t)[r_k(t) + \gamma \hat{p}_k(t) - p_k(t-1)] \tag{5.5}$$

Thus, we arrive at an equivalent form to the original TD-learning rule.

5.4 Discussion

We propose an interpretation of the cerebellum that draws correspondences between the Actor-Critic framework (Barto et al., 1983) and the functional cerebellar circuitry (Ito, 2006). The main result is that a theoretical model of learning at PF-MLI synapses can be seen to implement TD-learning.

The hypothesis that PF-MLI synapses implement TD-learning would predict that MLIs learn to predict motor error signals conveyed to the cerebellar cortex via climbing fibers. Indeed, a simple experimental paradigm exists for testing this prediction and preliminary evidence exists in support. The conditioned eyeblink response (CER) is a classical conditioning paradigm where an animal is presented with a conditioned stimulus (CS) -- usually a tone -- for several hundred milliseconds, and an unconditioned stimulus (US) -- usually an air puff to the eye -- for several tens of milliseconds which co-terminates with the CS (Thompson and Steinmetz, 2009). The CS causes the animal to reflexively blink. After many trials, the animal learns to blink in

response to the CS before the onset of the US to avoid the aversive US. This learned response is cerebellum dependent (McCormick and Thompson, 1984) and requires learning an appropriately timed PKJ response to the CS which is conveyed via the mossy fiber - parallel fiber input pathway into the cerebellum (Jirenhed et al., 2007). The climbing fibers convey the US which can be considered a reinforcement signal that reinforces the blink in response to the CS. If TD-learning were implemented at PF-MLI synapses, we would expect their activity to predict the arrival of the US upon presentation of the CS. Indeed, recordings from PKJs suggest feedforward inhibition from these neurons precedes the US and causes a decrease in the PKJ activity to disinhibits the deep cerebellar nuclei (DCN) which results in an eyeblink (Jirenhed et al., 2007). Preliminary evidence of direct recordings from stellate-type MLIs during this learned behavior also support this, while basket-type MLIs which receive PKJ recurrent collaterals synchronize to strongly inhibit PKJs immediately before the expected US onset (Halverson et al., 2014).More generally, the function of PF-MLI TD learning could be to predict motor errors and influence the activity of the PKJs towards choosing the appropriate output to mitigate these errors. Additional experimental investigation is needed to characterize the time-course of MLIs in naive and trained animal behaviors.

A number of differences between the Actor-Critic framework and the cerebellar circuitry exist as described in the Results. First, PKJs also receive CF inputs which drive PF-PKJ long term depression at these synapses. However, the Actor-Critic framework does not have the reinforcement signal conveyed directly to the 'actor'. Second, the output of the 'critic' is used in the 'actor' learning rule directly and does not directly affect the "activity" of the

'actor'. In the cerebellum, MLI output to PKJs provide feedforward inhibition to PKJs, directly affecting the PKJ activity. Finally, the model assumes that the targets of the PKJ -- the DCN -- are the 'controlled object'. One could also consider the network formed by the MLIs and PKJs as the 'critic' and the DCN as the 'actor'. Future theoretical work is needed to validate this idea, however.

5.5 Acknowledgements

Chapter 5, in part, is currently being prepared for submission for publication of the material. William Lennon, Tadashi Yamazaki, Robert Hecht-Nielsen. The dissertation author is the primary investigator and author of this material.

Chapter 6 Conclusion and Future Work

For more than 30 years of experimental and theoretical study, the molecular layer interneurons have been relegated to the background of cerebellar neuroscience. Like many inhibitory interneurons throughout the rest of the brain, the MLIs were once thought to simply provide "blanket" inhibition to the principal neurons (in this case the Purkinje cells) to prevent runaway activity. Through a series of surprising experimental results, the MLIs came to the foreground of study and in the past few years have been recognized by the cerebellar neuroscience community as playing a critical role in cerebellar learning and function. With the advent of new tools such as optogenetics and genetic knockouts, the next decade will be an exciting era of study of the molecular layer interneurons.

6.1 Future Work

Throughout the course of performing research a myriad of possibilities for further investigation inevitably present themselves. This section will briefly describe the next steps in extending the research described in this dissertation.

6.1.1 Improvements to the MLI-PKJ network

A number of improvements can be made to the MLI-PKJ network described in Chapter 3 to make it more biologically plausible. These improvements should endow the network with greater information processing

capabilities whose function can be investigated via simulation. We list a number of improvements that can be made below.

6.1.1.1 Add gap junctions to MLI-PKJ network

Gap junctions connect nearby MLIs in a patterned way and allow small amounts of current to flow between connected neurons (Rieubland et al., 2014). Gap junctions could enable connected neurons to quickly synchronize their activity and enable high frequency oscillations in MLIs. Since MLIs form inhibitory synapses with each other, gap junctions could operate like very fast, low gain excitatory synapses. This could result in *cell assemblies* of MLIs that become excited in response to stimulus (e.g. a sequence of PF input activity).

6.1.1.2 Add more realistic connectivity to MLI-PKJ net

We now know more details about the pattern of synaptic connectivity between the MLIs (Rieubland et al., 2014). This should be incorporated into a new iteration of the network model and can be done so with relative ease using the published code (Lennon et al., 2014) and Brian Simulator framework (Goodman and Brette, 2009).

6.1.1.3 Improve parallel fiber synaptic model: STP and probabilistic neurotransmitter release

Parallel fiber synapses exhibit rapid dynamics whereby increased amounts of neurotransmitter are released with shorter intervals between PF spikes (Goto et al., 2006;Bender et al., 2009). This phenomenon is known as short term plasticity (STP) and probably plays an important role in cerebellar information processing. STP has been proposed to act as a filtering mechanism for information transmission (Abbott and Regehr, 2004). It may also be

involved in producing sequences of activity in the target neuron population --
MLIs and PKJs.

An additional feature present in biologically PF synapses is probabilistic
release. Biological synapses do not release neurotransmitter in response to the
arrival of an action potential with perfect fidelity. PFs in particular exhibit
relatively low probabilities of releasing neurotransmitter (Bender et al., 2009).
This stochastic component should be included in the synapse model.

6.1.1.4 Improve neuron models

More realistic neuron models that capture the morphology and
membrane dynamics should be incorporated into the model. PKJs are large
neurons with complex dendritic morphology that most likely endows these
neurons with powerful information processing capabilities. The PKJ neurons
simulated in this dissertation are considered point models since they do not
directly model the volume and morphology of PKJs. By modeling PKJ
morphology, the model can also take advantage of the diversity of phenotype
of MLI morphology -- a gradient ranging from basket type to stellate type (see
Chapter 2 for details). In particular, the model can take advantage of
axodendritic synapses made by stellate cells onto PKJ dendrites that play a
role in local information processing in contrast to the more global inhibition by
basket-type synapses. Modeling membrane dynamics is important to capture
the *transfer function* implemented by these neurons. PKJs exhibit dynamics
where their firing rate can exist in multiple modes: spontaneous firing,
quiescence and periodic pauses in firing (Engbers et al., 2013).

6.1.2 PF-MLI Plasticity

6.1.2.1 Experimentally test plasticity model prediction

The model presented in Chapter 4 makes explicit predictions about the changes in synaptic efficacy based on different stimulation and MLI activity levels. Some experiments that have not been performed *in vitro* include stimulating the PF to a high rate of activity while allowing the MLIs to fire spontaneous (not voltage or current clamped). The model predicts a potentiation of synapses. Further experiments should investigate the role of climbing fiber activity to test whether it modifies the plasticity threshold as proposed.

6.1.2.2 Cerebellum network simulation with PF-MLI learning on multiple behavioral tasks

A full-scale model of the cerebellum should be implemented that includes the cerebellar cortex, deep cerebellar nuclei, and inferior olive. A starting place is to extend Yamazaki and Nagao (2012) by replacing the MLI-PKJ network in that model with Lennon et al. (2014) (the code for both models is freely available online). We describe preliminary experiments with this setup in Appendix A, however the PF-MLI plasticity implemented is not consistent with the learning rule proposed in Chapter 4. Finally, modify the GR neuron model to exhibit bursting dynamics. This model should be applied to learning on multiple behavioral tasks such as the optokinetic response (OKR), vestibulo-ocular reflex (VOR) learning, VOR phase reversal, and conditioned eyeblink response (CER). The latter is the simplest to implement and make predictions for. One prediction is that due to the PF-MLI learning rule implemented, MLIs learn to begin firing during the conditioned stimulus

and long before the onset of the conditioned stimulus (see Discussion of Chapter 5).

6.1.2.3 Biophysical Model PF-MLI learning

The PF-MLI learning model presented in Chapter 4 is a *phenomenological* model of learning based on the activities of PF, MLI and CF inputs. As such, it is difficult and/or impossible at times to explain the mechanisms of plasticity at a biophysical level. The current model should be extended to explain changes in synaptic efficacy as a function of changes in Ca2+ concentrations and eventually downstream signaling cascades (see discussion of Chapter 4). The work of Shouval et al. (2002) should be valuable as guidance.

6.1.3 MLI-MLI and MLI-PKJ Plasticity

Plasticity is known to occur at MLI-MLI and MLI-PKJ synapses (Gao et al., 2012), however a mathematical formulation of learning or "learning rule" has not been proposed. Understanding how plasticity is governed at these synapses will greatly enrich our understanding of the role of MLIs in cerebellar function. While PF-MLI plasticity may capture stimuli statistics and encode a control signal as their sequence of activity, this is relatively useless unless it appropriately affects PKJ activity. Achieving this requires tuning MLI-PKJ synapses. One possible scheme may be that sequences of MLI ensembles may encode control signals and MLI-PKJ synapses are tuned to either use or ignore them. Thus, understanding plasticity is key to utilizing MLI activity.

6.2 The Future

Computational neuroscience is a promising approach for solving problems in intelligent systems, robotics and control. If we understand the brain well-enough to simulate it, then endowing machines with brain-like capabilities is corollary. The cerebellum is one piece of this puzzle.

Presently, the human brain is the pinnacle of known intelligence, but even mice are more capable than today's best machine learning and control algorithms on many tasks. Theoretically, brain simulations will enable machines to *perceive* and *understand* the world as we do, to *control* their robotic anthropomorphic bodies as we do, and *imagine* and *feel* as we do. This possibility is both exciting and terrifying. Today, we are just beginning to understand the brain well enough to build brain simulations that perceive and perform elementary control. True *simulated intelligence* is probably over a century away. However, by understanding the principles of brain function, we can design powerful new applications in both perception and control that will greatly benefit the world.

6.3 Farewell

The cerebellum is a beautiful and fascinating brain structure with untold treasures waiting to be discovered. It is a rich system for study that provides rigorous training as a theoretical and computational neuroscientist -- covering neuroanatomy, neurophysiology, mathematics, and numerical methods in an accessible way for rapid progress. My work on the cerebellum studying the molecular layer interneurons was largely about overcoming biases in the mental models built up by the cerebellum neuroscience community over

the past several decades. I should state that even my own mental model of cerebellar function (see Chapter 2) excludes exhaustive understanding of a number of neuron types in the cerebellum; namely, unipolar brush cell and Lugaro cells. So, I too fall victim to certain biases. More generally, my mental model does not fully incorporate the role of certain connections and nuclei, sometimes due to lack of data. In particular, further investigation into the pontine nuclei, parvocellular red nucleus and inferior olive will likely lead to surprising results. I leave it to the next scientist to expose these biases and build upon the best models available at that time.

And that's all I have to say about that.

Appendix A   Cerebellum network simulations with parallel fiber plasticity

We simulated a learned optokinetic response (OKR) using the network model from Yamazaki and Nagao (2012) but replacing the MLI-PKJ network with the one described in Lennon et al. (2014). We simulate learning at PF-PKJ and PF-MLI synapses. The learning rule for PF-MLI synapses is complementary and synergistic to learning at PF-PKJ synapses, a theory espoused by some (Gao et al., 2012); however, it is not the learning rule described in Chapter 4.

A.1 Introduction

The functional role of the molecular layer interneurons (MLIs) (basket and stellate cells) in the cerebellar cortex is poorly understood. Experimental evidence from genetically modified mice lacking MLI feedforward inhibition onto Purkinje cells (PKJs) show significant impairments in their ability to consolidate VOR gain down learning over 24 hours and their ability to learn VOR phase reversals (Gao et al., 2012). These deficits suggest a significant role for MLIs in cerebellar function. To investigate the role of MLIs, we extend a spiking neural network model of the cerebellum (Yamazaki and Nagao, 2012) to account for MLI physiology, anatomy and plasticity at the parallel fiber (PF) - MLI synapses. We model MLIs as conductance-based leaky integrate-

and-fire neurons with a spontaneous depolarizing current and physiological parameters derived from the literature. We model plasticity at the PF-MLI synapse as a complementary and synergistic form of learning to plasticity at the PF-PKJ synapse, as argued by some (Gao et al., 2012). The network successfully learns an appropriate opto-kinetic response (OKR) given simulated mossy fiber (MF) and climbing fiber (CF) input. The network also exhibits additional physiological phenomena observed *in vivo:* blocking GABA shifts PKJ firing rate from out-of-phase with MF input to in-phase, as observed in the VOR (Miyashita and Nagao, 1984).

A.2 Simulated Behavior

We simulate the OKR -- a learned eye reflex that moves the eye in the opposite direction of a slowly moving visual scene to reduce image blur on the retina (Itō, 2012). Mossy fibers convey retinal information from the brainstem optic nuclei (accessory optic system (AOS), nucleus reticularis tegmenti pontis (NRTP)) about the flow of the visual scene. Figure A.1 shows the cerebellar and brainstem circuitry in a schematic system which receives visual input of a moving grating pattern. The IO also receives retinal slip information and conveys it to the cerebellar cortex via CFs. The output of the cerebellum -- via the vestibular nuclei (VN) -- sends control signals to the brainstem motor nuclei that control the muscles of the eye (AN and ON here).
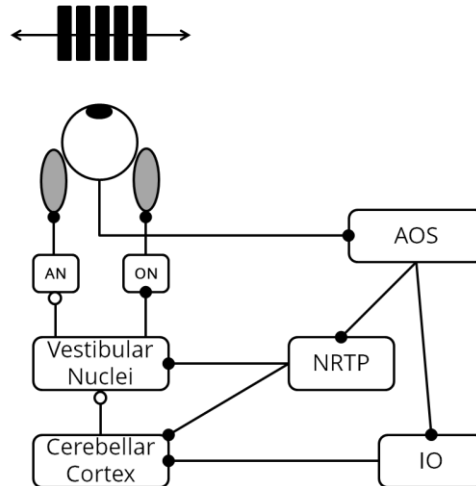
Figure A.1 OKR model schematic. Model of the brainstem nuclei and cerebellum responsible for OKR learning

A.3 Network Model

The model simulated is identical to network presented in Yamazaki and Nagao (2012) except that the MLI-PKJ network has been substituted for the one presented in Lennon et al. (2014). The network is depicted in Figure A.2. The network consists of a 160x160 grid of granule cells (GRs) and 32x32 grid of Golgi cells (GRs). GRs received mossy fiber (MF) input and send their outputs to GOs, MLIs and PKJs. GOs in turn provide reciprocal inhibition to GRs. Mossy fibers are simulated as Poisson spike trains with a variable rate that is sinusoidally modulated to represent sinusoidally modulated visual input from a visual grating pattern oscillating back-and-forth horizontally. Similarly, a single climbing fiber connecting to all MLIs and PKJs conveys a Poisson spike train with rate parameter modulated according to the
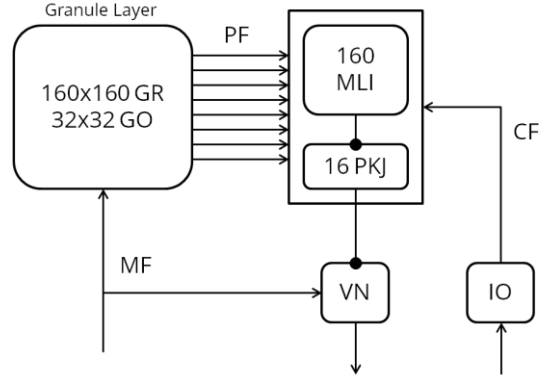
**Figure A.2** Cerebellum network model. The MLI-PKJ net is identical to the network in Lennon et al. (2014).

A.4 Plasticity Model

$$PF \text{ - } PKJ \; : w_{j,i} \leftarrow w_{j,i} + c_{LTP} \, (\hat{w} - w_{j,i}) PF_i(t) - c_{LTD} \, w_{j,i} \sum_{\Delta t = 0}^{50} CF(t) PF_i(t - \Delta t) \qquad (A.1)$$

$$PF \text{ - } MLI \; : v_{j,i} \leftarrow v_{j,i} - d_{LTD} \, v_{j,i} PF_i(t) + d_{LTP} \, (\hat{v} - v_{j,i}) \sum_{\Delta t = 0}^{50} CF(t) PF_i(t - \Delta t) \qquad (A.2)$$

A.5 Results

Figure A.3 shows the GR response to the input stimuli. Figure A.4 shows the MLI and PKJ response to the GR response (via parallel fibers) in the untrained model. After 150 trials, the model changes the PF-MLI and PF-PKJ synaptic weight sufficiently to reverse the phase of the PKJ response (Figure A.5). MLIs now firing in-phase with the GRs; previously their weights were so low the GRs had only a minor effect on their firing rates. Simulating block of feedforward inhibition shifts the PKJ response 180 degrees out of phase (Figure A.6). This reproduces the results seen in Miyashita and Nagao (1984).
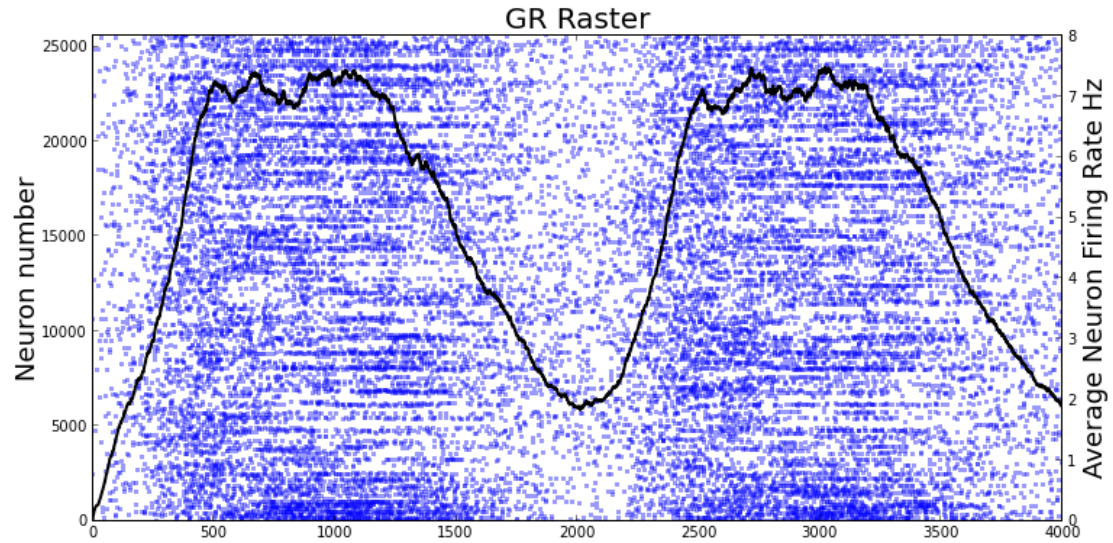
Figure A.3 The raster plot is the granule cell population response to sinusoidally modulated visual input via the mossy fibers. The climbing fiber response (not shown) is a Poisson spike process with sinusoidal rate in phase. Two cycles of the OKR are shown. All plots: sub-population raster plot (blue) with population mean firing rate superimposed (black).
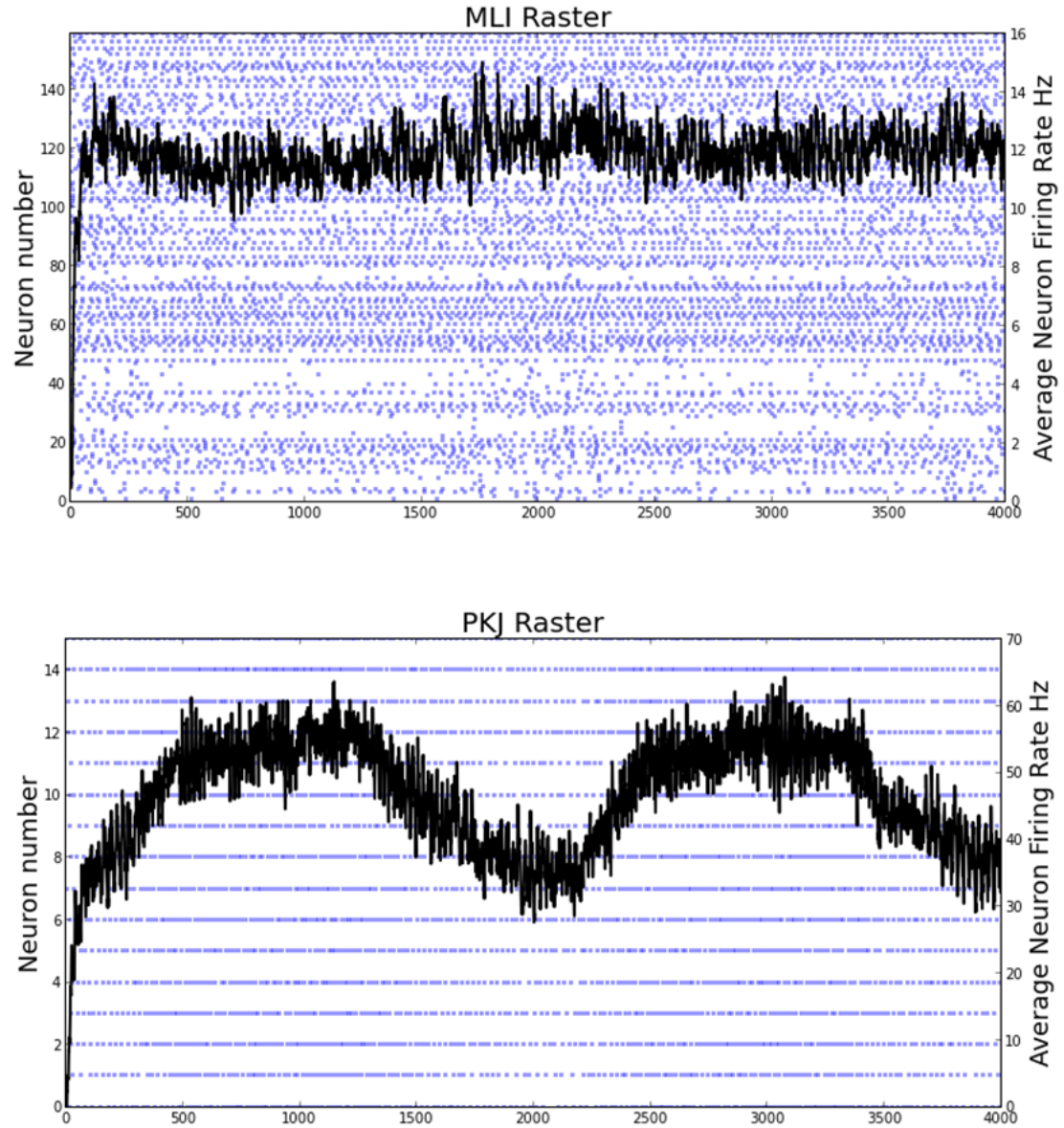
Figure A.4 MLI and PKJ response to PF input in naive model. In the untrained model, parallel fiber input strongly activates PKJs, modulating their firing rate in phase. The MLIs hardly respond since the PF-MLI weights are initialized small.
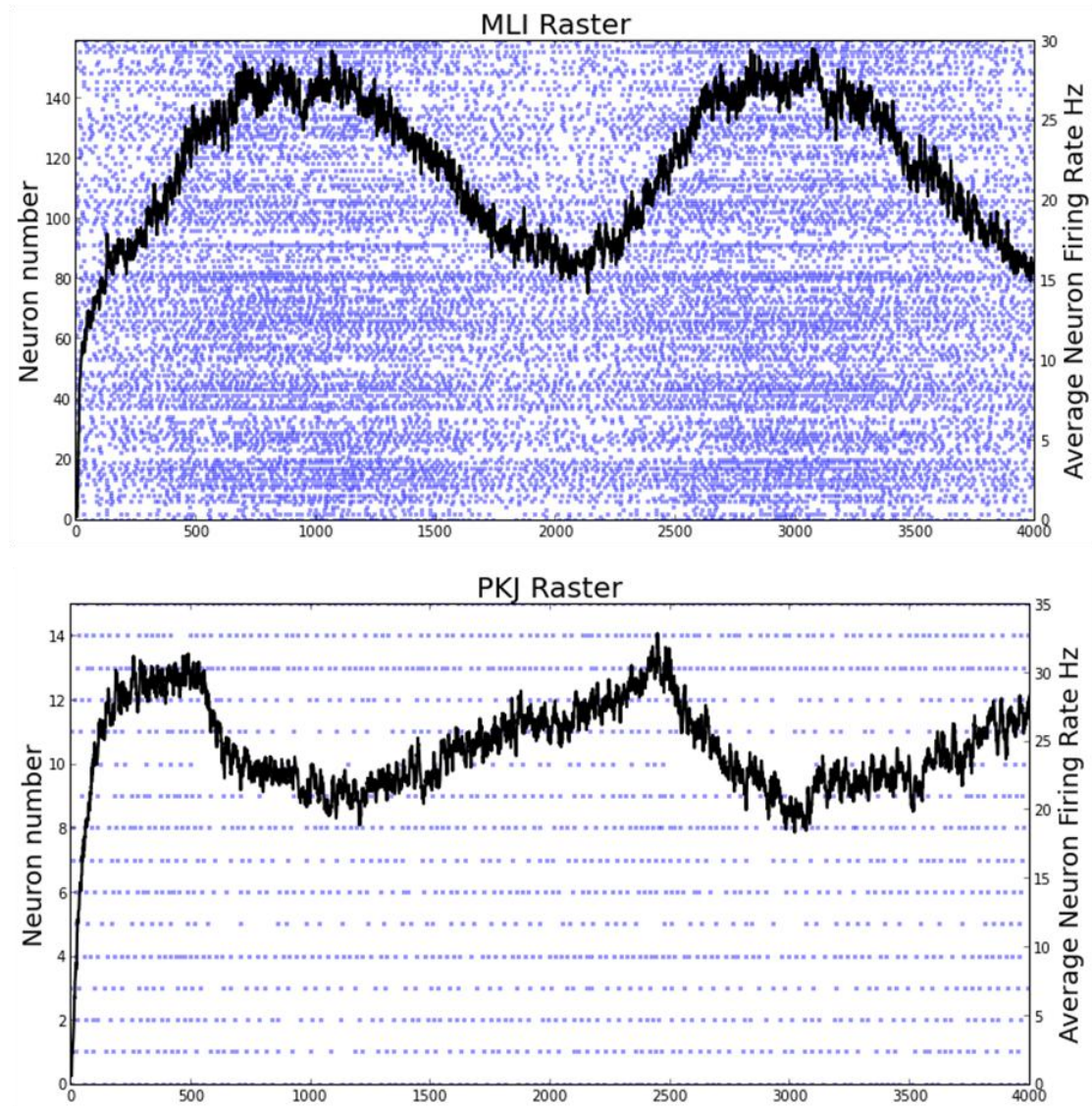
Figure A.5 MLI and PKJ response to PF input in trained model. After 150 trials, the model learns to decrease the PKJ firing rate (as observed in vitro) to disinhibit the DCN to increase the gain of the eye movement. The MLIs now fire in phase with the PF input and provide feedforward inhibition to the PKJs.
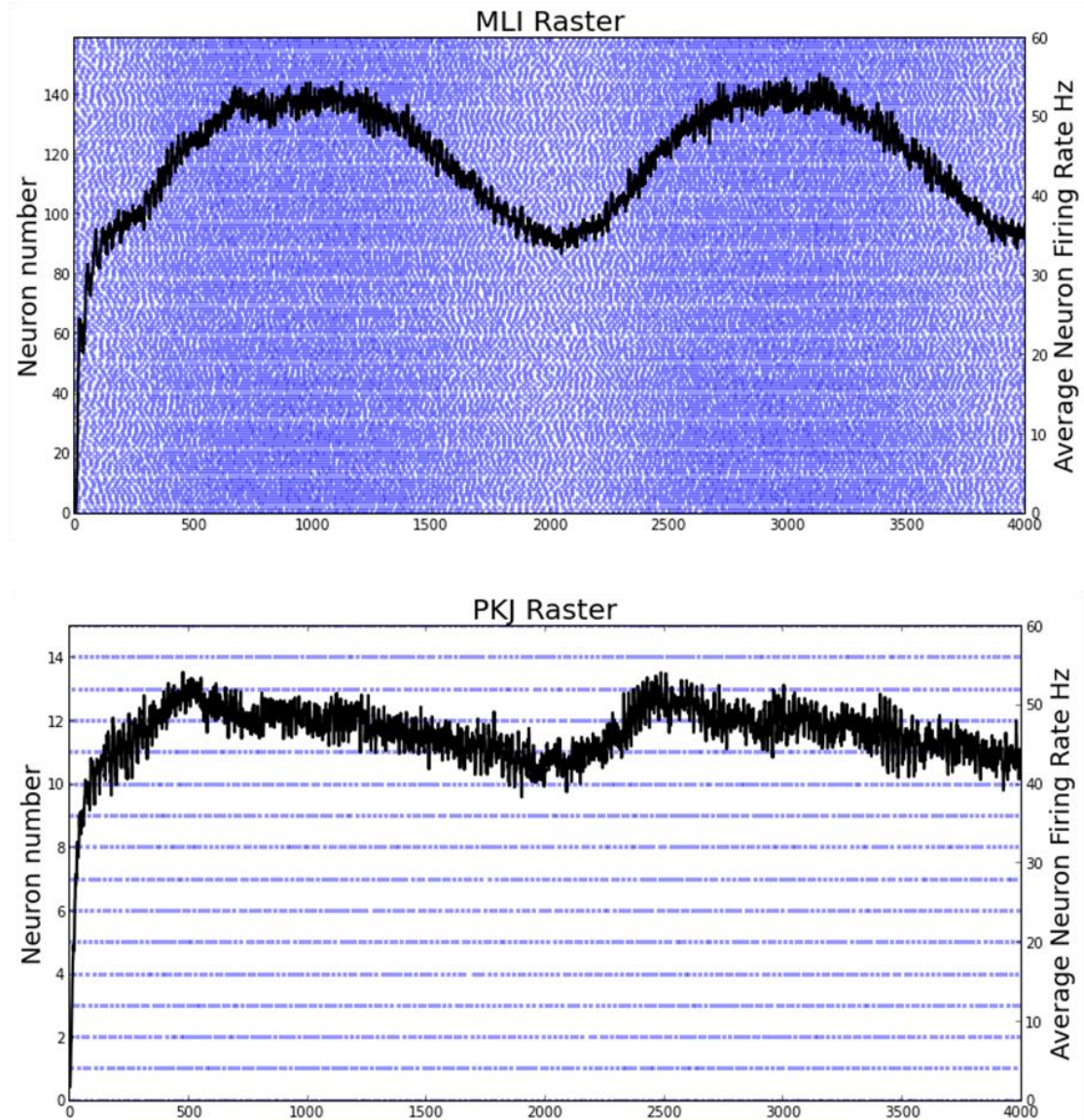
Figure A.6 MLI and PKJ response to PF input in trained model. Response of the trained model with GABA blocked (simulated). Notice the baseline firing rate of the PKJ shifts up compared to D. Also, the firing rate is now in-phase with the MF and PF input. We see a shift from out-of-phase to in-phase as in Miyashita and Nagao (1984).

References

Abbott, L.F., and Regehr, W.G. (2004). Synaptic computation. Nature 431, 796-803.

Aizenman, C.D., and Linden, D.J. (1999). Regulation of the rebound depolarization and spontaneous firing patterns of deep nuclear neurons in slices of rat cerebellum. J Neurophysiol 82, 1697-1709.

Albus, J.S. (1971). A theory of cerebellar function. *Mathematical Biosciences* 10, 25-61.

Apps, R., and Hawkes, R. (2009). Cerebellar cortical organization: a one-map hypothesis. *Nat Rev Neurosci* 10, 670-681.

Armstrong, D.M., and Edgley, S.A. (1984). Discharges of Purkinje cells in the paravermal part of the cerebellar anterior lobe during locomotion in the cat. *J Physiol* 352, 403-424.

Barto, A. (2007). Temporal difference learning. *Scholarpedia* 2, 1604.

Barto, A., Sutton, R., and Anderson, C. (1983). Neuronlike adaptive elements that can solve difficult learning control problems. *IEEE Transactions on Systems, Man and Cybernetics* 13, 835-846.

Bats, C., Farrant, M., and Cull-Candy, S.G. (2013). A role of TARPs in the expression and plasticity of calcium-permeable AMPARs: evidence from cerebellar neurons and glia. *Neuropharmacology* 74, 76-85.

Bender, V.A., Pugh, J.R., and Jahr, C.E. (2009). Presynaptically expressed long-term potentiation increases multivesicular release at parallel fiber synapses. *J Neurosci* 29, 10974-10978.

Bienenstock, E.L., Cooper, L.N., and Munro, P.W. (1982). Theory for the development of neuron selectivity: orientation specificity and binocular interaction in visual cortex. *J Neurosci* 2, 32-48.

Bloedel, J.R., and Bracha, V. (1998). Current concepts of climbing fiber function. *Anat Rec* 253, 118-126.

Bower, J.M. (2010). Model-founded explorations of the roles of molecular layer inhibition in regulating purkinje cell responses in cerebellar cortex: more trouble for the beam hypothesis. *Front Cell Neurosci* 4.

Brunel, N., Hakim, V., Isope, P., Nadal, J.P., and Barbour, B. (2004). Optimal information storage and the distribution of synaptic weights: perceptron versus Purkinje cell. *Neuron* 43, 745-757.

Buonomano, D.V., and Mauk, M.D. (1994). Neural network model of the cerebellum: temporal discrimination and the timing of motor responses. *Neural Computation* 6, 38-55.

Burman, K., Darian-Smith, C., and Darian-Smith, I. (2000). Macaque red nucleus: origins of spinal and olivary projections and terminations of cortical inputs. *J Comp Neurol* 423, 179-196.

Butler, A.B., and Hodos, W. (2005). *Comparative vertebrate neuroanatomy : evolution and adaptation.* Hoboken, N.J.: Wiley-Interscience.

Carter, A.G., and Regehr, W.G. (2000). Prolonged synaptic currents and glutamate spillover at the parallel fiber to stellate cell synapse. *J Neurosci* 20, 4423-4434.

Carter, A.G., and Regehr, W.G. (2002). Quantal events shape cerebellar interneuron firing. *Nat Neurosci* 5, 1309-1318.

Cerminara, N.L., and Rawson, J.A. (2004). Evidence that climbing fibers control an intrinsic spike generator in cerebellar Purkinje cells. *J Neurosci* 24, 4510-4517.

Chadderton, P., Margrie, T.W., and Hausser, M. (2004). Integration of quanta in cerebellar granule cells during sensory processing. *Nature* 428, 856-860.

Chan-Palay, V. (1971). The recurrent collaterals of Purkinje cell axons: a correlated study of the rat's cerebellar cortex with electron microscopy and the Golgi method. *Z Anat Entwicklungsgesch* 134, 200-234.

Chen, Z. (2007). *Correlative learning : a basis for brain and adaptive systems.* Hoboken, N.J.: Wiley-Interscience.

Chu, C.P., Bing, Y.H., Liu, H., and Qiu, D.L. (2012). Roles of molecular layer interneurons in sensory information processing in mouse cerebellar cortex Crus II in vivo. *PLoS One* 7, e37031.

Clark, B.A., and Cull-Candy, S.G. (2002). Activity-dependent recruitment of extrasynaptic NMDA receptor activation at an AMPA receptor-only synapse. *J Neurosci* 22, 4428-4436.

Clopath, C., Nadal, J.P., and Brunel, N. (2012). Storage of correlated patterns in standard and bistable Purkinje cell models. *PLoS Comput Biol* 8, e1002448.

Coddington, L.T., Rudolph, S., Vande Lune, P., Overstreet-Wadiche, L., and Wadiche, J.I. (2013). Spillover-mediated feedforward inhibition functionally segregates interneuron activity. *Neuron* 78, 1050-1062.

Contreras-Vidal, J.L., Grossberg, S., and Bullock, D. (1997). A neural model of cerebellar learning for arm movement control: cortico-spino-cerebellar dynamics. *Learn Mem* 3, 475-502.

D'angelo, E., and Casali, S. (2012). Seeking a unified framework for cerebellar function and dysfunction: from circuit operations to cognition. *Front Neural Circuits* 6, 116.

De Schutter, E., and Bower, J.M. (1994a). An active membrane model of the cerebellar Purkinje cell I. Simulation of current clamps in slice. *J Neurophysiol* 71, 375-400.

De Schutter, E., and Bower, J.M. (1994b). An active membrane model of the cerebellar Purkinje cell II. Simulation of synaptic responses. *J Neurophysiol* 71, 401-419.

Dean, P., Porrill, J., Ekerot, C.F., and Jorntell, H. (2010). The cerebellar microcircuit as an adaptive filter: experimental and computational evidence. *Nat Rev Neurosci* 11, 30-43.

Doya, K. (1999). What are the computations of the cerebellum, the basal ganglia and the cerebral cortex? *Neural Networks* 12, 961-974.

Eccles, J.C., Ito, M., and Szentá́Gothai, J.N. (1967). *The cerebellum as a neuronal machine.* Berlin, New York etc.: Springer-Verlag.

Engbers, J.D., Fernandez, F.R., and Turner, R.W. (2013). Bistability in Purkinje neurons: ups and downs in cerebellar research. *Neural Netw* 47, 18-31.

Franconville, R., Revet, G., Astorga, G., Schwaller, B., and Llano, I. (2011). Somatic calcium level reports integrated spiking activity of cerebellar interneurons in vitro and in vivo. *J Neurophysiol* 106, 1793-1805.

Fujita, M. (1982). Adaptive filter model of the cerebellum. *Biol Cybern* 45, 195-206.

Fulton, J.F. (1935). A note on the definition of the "motor" and "premotor" areas. *Brain* 58, 311-316.

Gabbiani, F., Midtgaard, J., and Knopfel, T. (1994). Synaptic integration in a model of cerebellar granule cells. *J Neurophysiol* 72, 999-1009.

Gao, Z., Van Beugen, B.J., and De Zeeuw, C.I. (2012). Distributed synergistic plasticity and cerebellar learning. *Nat Rev Neurosci* 13, 619-635.

Gardner, S.M., Takamiya, K., Xia, J., Suh, J.G., Johnson, R., Yu, S., and Huganir, R.L. (2005). Calcium-permeable AMPA receptor plasticity is mediated by subunit-specific interactions with PICK1 and NSF. *Neuron* 45, 903-915.

Gerstner, W., and Kistler, W.M. (2002). *Spiking neuron models : single neurons, populations, plasticity.* Cambridge, U.K. ; New York: Cambridge University Press.

Glickstein, M., Strata, P., and Voogd, J. (2009). Cerebellum: history. *Neuroscience* 162, 549-559.

Goodman, D.F., and Brette, R. (2009). The brian simulator. *Front Neurosci* 3, 192-197.

Goto, J., Inoue, T., Kuruma, A., and Mikoshiba, K. (2006). Short-term potentiation at the parallel fiber-Purkinje cell synapse. *Neurosci Res* 55, 28-33.

Grossberg, S. (1969). On learning of spatiotemporal patterns by networks with ordered sensory and motor components. 1. Excitatory components of the cerebellum. *Stud Appl Math*, 105-132.

Habas, C., Guillevin, R., and Abanou, A. (2010). In vivo structural and functional imaging of the human rubral and inferior olivary nuclei: A mini-review. *Cerebellum* 9, 167-173.

Halverson, H., Khilkevich, A., and Mauk, M.D. (Year). "Synchrony of learning-related activity in Purkinje cells is facilitated by basket cells during delay eyelid conditioning", in: *Program No. 341.13. 2014 Neuroscience Meeting Planner. Washington, DC: Society for Neuroscience, 2014. Online.*).

Hausser, M., and Clark, B.A. (1997). Tonic synaptic inhibition modulates neuronal output pattern and spatiotemporal synaptic integration. *Neuron* 19, 665-678.

Hawkes, R., and Leclerc, N. (1989). Purkinje cell axon collateral distributions reflect the chemical compartmentation of the rat cerebellar cortex. *Brain Res* 476, 279-290.

Heiney, S.A., Kim, J., Augustine, G.J., and Medina, J.F. (2014). Precise control of movement kinematics by optogenetic inhibition of Purkinje cell activity. *J Neurosci* 34, 2321-2330.

Isope, P., and Barbour, B. (2002). Properties of unitary granule cell-->Purkinje cell synapses in adult rat cerebellar slices. *J Neurosci* 22, 9668-9678.

Ito, M. (1982). Cerebellar control of the vestibulo-ocular reflex--around the flocculus hypothesis. *Annu Rev Neurosci* 5, 275-296.

Ito, M. (2006). Cerebellar circuitry as a neuronal machine. *Prog Neurobiol* 78, 272-303.

Ito, M. (1984). *The cerebellum and neural control.* New York: Raven Press.

Itō, M. (2012). *The cerebellum : brain for an implicit self.* Upper Saddle River, N.J.: FT Press.

Ito, M., Yamaguchi, K., Nagao, S., and Yamazaki, T. (2014). Long-term depression as a model of cerebellar plasticity. *Prog Brain Res* 210, 1-30.

Jirenhed, D.A., Bengtsson, F., and Hesslow, G. (2007). Acquisition, extinction, and reacquisition of a cerebellar cortical memory trace. *J Neurosci* 27, 2493-2502.

Jorntell, H., Bengtsson, F., Schonewille, M., and De Zeeuw, C.I. (2010). Cerebellar molecular layer interneurons - computational properties and roles in learning. *Trends Neurosci* 33, 524-532.

Jorntell, H., and Ekerot, C.F. (2002). Reciprocal bidirectional plasticity of parallel fiber receptive fields in cerebellar Purkinje cells and their afferent interneurons. *Neuron* 34, 797-806.

Jorntell, H., and Ekerot, C.F. (2003). Receptive field plasticity profoundly alters the cutaneous parallel fiber synaptic input to cerebellar interneurons in vivo. *J Neurosci* 23, 9620-9631.

Jorntell, H., and Ekerot, C.F. (2011). Receptive Field Remodeling Induced by Skin Stimulation in Cerebellar Neurons in vivo. *Front Neural Circuits* 5, 3.

Kandel, E.R. (2013). *Principles of neural science.* New York: McGraw-Hill.

Kassardjian, C.D., Tan, Y.F., Chung, J.Y., Heskin, R., Peterson, M.J., and Broussard, D.M. (2005). The site of a motor memory shifts with consolidation. *J Neurosci* 25, 7979-7985.

Kelly, L., Farrant, M., and Cull-Candy, S.G. (2009). Synaptic mGluR activation drives plasticity of calcium-permeable AMPA receptors. *Nat Neurosci* 12, 593-601.

Kenyon, G.T. (1997). A model of long-term memory storage in the cerebellar cortex: a possible role for plasticity at parallel fiber synapses onto stellate/basket interneurons. *Proc Natl Acad Sci U S A* 94, 14200-14205.

Kondo, S., and Marty, A. (1998). Synaptic currents at individual connections among stellate cells in rat cerebellar slices. *J Physiol* 509 (Pt 1), 221-232.

Korbo, L., Andersen, B.B., Ladefoged, O., and Moller, A. (1993). Total numbers of various cell types in rat cerebellar cortex estimated using an unbiased stereological method. *Brain Res* 609, 262-268.

Koziol, L.F., Budding, D., Andreasen, N., D'arrigo, S., Bulgheroni, S., Imamizu, H., Ito, M., Manto, M., Marvel, C., Parker, K., Pezzulo, G.,

Ramnani, N., Riva, D., Schmahmann, J., Vandervert, L., and Yamazaki, T. (2014). Consensus paper: the cerebellum's role in movement and cognition. *Cerebellum* 13, 151-177.

Lachamp, P.M., Liu, Y., and Liu, S.J. (2009). Glutamatergic modulation of cerebellar interneuron activity is mediated by an enhancement of GABA release and requires protein kinase A/RIM1alpha signaling. *J Neurosci* 29, 381-392.

Lennon, W., Hecht-Nielsen, R., and Yamazaki, T. (2014). A spiking network model of cerebellar Purkinje cells and molecular layer interneurons exhibiting irregular firing. *Front Comput Neurosci* 8, 157.

Liu, S.J., and Cull-Candy, S.G. (2002). Activity-dependent change in AMPA receptor properties in cerebellar stellate cells. *J Neurosci* 22, 3881-3889.

Liu, S.J., and Cull-Candy, S.G. (2005). Subunit interaction with PICK and GRIP controls Ca2+ permeability of AMPARs at cerebellar synapses. *Nat Neurosci* 8, 768-775.

Liu, S.J., and Savtchouk, I. (2012). Ca(2+) permeable AMPA receptors switch allegiances: mechanisms and consequences. *J Physiol* 590, 13-20.

Liu, S.Q., and Cull-Candy, S.G. (2000). Synaptic activity at calcium-permeable AMPA receptors induces a switch in receptor subtype. *Nature* 405, 454-458.

Llinas, R., Walton, K., and Lang, E. (2004). in *The synaptic organization of the brain,* ed. G.M. Shepherd. 5th ed (Oxford ; New York: Oxford University Press), 271-309.

Llinas, R.R. (2011). Cerebellar motor learning versus cerebellar motor timing: the climbing fibre story. *J Physiol* 589, 3423-3432.

Maex, R., and De Schutter, E. (2003). Resonant synchronization in heterogeneous networks of inhibitory neurons. *J Neurosci* 23, 10503-10514.

Maex, R., and Steuber, V. (2013). An integrator circuit in cerebellar cortex. *Eur J Neurosci* 38, 2917-2932.

Magal, A. (2013). A hypothetical universal model of cerebellar function: reconsideration of the current dogma. *Cerebellum* 12, 758-772.

Mann-Metzer, P., and Yarom, Y. (1999). Electrotonic coupling interacts with intrinsic properties to generate synchronized activity in cerebellar networks of inhibitory interneurons. *J Neurosci* 19, 3298-3306.

Marr, D. (1969). A theory of cerebellar cortex. *J Physiol* 202, 437-470.

Mccormick, D.A., and Thompson, R.F. (1984). Cerebellum: essential involvement in the classically conditioned eyelid response. *Science* 223, 296-299.

Mccormick, D.A., Wang, Z., and Huguenard, J. (1993). Neurotransmitter control of neocortical neuronal activity and excitability. *Cereb Cortex* 3, 387-398.

Mcelvain, L.E., Bagnall, M.W., Sakatos, A., and Du Lac, S. (2010). Bidirectional plasticity gated by hyperpolarization controls the gain of postsynaptic firing responses at central vestibular nerve synapses. *Neuron* 68, 763-775.

Medina, J.F., Garcia, K.S., Nores, W.L., Taylor, N.M., and Mauk, M.D. (2000). Timing mechanisms in the cerebellum: testing predictions of a large-scale computer simulation. *J Neurosci* 20, 5516-5525.

Midtgaard, J. (1992). Membrane properties and synaptic responses of Golgi cells and stellate cells in the turtle cerebellum in vitro. *J Physiol* 457, 329-354.

Miyashita, Y., and Nagao, S. (1984). Contribution of cerebellar intracortical inhibition to Purkinje cell response during vestibulo-ocular reflex of alert rabbits. *J Physiol* 351, 251-262.

Myoga, M.H., Beierlein, M., and Regehr, W.G. (2009). Somatic spikes regulate dendritic signaling in small neurons in the absence of backpropagating action potentials. *J Neurosci* 29, 7803-7814.

Nahir, B., and Jahr, C.E. (2013). Activation of extrasynaptic NMDARs at individual parallel fiber-molecular layer interneuron synapses in cerebellum. *J Neurosci* 33, 16323-16333.

O'donoghue, D.L., King, J.S., and Bishop, G.A. (1989). Physiological and anatomical studies of the interactions between Purkinje cells and basket cells in the cat's cerebellar cortex: evidence for a unitary relationship. *J Neurosci* 9, 2141-2150.

Palay, S.L., and Chan-Palay, V. (1974). *Cerebellar cortex: cytology and organization.* Berlin, Heidelberg, New York,: Springer.

Palkovits, M., Magyar, P., and Szentagothai, J. (1971). Quantitative histological analysis of the cerebellar cortex in the cat. I. Number and arrangement in space of the Purkinje cells. *Brain Res* 32, 1-13.

Park, S.M., Tara, E., and Khodakhah, K. (2012). Efficient generation of reciprocal signals by inhibition. *J Neurophysiol* 107, 2453-2462.

Person, A.L., and Raman, I.M. (2010). Deactivation of L-type Ca current by inhibition controls LTP at excitatory synapses in the cerebellar nuclei. *Neuron* 66, 550-559.

Person, A.L., and Raman, I.M. (2012). Purkinje neuron synchrony elicits time-locked spiking in the cerebellar nuclei. *Nature* 481, 502-505.

Phoka, E., Cuntz, H., Roth, A., and Hausser, M. (2010). A new approach for determining phase response curves reveals that Purkinje cells can act as perfect integrators. *PLoS Comput Biol* 6, e1000768.

Pouzat, C., and Marty, A. (1998). Autaptic inhibitory currents recorded from interneurones in rat cerebellar slices. *J Physiol* 509 (Pt 3), 777-783.

Pugh, J.R., and Raman, I.M. (2008). Mechanisms of potentiation of mossy fiber EPSCs in the cerebellar nuclei by coincident synaptic excitation and inhibition. *J Neurosci* 28, 10549-10560.

Puia, G., Costa, E., and Vicini, S. (1994). Functional diversity of GABA-activated Cl- currents in Purkinje versus granule neurons in rat cerebellar slices. *Neuron* 12, 117-126.

Raman, I.M., and Bean, B.P. (1997). Resurgent sodium current and action potential formation in dissociated cerebellar Purkinje neurons. *J Neurosci* 17, 4517-4526.

Raman, I.M., and Bean, B.P. (1999). Ionic currents underlying spontaneous action potentials in isolated cerebellar Purkinje neurons. *J Neurosci* 19, 1663-1674.

Rancillac, A., and Crepel, F. (2004). Synapses between parallel fibres and stellate cells express long-term changes in synaptic efficacy in rat cerebellum. *J Physiol* 554, 707-720.

Rieubland, S., Roth, A., and Hausser, M. (2014). Structured connectivity in cerebellar inhibitory networks. *Neuron* 81, 913-929.

Romaniello, R., and Borgatti, R. (2013). "Cerebellar Agenesis," in *Handbook of the Cerebellum and Cerebellar Disorders,* eds. M. Manto, J. Schmahmann, F. Rossi, D. Gruol & N. Koibuchi. Springer Netherlands), 1855-1872.

Ruigrok, T.J., Hensbroek, R.A., and Simpson, J.I. (2011). Spontaneous activity signatures of morphologically identified interneurons in the vestibulocerebellum. *J Neurosci* 31, 712-724.

Santamaria, F., Tripp, P.G., and Bower, J.M. (2007). Feedforward inhibition controls the spread of granule cell-induced Purkinje cell activity in the cerebellar cortex. *J Neurophysiol* 97, 248-263.

Satake, S., Inoue, T., and Imoto, K. (2012). Paired-pulse facilitation of multivesicular release and intersynaptic spillover of glutamate at rat cerebellar granule cell-interneurone synapses. *J Physiol* 590, 5653-5675.

Schmahmann, J.D. (2004). Disorders of the cerebellum: ataxia, dysmetria of thought, and the cerebellar cognitive affective syndrome. *J Neuropsychiatry Clin Neurosci* 16, 367-378.

Schonewille, M., Gao, Z., Boele, H.J., Veloz, M.F., Amerika, W.E., Simek, A.A., De Jeu, M.T., Steinberg, J.P., Takamiya, K., Hoebeek, F.E., Linden, D.J., Huganir, R.L., and De Zeeuw, C.I. (2011). Reevaluating the role of LTD in cerebellar motor learning. *Neuron* 70, 43-50.

Schweighofer, N., Spoelstra, J., Arbib, M.A., and Kawato, M. (1998). Role of the cerebellum in reaching movements in humans. II. A neural model of the intermediate cerebellum. *Eur J Neurosci* 10, 95-105.

Shouval, H.Z., Bear, M.F., and Cooper, L.N. (2002). A unified model of NMDA receptor-dependent bidirectional synaptic plasticity. *Proc Natl Acad Sci U S A* 99, 10831-10836.

Shutoh, F., Ohki, M., Kitazawa, H., Itohara, S., and Nagao, S. (2006). Memory trace of motor learning shifts transsynaptically from cerebellar cortex to nuclei for consolidation. *Neuroscience* 139, 767-777.

Smith, S.L., and Otis, T.S. (2005). Pattern-dependent, simultaneous plasticity differentially transforms the input-output relationship of a feedforward circuit. *Proc Natl Acad Sci U S A* 102, 14901-14906.

Soler-Llavina, G.J., and Sabatini, B.L. (2006). Synapse-specific plasticity and compartmentalized signaling in cerebellar stellate cells. *Nat Neurosci* 9, 798-806.

Sultan, F., and Bower, J.M. (1998). Quantitative Golgi study of the rat cerebellar molecular layer interneurons using principal component analysis. *J Comp Neurol* 393, 353-373.

Sun, L., and June Liu, S. (2007). Activation of extrasynaptic NMDA receptors induces a PKC-dependent switch in AMPA receptor subtypes in mouse cerebellar stellate cells. *J Physiol* 583, 537-553.

Sutton, R. (1988). Learning to predict by the method of temporal differences. *Machine Learning* 3, 9-44.

Swain, R.A., Kerr, A.L., and Thompson, R.F. (2011). The cerebellum: a neural system for the study of reinforcement learning. *Front Behav Neurosci* 5, 8.

Szapiro, G., and Barbour, B. (2007). Multiple climbing fibers signal to molecular layer interneurons exclusively via glutamate spillover. *Nat Neurosci* 10, 735-742.

Thompson, R.F., and Steinmetz, J.E. (2009). The role of the cerebellum in classical conditioning of discrete behavioral responses. *Neuroscience* 162, 732-755.

Turrigiano, G. (2012). Homeostatic synaptic plasticity: local and global mechanisms for stabilizing neuronal function. *Cold Spring Harb Perspect Biol* 4, a005736.

Van Beugen, B.J., Gao, Z., Boele, H.J., Hoebeek, F., and De Zeeuw, C.I. (2013). High frequency burst firing of granule cells ensures transmission at the parallel fiber to purkinje cell synapse at the cost of temporal coding. *Front Neural Circuits* 7, 95.

Walter, J.T., Alvina, K., Womack, M.D., Chevez, C., and Khodakhah, K. (2006). Decreases in the precision of Purkinje cell pacemaking cause cerebellar dysfunction and ataxia. *Nat Neurosci* 9, 389-397.

Watt, A.J., Cuntz, H., Mori, M., Nusser, Z., Sjostrom, P.J., and Hausser, M. (2009). Traveling waves in developing cerebellar cortex mediated by asymmetrical Purkinje cell connectivity. *Nat Neurosci* 12, 463-473.

Williams, R.W., and Herrup, K. (1988). The control of neuron number. *Annu Rev Neurosci* 11, 423-453.

Wulff, P., Schonewille, M., Renzi, M., Viltono, L., Sassoe-Pognetto, M., Badura, A., Gao, Z., Hoebeek, F.E., Van Dorp, S., Wisden, W., Farrant, M., and De Zeeuw, C.I. (2009). Synaptic inhibition of Purkinje cells mediates consolidation of vestibulo-cerebellar motor learning. *Nat Neurosci* 12, 1042-1049.

Yamazaki, T., and Nagao, S. (2012). A computational mechanism for unified gain and timing control in the cerebellum. *PLoS One* 7, e33319.

Yamazaki, T., Nagao, S., Lennon, W., and Tanaka, S. (In press). Modeling memory consolidation during post-training periods in cerebellovestibular learning. *Proc Natl Acad Sci U S A*.

Yamazaki, T., and Tanaka, S. (2005). Neural modeling of an internal clock. *Neural Comput* 17, 1032-1058.

Yeung, L.C., Shouval, H.Z., Blais, B.S., and Cooper, L.N. (2004). Synaptic homeostasis and input selectivity follow from a calcium-dependent plasticity model. *Proc Natl Acad Sci U S A* 101, 14943-14948.

Zheng, N., and Raman, I.M. (2010). Synaptic inhibition, excitation, and plasticity in neurons of the cerebellar nuclei. *Cerebellum* 9, 56-66.